Use of the environmentally controlled scanning vibrating electrode technique for the investigation of localised corrosion in pipeline steel.

Boughton, Jim

Use of the Environmentally Controlled Scanning Vibrating Electrode Technique for the Investigation of Localised Corrosion in Pipeline Steel

Jim Boughton

University of Wales Swansea
MPhil

Acknowledgements:

Many thanks to my supervisor, Dr. David Worsley, Dr. Neil McMurray and all those in the Corrosion Group in Swansea who helped and guided me throughout this project. I would also like to thank Ahmed Belghazi and Total Fina Elf who supported this project in the supply of materials and technical information.

Contents

Chapter 2

Chapter 3

Chapter 4

Chapter 5

Chapter 6

Abstract

The aim of this project was to explore the design criterion for a scanning vibrating electrode technique (SVET) assembly with partial environmental control. To facilitate this goal an SVET has been designed which incorporates an enclosed sample chamber equipped with a means of gas purging.

The design allows for prepurging of electrolyte prior to sample immersion since corrosion initiated prior to stabilising the atmosphere is likely to dominate the corrosion profile. In addition, dosing of the electrolyte with prepurged solution such as corrosion inhibitor is possible through injection ports

The apparatus has been built and rigorously calibrated using a point current source as described in Chapter 3. The apparatus has a spatial resolution of ~220μm at 100μm scan height, this is slightly larger than the theoretical value due to the finite size of the SVET tip. The use of the point current source enabled a calibration factor of 5445 $Am^{-2}V^{-1}$ to be obtained in 0.1% NaCl. This acts as a means of converting SVET voltages to current densities and is also a routine calibration check.

The first use of the equipment described in chapter 4 has been to analyse the efficiency of a commercial filming amine inhibitor on the kinetics and mechanisms of corrosion. The addition of inhibitor to the electrolyte served to reduce the levels of corrosion of the pipeline material. However low concentrations (<5ppm) did, whilst reducing the overall corrosion levels, cause the formation of intense localised pits. Measurement of the E_{corr} showed an increase on addition of the inhibitor implying partial anodic inhibition. Total metal loss (TML) for varying levels of inhibitor concentration and atmospheric conditions were calculated over a three hour period; under normal atmospheric conditions the TML for a $10mm^2$ area was 24.8μg, under

CO_2 purged conditions this decreased to 12.1μg, the addition of 5 parts per million inhibitor solution reduced the TML further to 4.65μg and finally the addition of 10ppm inhibitor yielded the lowest total metal loss figure of 2.84μg. Due to the fact that the inhibitor is a positively charged species the inhibitor solution served to actually increase crevice corrosion activity by a factor of three in the crevice region whilst reducing corrosion across the bulk surface. In the second application, described in chapter 5, the environmental SVET has been used to visualise galvanic coupling between weld metal and base materials in a field failure supplied by Total Elf Fina. The weld and the heat affected zones are anodic to the tube base metal and this is related to their lower chromium level and elevated aluminium content. Comparing total metal loss values of the welded sample in a CO_2 saturated atmosphere with a single metal material under the same conditions; the galvanic corrosion effectively doubles the corrosion activity, bringing it back up to the levels found with samples corroding in air saturated sodium chloride solution. Further more the corrosion is focused on the small area of the weld metal, and in the field the ratio of areas between the cathodic pipeline and anodic welded joints will be significantly greater therefore accelerating time to failure.

CHAPTER 1

Introduction

1. Introduction

The oil industry is among the most wealthy and dynamic industries in the world. As such effective means of moving the oil and other petrochemical materials is paramount in the petrochemicals industry. Pipelines can stretch for many miles, however the industry is so cutthroat that economic factors must take a front seat in materials selection. Since pipelines must be made as cheaply as possible they are constructed from carbon steels, and in most cases welded joints are necessary to make suitable lengths of pipeline. Corrosion is therefore inevitable since the environment can contain significant corrosive species (chloride, acetic acid, CO_2, H_2S etc...). Corrosion failure of the materials in service could lead to a disaster both ecologically and financially, with regards to remedial action. This is the driving force behind the study of pipeline corrosion; in order to maximise in-service performance it is essential to understand the corrosion processes from a mechanistic standpoint.

1.1 Socio Economic cost of corrosion:

The cost of corrosion is seldom thought of in its full enormity. A study by the Government Committee on Corrosion and Protection showed that in 1971[1] the total cost of corrosion to the economy was nearly £1.5billion, which at that time accounted for three percent of the gross national product (GNP). With reference to the cost of corrosion in today's terms, 3% of the UK's GNP would be £26billion. It is not only the cost of replacement of corroded parts that accounts for this vast sum of money:

- Component maintenance; application of barrier coatings such as paint, greasing and oiling of components.
- Replacement of failed components; the down time involved with component failure, and replacement of the failed component. It has been estimated that in the UK alone one tonne of steel is converted to rust every 90 seconds.
- Compliance with European environmental regulations; contamination of soils by corrosion products etc.

In 1981, the agricultural industry in the UK was estimated to have lost £600million due to corrosion, and that this could have been halved by the use of effective corrosion prevention methods[2]. As such it is important for the mechanisms of corrosion to be fully understood so that they can be combated effectively.

1.2 Pipeline materials:

Economic factors have pushed forward mild steel as the material of choice in the construction of oil pipelines, regardless of the fact that its corrosion characteristics are not ideal. A table showing typical compositions of mild steels used in a pipelines is shown below (table 1.1)[3]

	Chemical Compositions (mass %) (*ppm)													Strength (MPa)	
Steel	**C**	**Si**	**Mn**	***P**	***S**	**Nb**	**Ti**	**Al**	**Ni**	**Mo**	**Cu**	**V**	***B**	**Ys**	**Ts**
X65TMCP	0.05	0.21	1.31	50	10	0.04	0.014	0.029	0.16	0	0.27	0.05	0	524	557
X65CR	0.08	0.25	1.53	80	20	0.03	0.008	0.032	0	0	0	0.07	0	575	614
X65QT	0.08	0.22	1.29	110	10	0.04	0	0.041	0	0.16	0	0	0	465	587
X80TMCP	0.26	0.24	1.94	30	10	0.03	0.12	0.024	0.36	0.21	0.4	0	10	615	794
X52CR	0.16	0.26	1.3	90	40	0.02	0.017	0.025	0	0	0	0	0	439	537

Table 1.1 shows the compositions of common pipeline materials, Ys and Ts are the yield and tensile strengths of the material shown respectively. Steel X65QT (highlighted in red) is the pipeline steel under investigation.

The steel pipeline sections are welded together using fusion or TIG techniques. Should care not be taken, this can introduce such phenomena as galvanic corrosion, crevice corrosion and embrittlement of the heat affected zone all of which could precipitate in catastrophic failure of the line. The materials studied in this investigation are derived from a welded component that failed unexpectedly in the field.

1.3 Corrosion of metals:

The majority of metals used today for structural applications are derived from ores of some sort (usually oxides), i.e. they do not tend to be found naturally in their metallic form. This is due to the fact that these ores are thermodynamically more stable than the uncombined metals. Extraction of metals from their respective ores is an extremely energy intensive process (e.g. the extraction of aluminium from bauxite by electrolysis or carbon reduction of iron ores such as haematite) due to the end product being at a higher energy state than its constituents. As such the metal exists in a metastable state with only a relatively small activation energy barrier to overcome before corrosion can occur (see fig 1.1). Thus there is a relentless tendency for the uncombined metal to transform into an entropically lower energy state via interaction with components in the environment to form corrosion products of a similar energy state to the original ore. Of course, the rate at which this transition occurs is dependant on many different factors, such as the free energy difference between the uncombined metal and the corrosion product. Another factor would be what type of corrosion product is formed, i.e. aluminium although having a large ΔG can be more

stable than iron due to the fact that aluminium forms a protective oxide layer on its exposed surfaces preventing further corrosion taking place. Whereas in the case of iron the corrosion product flakes away, exposing fresh material to the environment which can then in turn be corroded and so on.

The definition for corrosion of metals according to the international standard ISO 8044 is, "A physiochemical interaction (usually electrochemical in nature) between a metal and its environment which results in changes in the properties of the metal, the environment, or the technical system of which these form a part."[19 p29]

1.4 Mechanisms of Corrosion:

Corrosion of mild steel predominantly occurs under wet or aqueous conditions. This is where the steel surface is brought into contact with an electrolyte, facilitating electrochemical reactions by reducing the activation energy barrier between the metal and the oxidised states. Under aqueous conditions, an electrochemical cell can be formed; this consists of an anode and a cathode with current flow between them through the electrolyte and the metal itself (see fig 1.2)[6].

At the anode, oxidation occurs where the more reactive metal gives up electrons to form a metal ion and an electron as shown in equation 1.1

$$M \rightarrow M^{n+} + ne^{-} \qquad 1.1$$

In the case of steel, this reaction would be expressed:

$$Fe \rightarrow Fe^{2+} + 2e^{-} \qquad 1.2$$

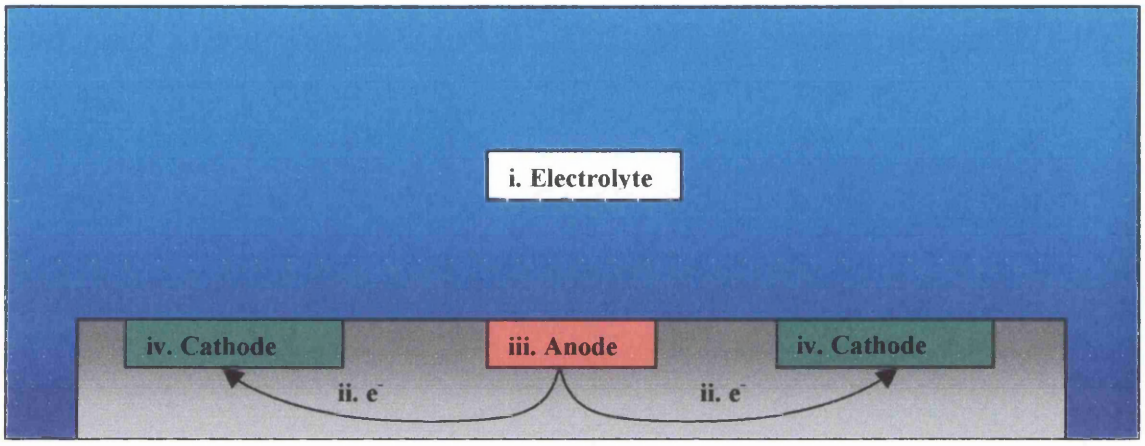

Figure 1.2 A diagram showing the four components of the electrochemical cell i.) the electrolyte. ii) the electrical connection. iii) the anode. iv) the cathode

The electrons produced by the anodic reaction pass through the electrolyte to the cathodic site where the reduction reaction occurs. The reduction reaction can take on a number of different forms such as: -

Hydrogen evolution $2H^+ + 2e^- \rightarrow H_2$ 1.3

Replating $M^{n+} + ne^- \rightarrow M$ 1.4

Reduction of dissolved oxygen $2H_2O + O_2 + 4e^- \rightarrow 4OH^-$ 1.5

Reaction 1.3 requires the presence of dissolved oxygen in the electrolyte. While this is common under aerobic conditions, within an oil pipeline the atmosphere would be predominately CO_2 saturated thus eliminating this form of cathodic reaction. However in these conditions of CO_2 saturation the pH of the electrolyte is ~4. As such hydrogen evolution (1.1) becomes the predominant reduction reaction. Since there is electronic flow from the anode to the cathode site their electrochemical potential is different. The magnitude of this potential difference between anode and cathode gives information on the thermodynamic likelihood of corrosion. Each metal has its own environment specific potential. In terms of defining a value, it is common to express standard electrode potentials measured using a metal electrode in a 1mol dm^{-3} solution of its ions at 298K and against a standard hydrogen half-cell who's E^0 is set at zero. A table of typical E^0 data[4 p31] is shown below in table 1.2

Electrode Reaction	*E^{θ}/V*
$Mg^{2+} + 2e^- \rightarrow Mg$	-2.363
$Al^{3+} + 3e^- \rightarrow Al$	-1.662
$Sn^{2+} + 2e^- \rightarrow Sn$	-1.36
$Pb^{2+} + 2e^- \rightarrow Pb$	-1.26
$Zn^{2+} + 2e^- \rightarrow Zn$	-0.763
$Fe^{2+} + 2e^- \rightarrow Fe$	-0.44
$Cu^{2+} + 2e^- \rightarrow Cu$	-0.34
$Pt^{2+} + 2e^- \rightarrow Pt$	1.2

Table 1.2 The Standard EMF series

The data shown in table 1.2 is for standard conditions. A more useful set of data is the galvanic series, which gives the free corrosion potentials of a metal under specific conditions. Fig 1.3 shows the galvanic series for a number of metals in sea water[5 p137]. The more negative the free corrosion potential correlates to the metal being less noble.

The effects of overpotential on the anodic (oxidation) and cathodic (reduction) reactions can be represented in a simplified manner using a Tafel plot[7], shown in figure 1.4 below. The intersection of the anodic and cathodic lines is i_0, the exchange current.

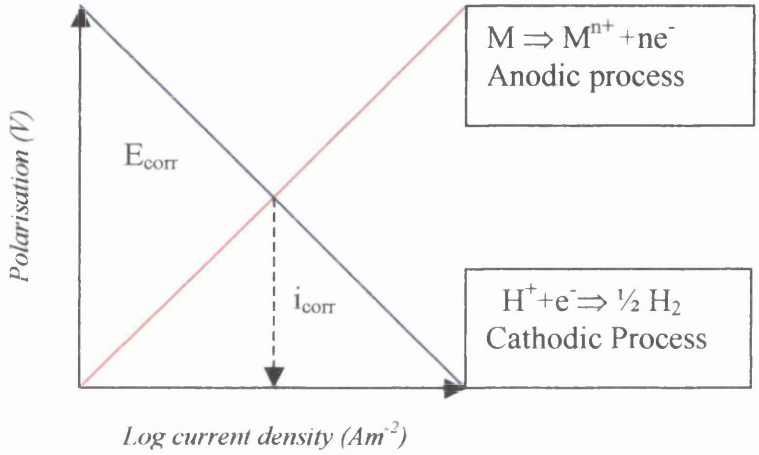

Figure 1.4 showing a Tafel plot

In practice, there will be a range of cathodic and anodic reactions occurring on the metal surface at a given time. However there must be an overall balance of reactions i.e. for every anodic reaction there must be an equivalent cathodic reaction.

$$\sum i_{anodic} = -\sum i_{cathodic} = i_{corr} \tag{3}$$

Where i_{anodic} is the partial current associated with the anodic reactions, $i_{cathodic}$ is the current associated with the cathodic reactions and i_{corr} is the rate of corrosion in terms of current.

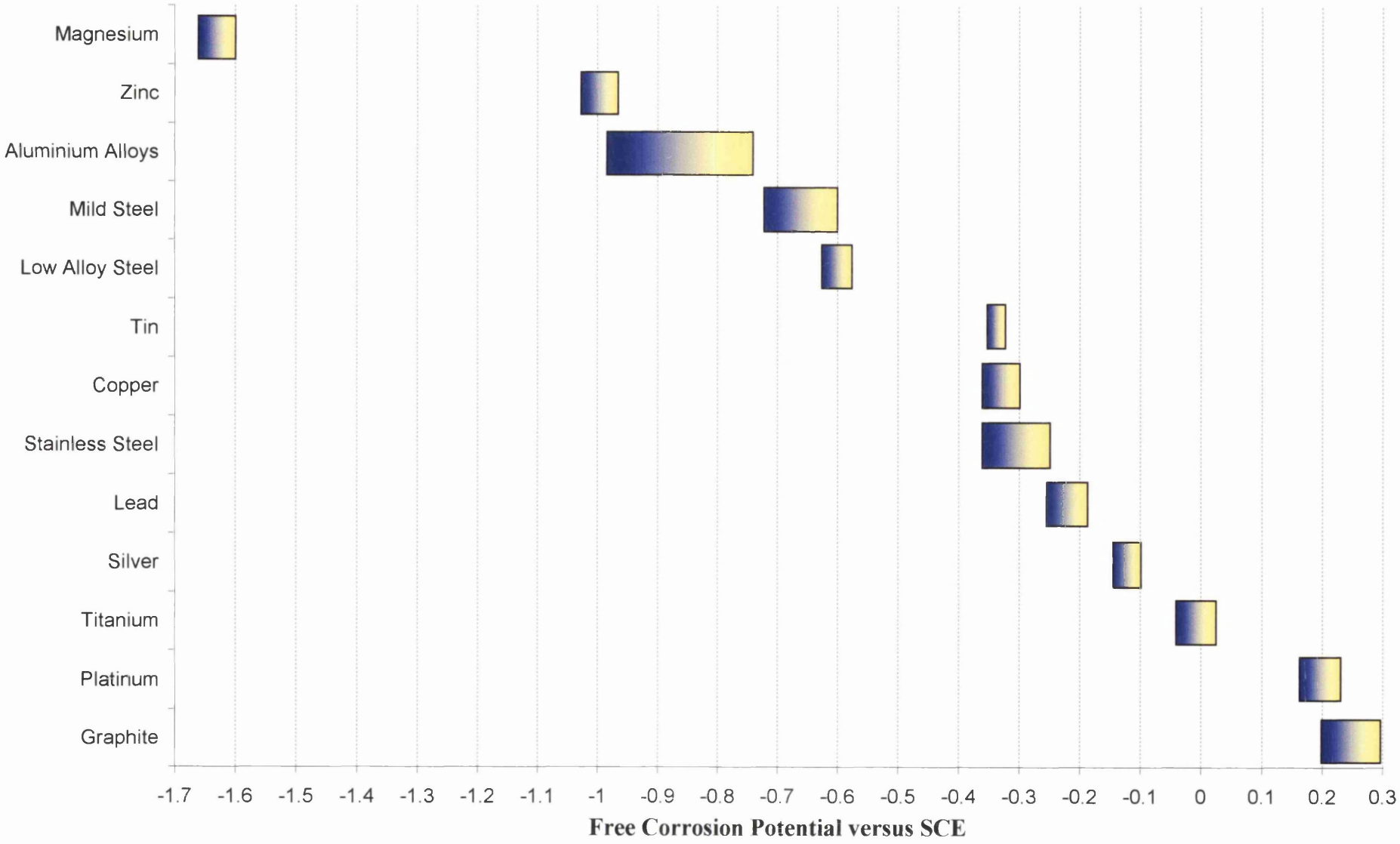

Figure 1.3 A graph showing the galvanic series for a range of metals in sea water[5 p137]

Corrosion of the metal can be termed as either generalised or localised corrosion. Generalised corrosion is where the anodic and cathodic reaction sites cannot be spatially resolved; localised corrosion is where, there are clearly identifiable anodic and cathodic sites and regions. It is the latter form that causes most component failures due the focused anodic activity resulting in increased rates of depth penetration.

Electrochemical cells will only be formed if there are local differences in conditions (such as composition, geometry of location etc) for different areas of the exposed metal surface that allow anodes to preferentially form in certain locations. These differences may be due to local composition, structural differences or physical location such as crevices.

1.4.1 Generalised Corrosion:

Also known as uniform corrosion this form of electrochemical attack occurs with a uniform intensity over the exposed metal surface. Other than affecting the aesthetics of a component, this form of corrosion rarely results in component failure; penetration of corrosion into the metal takes place over a significantly longer period of time. In addition, where general corrosion occurs the prediction of component failure is made relatively simple, since extrapolation of corrosion data is easy.

1.4.2 Localised Corrosion:

This form of corrosion tends to be far more damaging than generalised corrosion and can often be significantly more difficult to detect. Localised corrosion has been investigated for many years[6,8]. There are numerous mechanisms for localised corrosion some of which are discussed below.

1.4.3 Dissimilar Metals Corrosion:

This form of corrosion is also known as bimetallic or galvanic corrosion. It arises when two metals that are well separated in the galvanic series (see figure 1.3), or a metal and a non-metallic conductor (e.g. graphite) are in contact whilst being submersed in an electrolyte see figure 1.5 Should this situation occur, the metal positioned lower down the galvanic series (e.g. aluminium) becomes the anode, and the more noble metal (e.g. iron) becomes the cathode. Thus the anode experiences significantly more rapid corrosion, while the cathode remains intact.

When dissimilar metals corrosion strikes, it can cause catastrophic component failure, especially as many of the less noble metals such as magnesium and aluminium are often used in critical applications such as the aircraft industry. This form of corrosion can also result in failures around welds and joints as will be discussed in chapter 5.

It is however possible to harness galvanic corrosion to obtain favourable results, by using a more reactive metal to sacrificially protect the more structurally important cathode. An example of this would be the use of sacrificial zinc anodes on

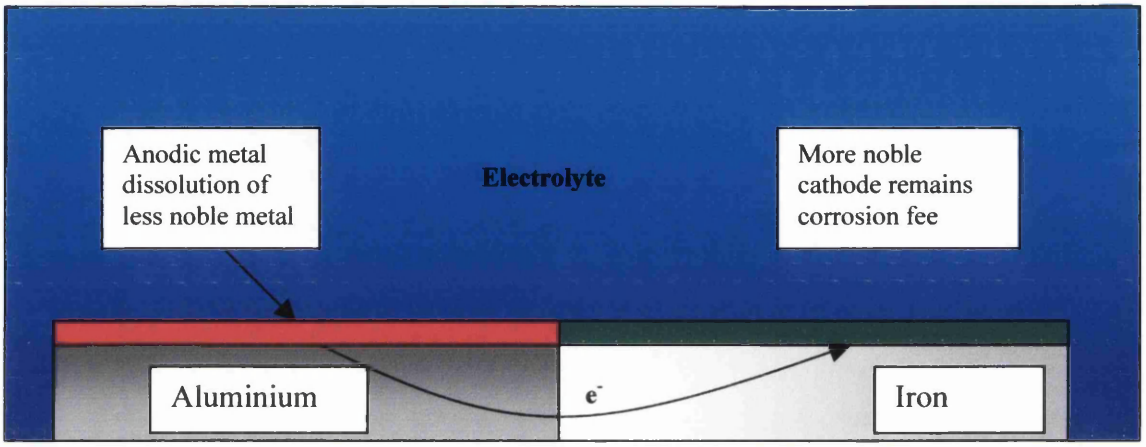

Figure 1.5 A schematic of dissimilar metals corrosion, the less noble metal becomes a sacrificial anode to the more noble metal, provided there is direct electrical contact between the two.

the steel superstructures of oilrigs. The steel legs of the oilrig would, under the harsh marine conditions, soon corrode limiting the lifespan of the rigs massively. Using another more inert material for the task would be economically impossible, so zinc is used. Looking at figure 1.3 it can be seen that the free corrosion potentials for zinc and steel are –1.05V and –0.65V respectively. Thus as the steel is the more noble of the two metals, the zinc will become the anode and the steel will act as the cathode. So the steel superstructure can remain in service for extended periods while the zinc anodes can be periodically replaced after they dissolve at a fraction of the cost of building a new oilrig or replacing corroded supports. Indeed in typical galvanised products, E_{corr} is ~ -1.05V reflecting the galvanic protection afforded to the iron.

Solutions to the problem of Dissimilar Metals Corrosion:

i) Insulate the two metals from one another, so that an electrochemical cell cannot be formed

ii) Use a less noble third metal as a sacrificial anode to the other metals, allowing metals further apart in the galvanic series to be coupled.

iii) When attaching two or more different metals together, try to ensure that they occupy similar positions in the galvanic series.

iv) Corrosion occurs at the anode. As such, if the anode is large compared to the cathode then corrosion will be spread over a larger area reducing the risk of failure.

v) Use of suitable inhibitors to slow down or prevent the corrosion process.

1.4.4 Crevice Corrosion:

Crevice corrosion can be initiated by differential aeration, but can also occur without oxygen. This is an intense form of localised corrosion that is prevalent in complex structures, or simple overlaps where a crevice is formed between the panels. Trethewey defines crevice corrosion thus: 'The attack which occurs because part of a metal surface is in a shielded or restricted environment, compared to the rest of the metal which is exposed to large volumes of electrolyte'[5 p165]. Corrosion can be accelerated by local changes in the environment surrounding the exposed metal i.e. differing concentrations of ions or dissolved gasses. It is because of this that crevice corrosion occurs in locations where there is sufficient gap for electrolyte to penetrate, but where the solution becomes stagnant or inaccessible to the ions and gases in solution.

In a solution where there is dissolved oxygen in the electrolyte, in the locations where electrolyte flow is restricted oxygen levels become depleted i.e. a crevice. This then promotes oxidation of the metal as shown in equation 1.1. The electrons produced flow through the metal to the cathodic sites where the reduction reaction takes place (see equation 1.3, 1.4, 1.5). To further increase the vigour of the anodic corrosion there is often a build up of H^+ and Cl^- ions that serve to break down any passivating layers and are hence actively corrosive themselves.

The Fontana Green mechanism of crevice corrosion[4 p43] is shown in figures 1.6a and 1.6b. Figure a shows the initial state where there is sufficient oxygen available within the crevice, so that no preferential anode is formed. However as the oxygen is used up in the crevice, it cannot be easily replaced and thus becomes

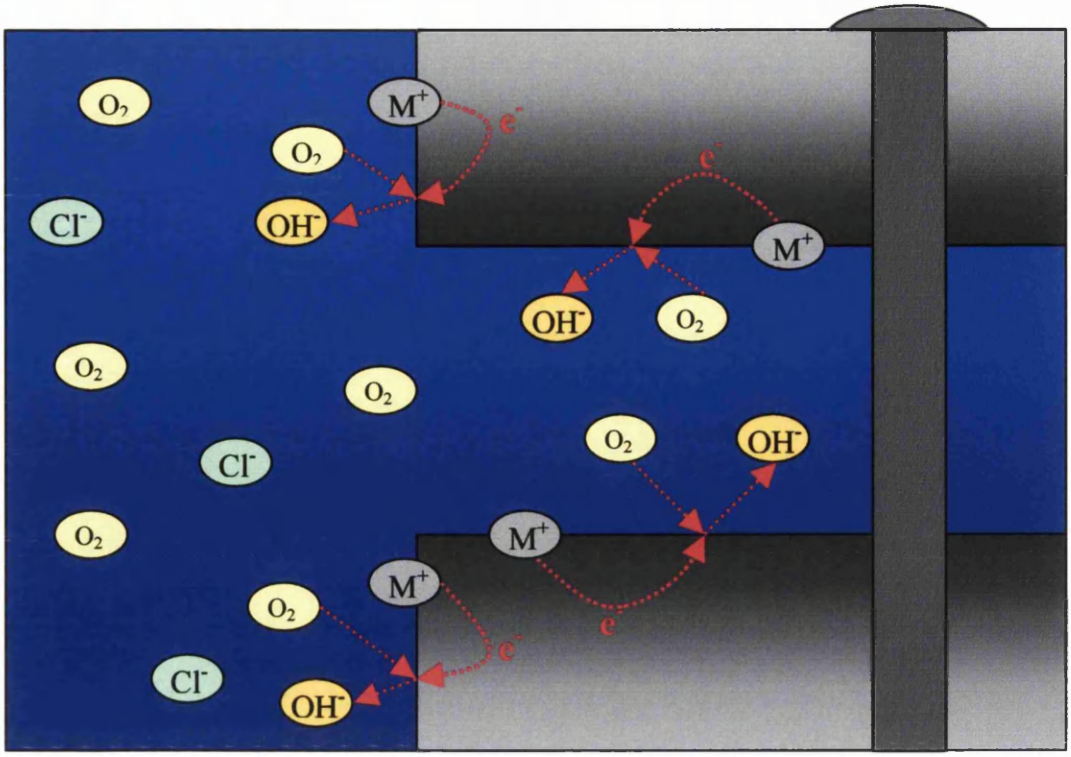

Figure 1.6a Shows the mechanism of wet corrosion at a crevice site prior to the oxygen being used up.

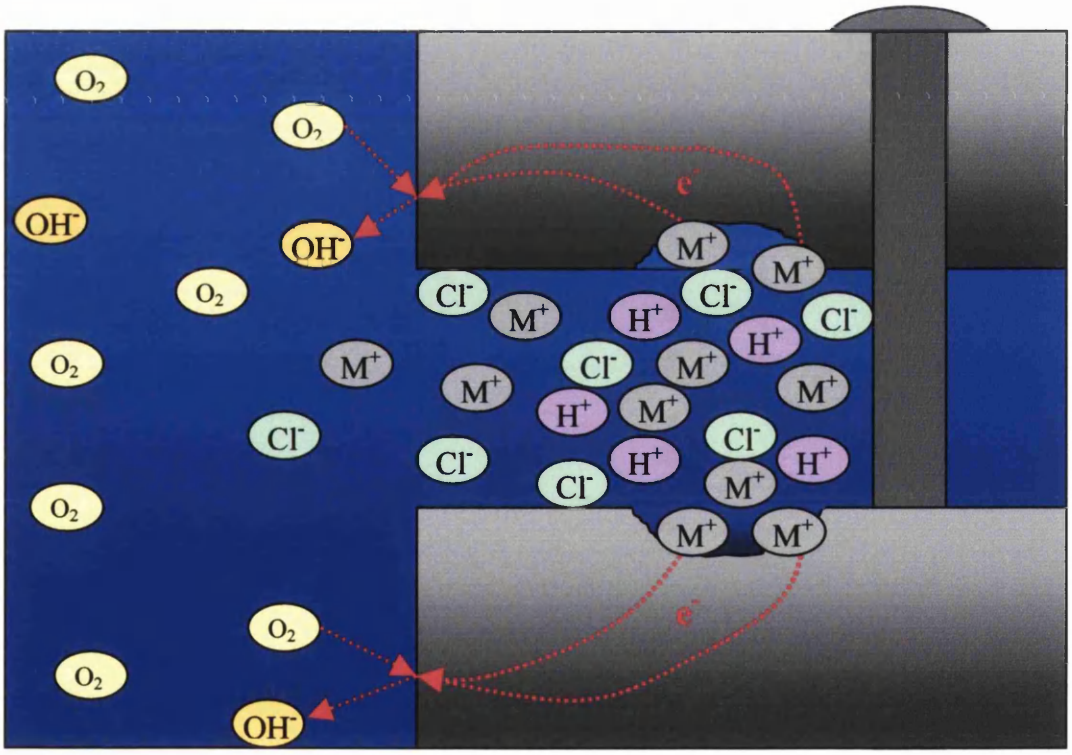

Figure 1.6b Shows the Fontana Green mechanism of wet corrosion at a crevice site when crevice becomes oxygen depleted.

oxygen depleted; therefore promoting oxidation reactions within the crevice. This corrosion mechanism is shown in figure 1.6b. When looking at the oxygen free environment within an oil pipeline, the crevice will not have any oxygen initially. In this case it is quite simple, hydrogen evolution occurs outside the crevice, metal dissolution occurs within the crevice creating a positive charge. The electrons generated by the oxidation reaction are used up in the cathodic reduction reaction outside the crevice. As metal ions begin to populate the electrolyte within the crevice, a positive charge is created attracting any chloride ions in solution into the crevice in order to balance the charge. These chloride ions serve to further the extent of the problem, and the process becomes self-sustaining.

Solutions to Crevice Corrosion:

i) Careful design of the artefact, ensuring minimal crevices and areas where stagnant electrolyte may pool e.g. rounded corners, curved rather then angular joints.

ii) Use of sealing joining methods that do not allow any electrolyte to penetrate into the crevices e.g. welding, gluing, siliconing.

iii) Regular removal of any deposits that may trap electrolyte next to the metal surface e.g. leaves, dirt.

iv) Use of inhibitors to control or eliminate corrosion.

1.4.5 Pitting Corrosion:

A highly focused form of localised corrosion in which small areas of the metal surface are selectively attacked, the mechanism of pitting has been researched extensively[4,6,11-12]. It predominantly occurs on horizontal surfaces at sites of compositional irregularities (such as precipitates of less noble metals), or where there is an existing flaw such as a scratch or knick. After initiation the mechanism for pitting corrosion is very similar to that for crevice corrosion where the pit becomes depleted in oxygen. The pit becomes the anode and oxidation reactions within the pit are complimented by cathodic reduction reactions on the exposed surface. Pitting can also be induced by the break down of a passive oxide layer by chloride ions. The layer is attacked, and where the passive layer is thinner the metal surface is exposed, making it highly anodic in comparison to the surrounding material with passive layer. After initiation, pits can be classified into two categories:

i) Unstable pitting; pits do not propagate, and after the initiation stage the pits die, the nucleation current decreases and the pit is terminated. Unstable pitting can occur if the pit becomes clogged with corrosion product.

ii) Metastable pitting; in this scenario the pit survives nucleation, and is in a metastable state, as its existence depends on a continued current density, and exposed surface. The pit can therefore propagate into the metal surface causing premature failure of the component. A difficulty in dealing with pitting corrosion is that it is very localised and can be difficult to detect before failure occurs.

Solutions to Pitting Corrosion:

i) Use a material or additive that reduces pitting corrosion e.g. molybdenum in stainless steel.

ii) Use of a barrier coating or filming inhibitor to prevent contact between the electrolyte and metal surface.

iii) Use a highly polished surface with minimal surface defects to reduce the numbers of initiation sites for pitting corrosion.

1.4.6 Sweet Corrosion:

Also known as carbon dioxide corrosion, sweet corrosion is particularly prevalent in the petrochemicals industry often causing premature failure of oil pipelines. The CO_2 in question is derived from injection techniques used to extract oil from underground reserves. The nature of sweet corrosion is well-documented [13-15] and understanding the mechanisms of it allow preventative measures to be taken.

The anodic reaction in the corrosion of pipeline is shown below:

$$Fe = Fe^{2+} + 2e^-$$

The cathodic reactions that occur are:

$$2H^+ + 2e^- = H_2$$

$$2H_2CO_3 + 2e^- = H_2 + 2HCO_3^-$$

A number of factors affect the rate at which CO_2 corrosion occurs

- Type of metal; unfortunately the materials mainly used in oil pipeline production are plain carbon steels, due to the economic constraints, however these steels are particularly susceptible to sweet corrosion.

- Liquid flow; areas of turbulent flow can experience enhanced sweet corrosion.
- pH of the oil, corrosion will occur more readily in more acidic conditions.
- Partial pressure of the carbon dioxide.
- As the pipeline corrodes, carbonates can form on the exposed metal surface, offering barrier protection, which can significantly reduce the corrosion rates experienced. However, should the carbonate scale ($FeCO_3$) not cover the entire surface, the small exposed area becomes a focal anode and accelerated pitting can occur at the exposed site.

Solutions to sweet corrosion:

i) Try to make the solution as pH neutral as is possible.

ii) Avoid complex pipeline geometry to prevent turbulent flow

iii) Use a filming inhibitor as barrier protection

iv) Reduce operating temperatures to decrease the intensity of the sweet corrosion.

1.5 Corrosion Inhibition:

Inhibitors are substances that when added in relatively low concentrations to the environment, decrease its corrosive nature[18]. The type of inhibitor used is dependant on the metals involved, and the environment under which they will operate. Within the bracket of aqueous metallic corrosion, inhibitors can be classified as either anodic or cathodic, depending on which reactions they impede. They can work in a

variety of ways e.g. interference with the anodic or cathodic reactions or by the formation of a thin barrier coating on the corroding surface.

1.5.1 Anodic Inhibitors:

Anodic inhibitors operate by means of eliminating or impeding the anodic reactions. Therefore at a given E_{corr}, the electrochemical cell will exhibit a lower i_{corr}. This is shown graphically in figure 1.7a. The anodic line is effectively shifted left, increasing the E_{corr} and decreasing the i_{corr}. The reduction in the current density will under suitable conditions inhibit overall corrosion. The increase in potential effected by anodic inhibitors means that should there be insufficient inhibitor to protect the entire surface, the remaining unprotected areas will experience significantly increased local corrosion rates. This characteristic has earned anodic inhibitors the appellation 'dangerous inhibitors'[5].

These inhibitors are available in a number of guises: -

i) Precipitation inhibitors: anionic substances are added which control the anodic reactions by the formation of insoluble salts with the metal cations emerging from the anodic sites, plugging the site.

$$3M^{2+} + 2PO_4^{3-} \rightarrow M_3(PO_4)_2$$

e.g. Phosphates, Molybdate, Silicate

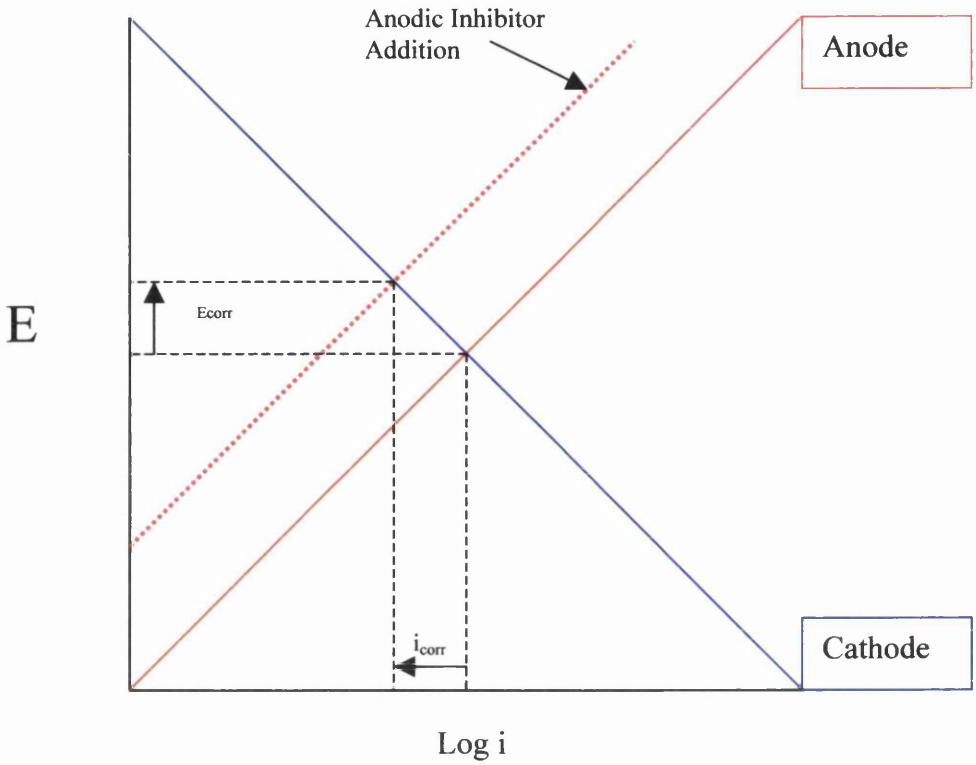

Figure 1.7a A Tafel plot showing the effects of anodic inhibitor solutions on the E_{corr} and i_{corr} of an electrochemical cell

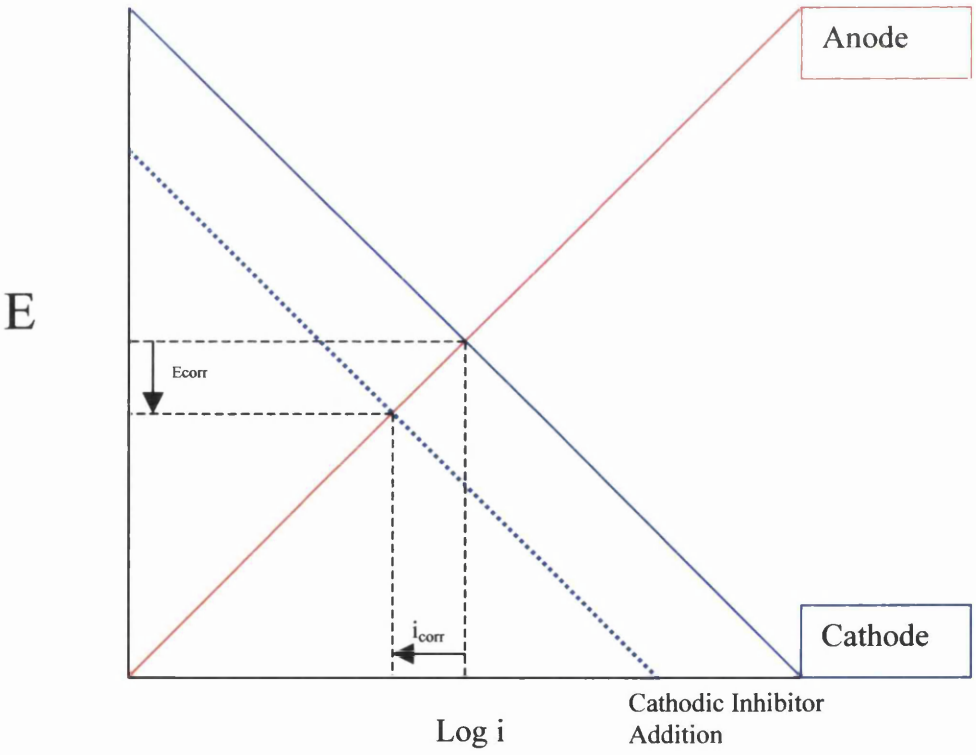

Figure 1.7b A Tafel plot showing the effects of cathodic inhibitor solutions on the E_{corr} and i_{corr} of an electrochemical cell

ii) Oxidizing Agents (cathodic depolarisers): these operate by means of pushing up the E_{corr} (Tafel line) into the passive region for those materials with an active passive transition such as iron.

iii) Anodic Filming Inhibitors: used extensively in the petrochemical industry, these inhibitors form a protective, non conductive film over the entire material surface, effectively insulating it from the electrolyte, breaking down the electrochemical corrosion cell. This results in elimination of corrosion if the coating is perfectly complete, or as happens in practice, corrosion can be significantly retarded by sufficient inhibitor treatment.

Advantages of anodic inhibitors:

- Very efficient, therefore only very small amounts required to offer protection.
- Variety of delivery methods e.g. can be included in the primer of paint, or as a liquid passed through a pipeline

Disadvantages of anodic inhibitors:

- 'Dangerous' so that if passive layer is not complete, aggressive localised corrosion events can occur at exposed sites due to increased E_{corr}.
- Aggressive ions may serve to break down the passive layer again exposing areas that will experience extensive corrosion.

- Many anodic inhibitors used in coatings are potentially damaging to the environment should they be out of the coating etc.

1.5.2 Cathodic inhibitors

These operate by interfering with the cathodic reactions within an electrochemical cell. With reference to the Tafel diagram shown in figure 1.7b, the cathodic reaction line is moved left, resulting in a decrease in both the E_{corr} and the i_{corr}. As such these inhibitors are significantly 'safer' than the anodic inhibitors and will not result in accelerated corrosion if insufficient amounts are added. Some of the mechanisms are described below: -

i) Precipitation inhibitors- metal ions are introduced which form insoluble salts with the hydroxide ions at the cathodic sites of oxygen reduction e.g. zinc, magnesium or calcium ions. Cerium, Yttrium and Lanthanum (all trivalent cations) offer enhanced efficiency.

ii) Cathodic Poisons- these are added to hinder the recombination of hydrogen atoms by preventing hydrogen diffusion at the metal surface e.g. arsenic or antimony. However this method effectively keeps hydrogen at the surface some of which can be absorbed into the metal causing hydrogen embrittlement problems.

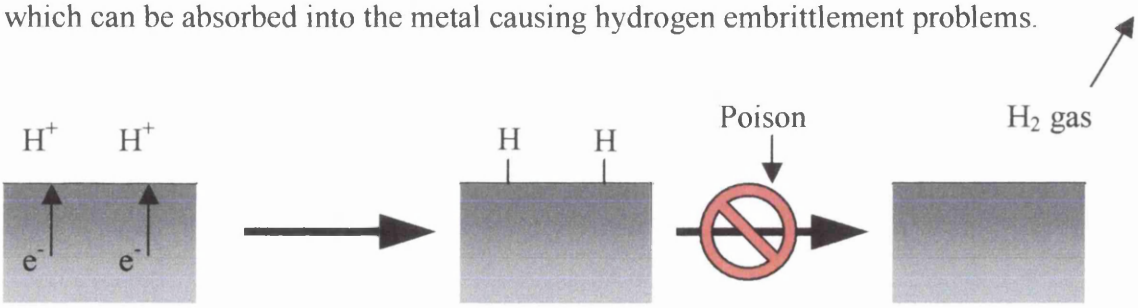

Figure 1.8 showing the cathodic poisoning mechanism.

Advantages of Cathodic inhibitors:

- Safer than anodic inhibitors, due to the reduction of the E_{corr} and i_{corr}, so control of inhibitor distribution is significantly less critical.
- Ionic metal additions are relatively cheap
- Yttrium, lanthanum and cerium, do offer increased efficiency over traditional cathodic inhibitors.

Disadvantages of Cathodic inhibitors:

- Do not tend to be as efficient as their anodic counterparts, and the more efficient species such as yttrium, lanthanum and cerium are more costly.
- Require greater amounts of cathodic inhibitor to hinder corrosion.

1.6 Corrosion Monitoring:

The pipelines used to transport oil are usually in service for many years, should premature failure occur, large oil spillage could occur at great economical and environmental cost. Furthermore it is extremely costly to replace the pipelines should they need to be taken out of service prematurely. As such there is a fine line to tread between maximising the service life of the pipe without compromising its integrity. It is because of this that techniques have been developed to produce lifetime estimates for the materials, as well as to investigate means of extending these lifetimes by use of careful design and corrosion inhibition. The are a wide range of survey methods[25,26,27] used to monitor corrosion behaviour of pipelines in service, the main ones are listed below

1. Potential Surveys:

This involves the measurement of the electrical potential between the buried pipeline and its environment. This is done simply by using a high resistance voltmeter with the negative terminal connected to the pipeline and the positive terminal connected to a copper sulphate reference electrode in contact with the environment. The potential measured gives indications of the extent of corrosion, the location of corrosion hotspots, allowing remedial action to be taken. Further testing can be done using line current surveys, soil resistivity and earth current measurements[25].

2. Bellhole Examinations:

While the potential surveys and line current surveys are relatively simple and convenient, it is sometimes necessary to conduct a physical examination of the pipeline, often where corrosion 'hot spots' have been detected using the above techniques. Simple tests can be performed at bellhole examinations to identify the corrosion activity occurring e.g. when anaerobic corrosion is suspected one would see a layer of black iron sulphide on the metal surface. The first hand data from the bellhole examination can be used as a measure of how the data obtained from potential surveys tallies with actual corrosion activity.

3. Internal Examination:

When inhibitors are used to dose pipelines with inhibitor, so called 'pigs' are used. A region of high concentration inhibitor can be swept down the pipeline

between two such pigs. This also affords a means of internal investigation using 'pig' mounted inspection cameras.

4. Mechanistic studies:

Conventional DC and AC electrochemical techniques can be used to provide a mechanistic understanding of processes leading to corrosion failure in pipeline steels. It is however true that whilst these techniques can provide mechanistic insight they do not provide any spatial resolution. Work has been done in the field of electrochemical noise in the analysis of corrosion activity[29] which does allow for analysis of crevice and pitting corrosion, however the work done thus far does not involve effective control of the atmosphere. This is why this project was established to review in broad terms the potential for scanning techniques to enable spatially resolved corrosion measurements to be made under environmentally controlled conditions.

1.7 Theory of the Scanning Vibrating Electrode Technique

An evolution of the scanning reference electrode technique (SRET)[16], the scanning vibrating electrode technique detects and records potential differences in the electrolyte above corroding metals. As a metal corrodes in an electrolyte, anodic and cathodic sites are formed with an ionic current running between them through the electrolyte. The conductivity of an electrolyte is significantly lower (many orders of magnitude) than that of a metal. As such the distribution of ionic current through the electrolyte facilitates ohmic potential gradients[17] as shown in figure 1.9. These potentials are generated by the ionic current flux passing through the electrolyte. The magnitude of the current flux and therefore the potential recorded is directly

proportional to the intensity of the corrosion events occurring on the adjacent metal surface, at a given scan height. To summarise the SVET records a potential directly proportional to the normal component of current flux in the plane of scan. It does this by means of a vibrating platinum electrode above the area of metal to be monitored.

Due to the finite resistivity of the solution, lines of isopotential can be plotted perpendicular to the current flux as shown in figure 1.9. The Laplace equation can be used to theoretically determine the distribution of potential and ionic currents.

$$\nabla^2 E = 0 \tag{1.1}$$

Where E is the electropotential and Ohm's law:

$$i = -\kappa \nabla E \tag{1.2}$$

Where i is the current and κ is the conductivity of the solution.

The solutions to these equations are impossible to calculate when considering a corroding sample with distributed cathodes and varying gradients. The point source is one of the few cases where a solution for the current voltage problem is possible, hence a point source with a remote cathode must be considered, so that a known current can be passed through the point source, and the current distribution will be linear, as shown in figure 1.9. Curved potential gradients are no longer prevalent due to the fact that the cathode is in effect at an infinite distance from the cell. The relationship between potential difference and current can now be shown to be:

$$F = \frac{dE}{dz} = \frac{iz}{2\pi\kappa\left(x^2 + y^2 + z^2\right)^{1.5}} \tag{1.3}$$

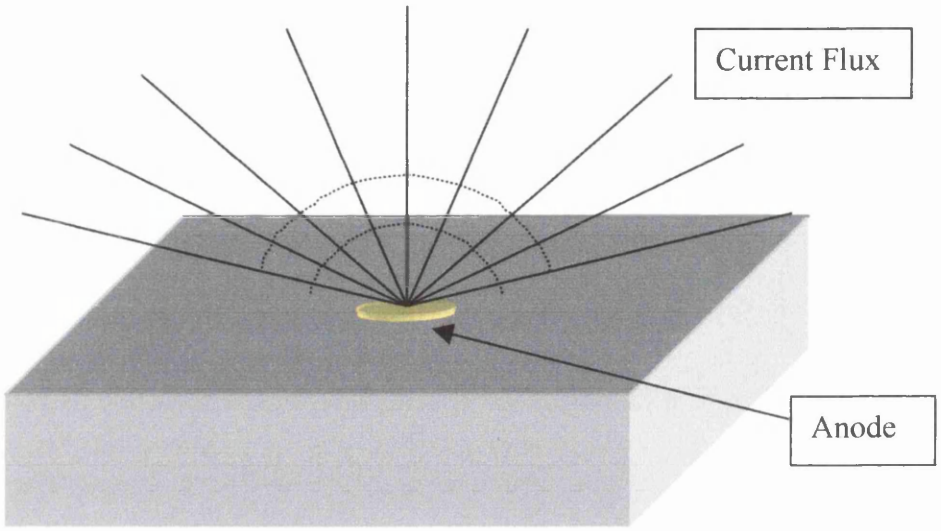

Figure 1.9 A schematic diagram of a point source, with a remote cathode.

Where F is normal electrical field strength, i is the current, κ is the conductivity of the solution and xyz is the position of the SVET tip in relation to the point source. The value of F_{max} is directly proportional to the SVET voltage detected.

The potential measured by the tip will be at its greatest when directly above the point source, when x and y (the coordinates in the plane of scan) are zero. Equation 1.3 can therefore be written as:

$$F_{max} = \frac{i}{2\pi\kappa z^2} \tag{1.4}$$

Taking the constants out of the above equation gives:

$$F_{max} = C\frac{i}{z^2} \tag{1.5}$$

Where C is a constant and i and z are controlled variables.

As can be seen in equation 1.5, the height term 'z' is squared, meaning that the SVET is very sensitive to height so that samples being scanned by the SVET must be planar and level (see section 2.16 as to how this is achieved.)

Calibration experiments that provide a constant that allow recorded SVET potentials to be readily converted into current density can be carried out using a point current source, this is discussed in section 3.

The SVET logs the potential gradient in solution at a given point, however by means of software and a triaxial micromanipulator the vibrating tip (at a frequency of 140Hz and an operational amplitude of 40μm) can be moved around a defined area logging the potential at each point until the entire surface has been scanned. Software outputs the data as a two dimensional grid, which can either be plotted as a contour

map or 3D plot. SVET plots for the corrosion of mild carbon steel in 0.1%NaCl solution are shown in figures 3.3a (3d plot) and 3.3b (contour map). Due to the fact that there is no physical contact with the metal's surface, corrosion can occur under non-perturbed conditions i.e. surface deposits are not disturbed. As such scans can be repeated on the same sample over a period of time to show the corrosion mechanisms over time i.e. scanning every hour for 24 hours would show how long anodes remain active, the intensity of corrosion at given times and provide hourly snap shots of the corrosion process. An excellent application of this is looking at the effectiveness of inhibitors.

SVET Advantages:

- The SVET provides excellent spatial resolution in comparison to other electrochemical corrosion monitoring techniques such as the SRET.
- After calibration the data obtained can be readily converted into current density or total metal loss to provide quantitative measures of the levels of corrosion occurring.
- Scans can be performed in a wide variety of different electrolytes and atmospheric conditions in order to simulate the actual field conditions of a given component.
- As the corroding surface remains undisturbed by the scanning technique, repeated scans can be performed without altering the course of the corrosion. This allows snap shots of the corrosion mechanism to take place which can be built up to make animations. Furthermore scanning conditions can be altered

during the experiment such as the addition of inhibitors after a given time period

Disadvantages:

- The SVET is highly sensitive to height changes; therefore samples must be totally planar and level.
- Corrosion product building up on the sample can impinge on the vibrating probe tip
- Entire experiments must take place under aqueous conditions which is not always the case in the field i.e. some components will only get contaminated by humidity films and may also dry out
- There is a finite size of samples that can be scanned due to limitations of the stepper motors. Maximum scan area is approximately 50mm x 50mm.
- Currently the temperature at which the experiment is run out is not controlled. As such experimentation occurs at room temperature (23°C)

1.7.1 Applications of the SVET

The SVET is holding ever more store in the corrosion science field. Its non-perturbing and quantitative operation makes it an ideal tool in the analysis of pitting corrosion, cut edge corrosion and many other types. It offers a time frame analysis of the corrosion mechanisms in operation during the real time corrosion of a sample in electrolyte. Worsley and McMurray have conducted an extensive review into the applications of the technique[16]. An early use of the SVET by Isaacs et al. was the analysis of pitting behaviour of pure iron in an electrolyte of 1mM NaCl / 1mM

Na_2SO_4[20]. It was found that immediately subsequent to submersion in electrolyte, intense localised pitting corrosion was prevalent, as time progressed up to ~20hours this localised corrosion became significantly more generalised.

More relevant to this study is Komai's research into the corrosion of offshore steels[21]. Steel was submersed in synthetic seawater and scanned using the SVET. This too yielded similar results, in that corrosion was initially localised at the sample edge before becoming more generalised as time progressed. Other research has been done on the effect of bacteria on pitting corrosion[22], galvanic corrosion of solders, and corrosion in coated steels[23-24].

Work in our group has primarily focused on galvanised steel[18], and aluminium to date with no environmental control. Therefore only allowing measurement of corrosion activity in uncontrolled aerated electrolyte, which whilst fine when analysing cut edge corrosion of galvanised steel where the electrolyte would be aerated in the real world, it is not suitable as a representation of an oil pipeline where the conditions would be CO_2 saturated. It is sweet (CO_2) corrosion that is a major cause of premature pipeline failure and in the following chapter it is our aim develop a SVET capable of environmental control.

1.7.2 Conclusions

The fight against corrosion is a costly one, with many billions of pounds spent on prevention and replacement of corroded components. There are many different mechanisms of corrosion attack; dissimilar metals corrosion, crevice corrosion, pitting corrosion and sweet corrosion to name a few (see section 1.4). Extensive research has

gone into better understanding these mechanisms allowing preventative measures to be taken, such as careful component design and materials selection, use of inhibitors, barrier protection etc...

The SVET apparatus has been used extensively in the investigation of corrosion mechanisms, and the technique is constantly evolving. Recent advances include the height scanning SVET which allows non-planar samples to be scanned. As discussed the SVET can be used quantitatively and gives an excellent insight into the mechanism of corrosion occurring on a given sample.

The focus of this project is on the corrosion of oil pipeline materials. The environment in which corrosion occurs is CO_2 saturated so the primary mechanism of attack would be sweet corrosion. Corrosion inhibitors are used in the pipelines in order to prolong the life of the mild steel. Corrosion monitoring techniques are used extensively in the field to avoid any catastrophic failures, however these methods only highlight the areas where corrosion is occurring and do not give an insight into why the corrosion is occurring at that point or the mechanism itself. As of yet the phenomenon of sweet corrosion has not been investigated using the SVET due to problems in controlling the atmosphere in the scan area. Using the SVET, the modes of operation of inhibitors could be studied, and the optimum concentrations calculated. Corrosion 'hotspots' could be identified at welded or complex sections. Furthermore metal loss of the pipelines could be calculated to give a quantitative account of corrosion activity under a range of conditions.

References

1. Hoar T.P. Report of the committee on corrosion protection. HMSO London (1971)

2. Editorial "Corrosion Prevention and Control" 29(1):1 (1982)

3. Asaki H, Kushida T, Kimura M, Fukai H, Okano S. "Role of microstructures on stress corrosion cracking of pipeline steels in carbonate-bicarbonate solution" Journal of science and engineering corrosion 55, 7, 644 (1999)

4. Fontana MG, Green ND "Corrosion Engineering 2nd Edition" McGraw book company (1978)

5. Trethewey KR, Chamberlain J "Corrosion for Science and Engineering 2nd Edition" (1995)

6. H Bonhi, in Corrosion Mechanisms. Mansfield F, Dekker M, N.Y 285 (1985)

7. Tafel J, Dhysic Z. Chem, 50, 641, (1905)

8. Brown F, Kruger J, Staehle RW, "Localised Corrosion" NACE (1974)

9. Al-Hassan S, Mishra B, Olson D, Salama M, "Effect of Microstructure on Corrosion of Steels in Aqueous Solutions Containing Carbon Dioxide" 54, 6, 480 (1998)

10. Callister WD "Materials Science and Engineering an Introduction" fourth edition (1997)

11. Shreir LL, Jarman RA, Burstein GT "Corrosion, Metal/Environment Reactions" Third edition (1994)

12. Shreir LL, Jarman RA, Burstein GT "Corrosion, Corrosion Control" Third edition (1994)

13. Newton LE, Hausler RH "CO_2 Corrosion in Oil and Gas Production" Houston Texas, National Association of Corrosion Engineers (1984)

14. Dugstad A, Lunde L, Videm K "Parametric Study of CO_2 Corrosion in Carbon Steel" Corrosion/94, paper 14 (1994)

15. Srinivasan S, Kane R.D. "Prediction of Corrosivity of CO_2/H_2S Production Environments" Corrosion/96 paper 11 (1996)

16. McMurray HN, Worsley DA "Scanning Electrochemical Techniques for Studying Metal" Blackwell Science Ltd (1997)

17. Isaacs HS, "Journal of the Electrochemistry Society" 138, 723 (1991)

18. Powell S "Scanning Electrochemical Techniques for Monitoring Localised Corrosion in Organically Coated Galvanised Steels" Thesis, UW Swansea (2001)

19. Einar Mattsson "Basic Corrosion for Scientists and Engineers" Second edition, Institute of Materials (1996)

20. Isaacs HS, "Advances in Localised Corrosion" Isaacs H, Bertocci U, Kruger J, Smialowska S (Eds) 221 (1988)

21. Komai K, Minoshima K, Kim G, "JSME International journal series I- Solid Mechanics Strength of Materials" 32, 282, (1989)

22. Franklin MJ, White DC, Isaacs HS "Corrosion Science" 32, 945 (1991)

23. Isaacs HS "Corrosion/86" Houston Texas, paper 194, (1986)

24. Isaacs HS "Corrosion/87" Houston Texas, paper 594, (1987)

25. Peabody AW "Control of Pipeline Corrosion" NACE (1971)

26. Wright JE "Practical Corrosion Control Methods for Gas Utility Piping" NACE Fourth Edition (1974).

27. Parker ME "Pipeline Corrosion and Cathodic Protection" Second Edition, Gulf Publishing Company (1962)

28. Bonnel A, Dabosi F, Deslouis C, Duprat M, Kedam M, Tribollet B "Journal of the Electrochem Society" 130, 753-761, (1983)

29. Cottis RA, Al Ansari, Bagley G, Pettiti I "Electrochemical Noise Measurements for Corrosion" EMCR, Trento. Materials Science Forum (1997)

CHAPTER 2

EXPERIMENTAL:

Instrument Design and Construction

2.1 Apparatus

2.1.1 General Overview of Apparatus:

As outlined in chapter 1 section 1.7 the scanning vibrating electrode technique (SVET) can detect local potential gradients in the solution above a corroding sample. These enable the location of anodic and cathodic events to be recorded. The SVET 'potential' is also a measure of normal ionic current density enabling the technique to be used in a semi quantitative manner.

A schematic illustration of the equipment is shown in figure 2.1. The lockin amplifier outputs an a.c. signal which is then amplified by the signal amplifier and connected to the terminals of the speaker mounted in the SVET head. The speaker then vibrates at a frequency of 140Hz at an amplitude of ~10μm measured using a strobe light source. A platinum electrode is attached to the end of a capillary tube that is in turn glued to the cone of the speaker, and is positioned at a small distance above the sample surface (100μm). A silver reference electrode is connected to the outer core of the smc coaxial cable that is connected to the lockin amplifier. As the electrode vibrates, it is able to detect any potential gradients in the electrolyte above the sample; these are recorded by the lockin amplifier and sent to the PC where the data is stored in conjunction with the coordinates of the data point. The PC then sends an instruction to the motors via the motor interface coupling to move a given displacement where the SVET potential is once again recorded. The process is continued until typically a 40x40mm matrix of the SVET potentials has been formed. Anodic sites can then be identified as areas of positive potential and cathodic regions

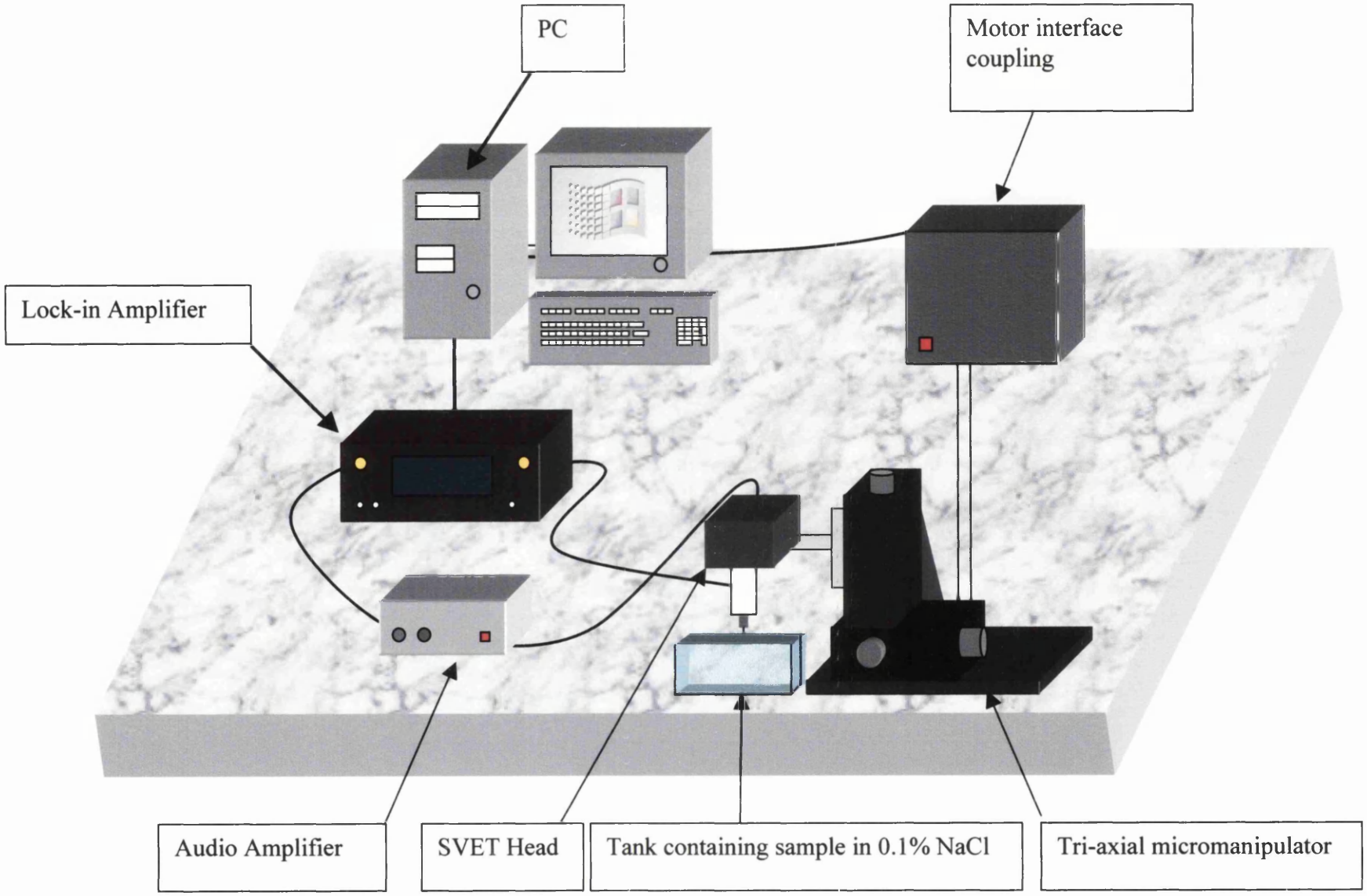

Figure 2.1. A Schematic diagram of the SVET apparatus.

are identified as having negative potential differences. The rate of corrosion is directly proportional to the magnitude of the anodic and cathodic currents recorded. Scans are then repeated over a 24-hour period giving a measure of how the sample corrodes over time.

The SVET potentials can be converted into current densities simply by multiplying the data by the calibration factor for the SVET. Thus electrochemical activity over a given time period can be quantitatively mapped using this technique. Details of how the calibration factor is obtained using the test cell apparatus are given in section 3.3. As the SVET signal is inversely proportional to the square of the scan height the apparatus had to be mounted on a concrete slab in order to minimise any vibration effects and ensure that the scanner and the tip were mounted on the same immovable plane.

2.1.2 The SVET head and tip:

The SVET head used in this work is shown schematically in figure 2.2a and the actual head is illustrated in figure 2.2b.

The SVET tip comprises of a 125μm platinum wire encased in a narrow glass sheath. The method used is to thread a 125μm platinum wire through a capillary tube, which is then heated and drawn to a fine point. The end is then snipped, and filed to produce a tip with an overall diameter of ~200μm, which is sufficiently small to allow maximum resolution, and yet rigid enough to withstand impacts with the surface.

The SVET head is carefully designed to ensure that the electrode vibrates normal to the sample surface and to minimise any electromagnetic or electrostatic

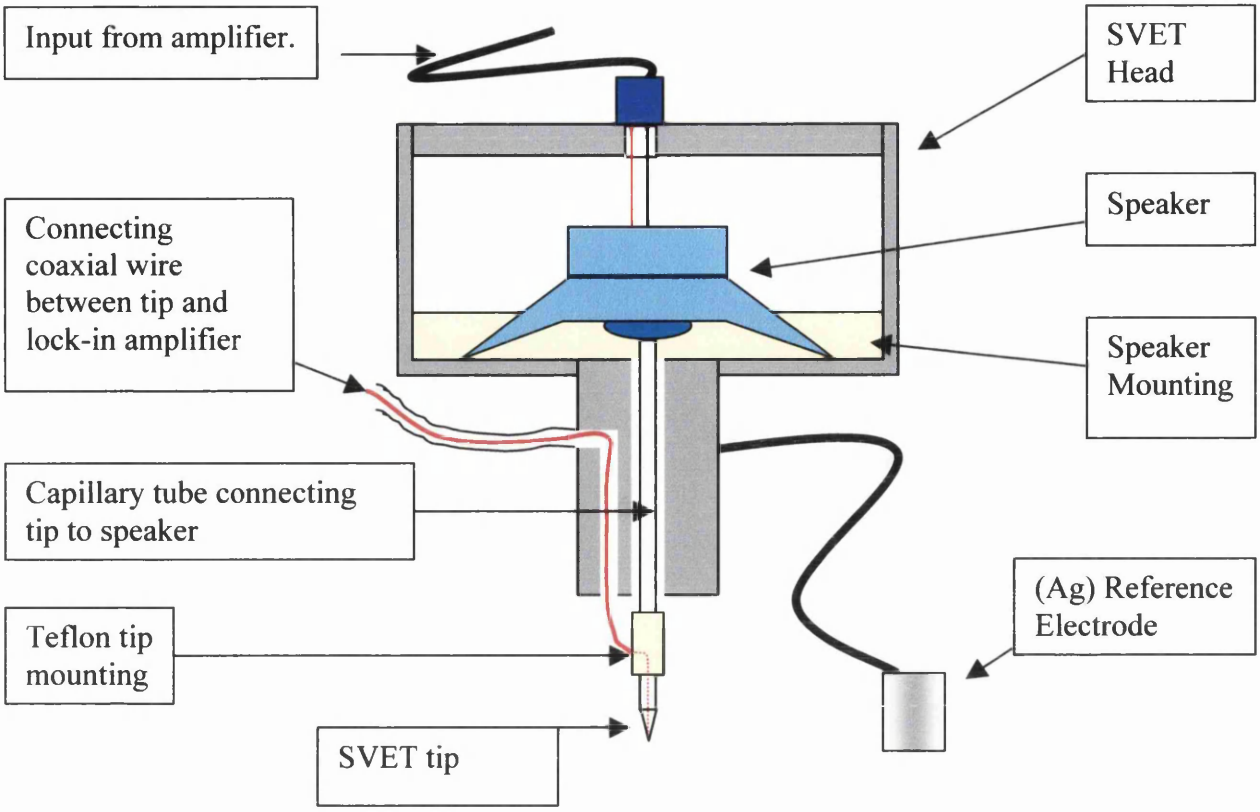

Figure 2.2a. A schematic diagram of the SVET Head

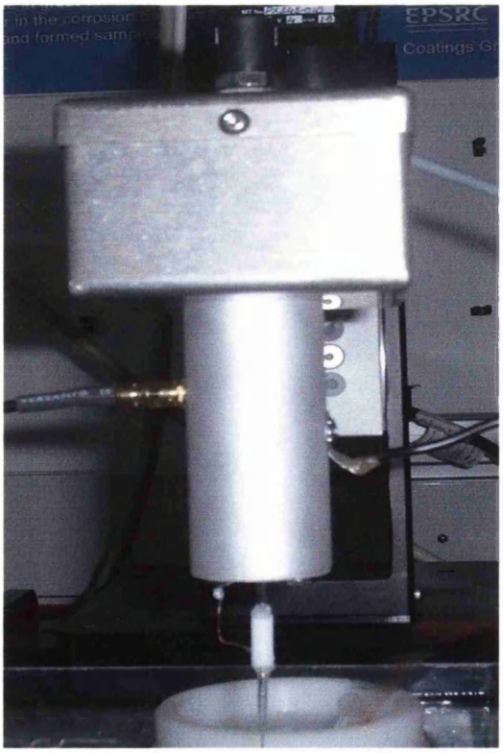

Figure 2.2b A close up of the SVET Head

interference with the SVET signal. A glass capillary tube is attached to the centre of the speaker cone using epoxy resin, the tube is then passed through a hole machined through the nose of the SVET with minimal clearance, in order to eliminate any lateral movement of the probe. Confirmation of normal tip vibration is achieved in two ways, observation of its movement under stroboscopic light at a multiple of the frequency of vibration; and scanning over a point source to confirm radially symmetric current flux about the point source (see section 3.1). The tip is then connected to the tube using a teflon sheath that fits over both the glass surround of the tip, and the capillary tube. The wire connecting the tip to the lockin amplifier is fed through another machined hole in the head, so that any interference can be minimised. A $2cm^2$ silver reference electrode is attached to the main body of the head, which is in turn connected to the earth of the lockin using the outer core of the smc cable. The drive speaker itself is securely mounted in the μ metal box in order to eliminate any electromagnetic signals that may interfere with the signals detected by the tip. The speaker is driven by an amplified signal from the lockin, and is driven at a frequency of 140Hz and amplitude of 10μm which can be checked using the stroboscope.

2.1.3 The Lockin and Signal Amplifier:

The lockin amplifier (model EG&G 7265) and signal amplifiers (built at UW Swansea) used in this work are shown in figures 2.3a and 2.3b.

The signal amplifier is a simple mono amplifier that had to be constructed in order to amplify the signal generated by the lockin by a factor of ten. Thus the 0.1V AC current generated by the lockin is amplified, and drives the speaker at a voltage of

Figure 2.3a A digital photo of the lock-in amplifier

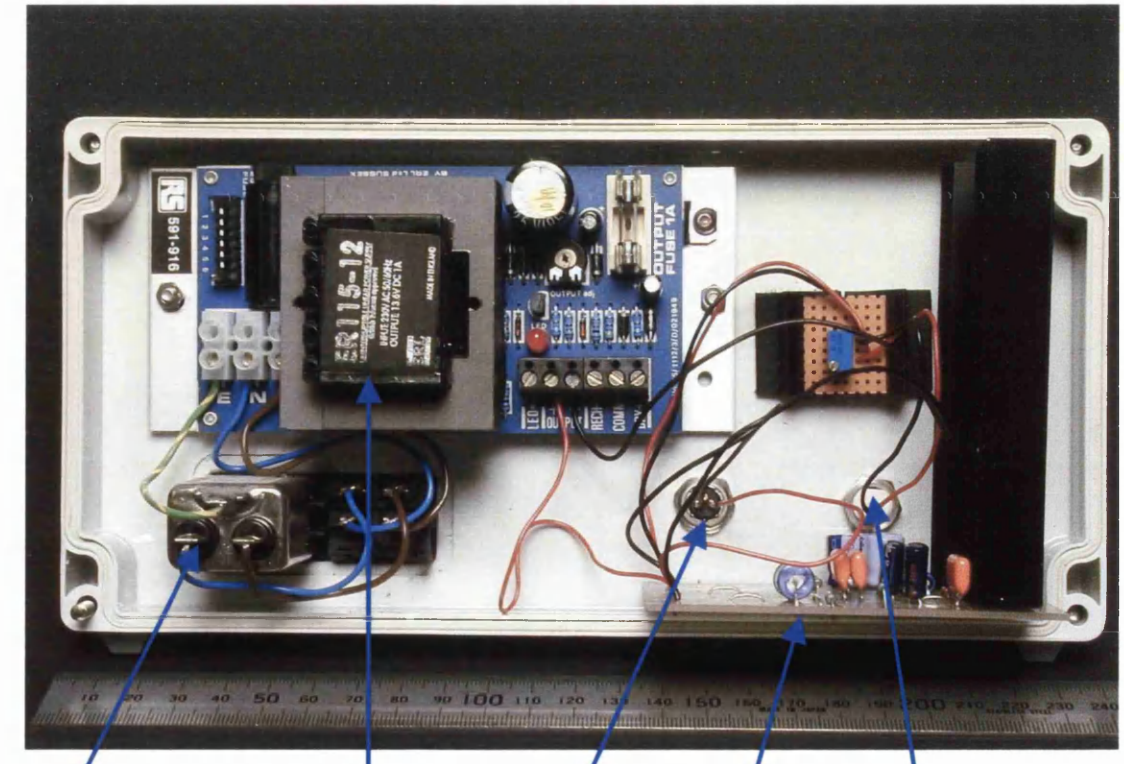

Figure 2.3b A digital photo of the signal amplifier that was constructed

1V, which gives the desired 10μm vibrational amplitude. A picture of the amplifier during construction is shown in figure 2.3b.

The lockin amplifier has two roles; the first is to generate the 140Hz AC signal that will, after amplification, drive the speaker mounted in the SVET head. The second is to record the potential gradients measured by the vibrating electrode which have a frequency of 140Hz, and communicate them to the scanning software on the pc through the GPIB connection.

2.1.4 The Personal Computer:

The PC used in this setup is a Pentium 733MHz with 128Mb of RAM, it has a GPIB card installed to communicate with the lockin amplifier, and uses the parallel port to connect to the motor interface coupling. A visual basic program has been written to log the data communicated by the lockin into a two dimensional matrix. Thus each SVET potential detected is stored along with its x and y coordinates producing a grid file of results. This grid file can then be loaded into a cartography package called 'Surfer' produced by Golden Software. Using the software the data from a scan over a surface can be plotted as a false colour contour map, or as three-dimensional contour map (see figures 3.3a and 3.3b). After converting the data into current density, the total volume of current density can be obtained using the software to give a measure of how much corrosion is occurring. By repeatedly scanning the sample every hour whilst immersed in electrolyte, the rates and systems by which corrosion occurs on a sample surface over time can be determined.

2.1.5 The Triaxial Micromanipulator and Motor Interface Coupling:

Since the SVET is used to map the corrosion activity occurring over the exposed sample area, it is critical that the software can precisely determine the location of the SVET tip. This is done by moving the tip to the top left corner of the square or rectangular area to be scanned, then setting the size of the area to be scanned. The software calculates the position of the tip by knowing the start point and the number of steps taken in the X and Y directions. The stepper motors have 400 steps per revolution and each complete revolution is equivalent to 500μm of linear travel in the X, Y and Z directions. Thus the minimum step size is 1.25μm; since the resolution of the apparatus is of the order of 100-200μm this is entirely adequate. The SVET makes a measurement whilst stationary, the software then moves the probe to a new location where it stops and records an averaged (usually three point) value of the SVET signal. This was done not only to enable precise height control but precise positioning and to avoid any convection effects caused by a fast moving probe

2.1.6 The Levelling table:

As outlined in section 1.7 the SVET technique is extremely sensitive to height and as such can only be used in its basic form to scan over planar samples. These samples must then be levelled to within less than ten microns, in the plane of scan. To achieve this a levelling table was designed (see figures 2.4a and 2.4b). The design

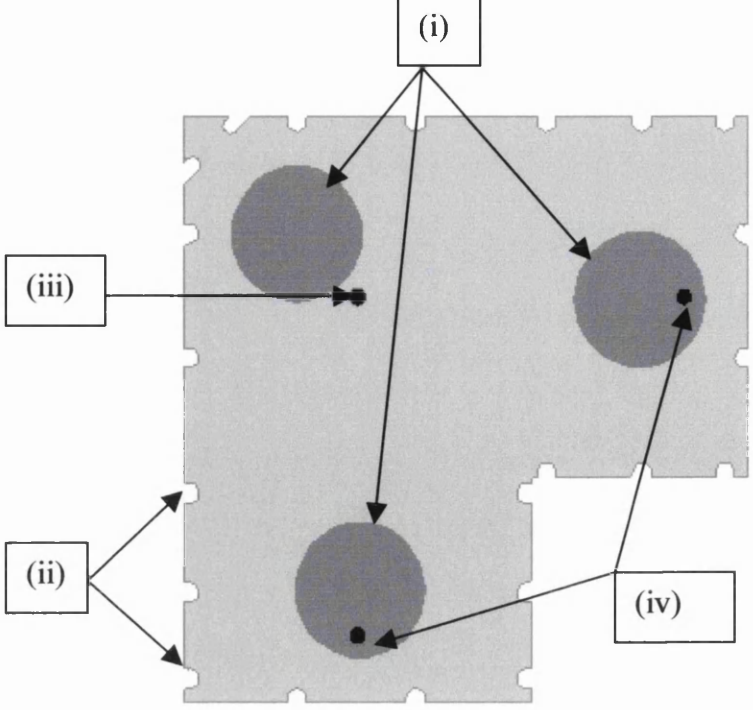

Figure 2.4a Part of the technical drawing of the levelling table showing (i) the legs of the levelling table. (ii) the notches for the elastic bands which holds the two plates together, (iii) the locating holes for the pivot in the top plate to locate in. (iv) the locating holes for the adjusting screws in the top plate of the levelling table.

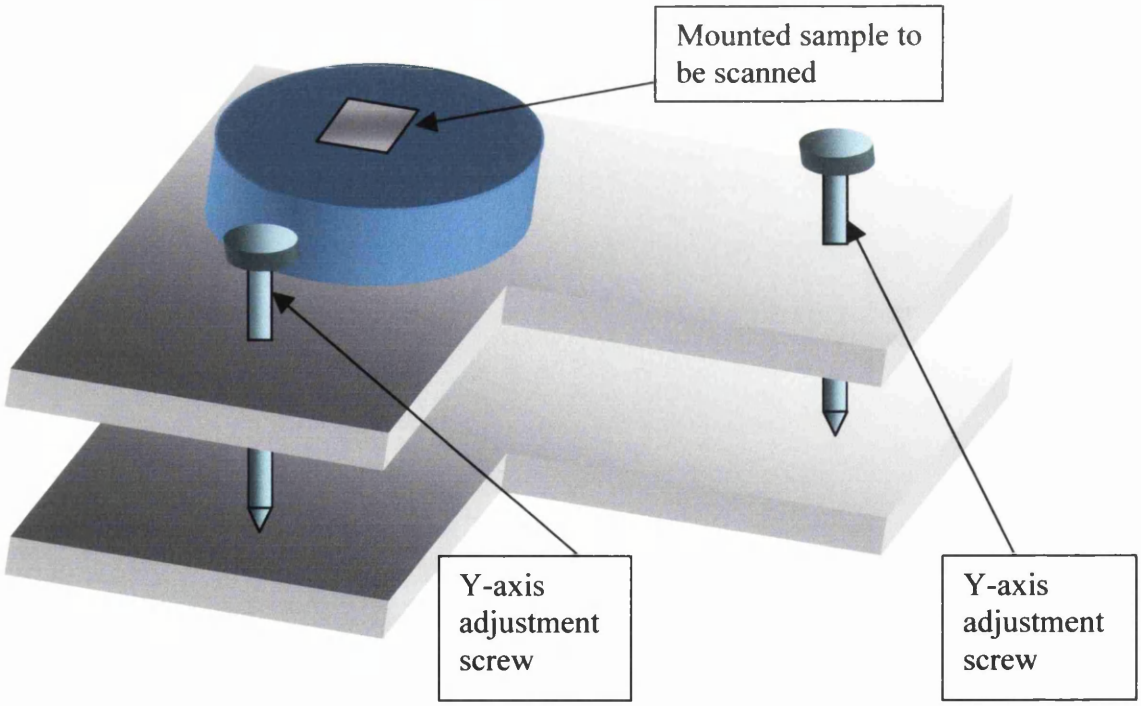

Figure 2.4b A 3d diagram of the complete levelling table showing the x and y adjustment screws, and the positioning of the sample

of the table was two perspex plates, with three pivots between them, one fixed and two adjustable. Figure 2.4a shows the lower plate of the levelling table, it is constructed of 5mm Perspex, with three feet on the lower side (i). On the upper side of the plate there are three locating holes for the pivot (iii) and adjusting screws (iv) to locate in.

The sample is placed above the central pivot as shown above point (iii) on figure 2.4a. The probe tip is then moved down until it touches the sample surface above the pivot. It is then raised up 100μm and the tip is then moved 4mm in the Y direction, before being lowered back down 100μm. The adjustable screws located at symmetrical positions (iv) are used to raise or lower the table so that the tip just comes into contact with the sample surface, the specimen is now level in the Y direction. This process is repeated for the X direction and as the two planes of levelling lie perpendicular to one another, the Y plane remains level. The specimen is now level to within 10μm, and is checked at the four extreme corners of the area to be scanned before scanning can commence. In order to prevent the sample moving during the scan, an adapter plate was manufactured for each of the different sized specimens to be used. The adapter plates fitted snugly around the samples, and screwed into them to ensure that there was no movement during the scan period.

2.1.7 Atmosphere Control:

In the corrosion of carbon steel pipeline materials control of the atmosphere is critical. To this end the SVET sample, tank and head were enclosed in a purpose built environment chamber as illustrated in figures 2.6 and 2.7. The chamber was

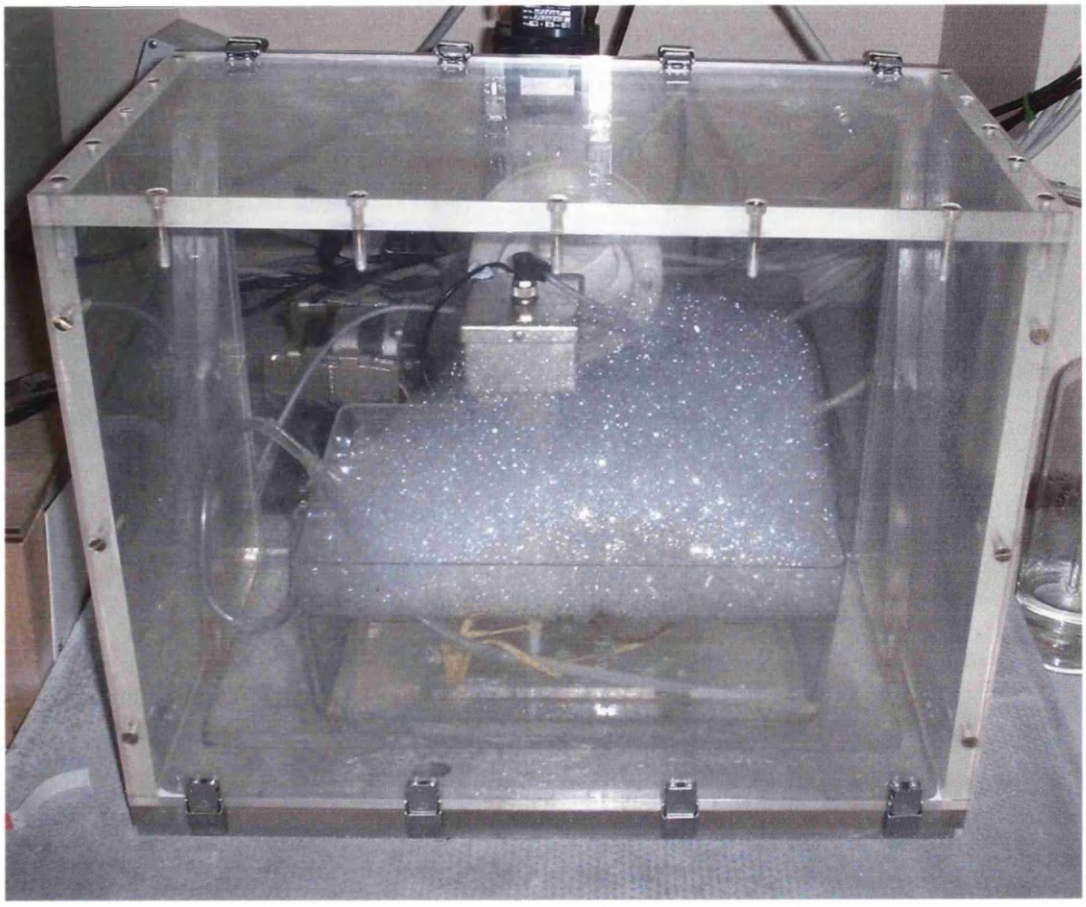

Figure 2.5a. The environment chamber in use during an experiment using high concentrations of filming inhibitor. Surprisingly the foaming of the inhibitor did not affect the performance of the SVET, although excessive foaming should be avoided as it will strip out the inhibitor in solution, therefore reducing the concentration.

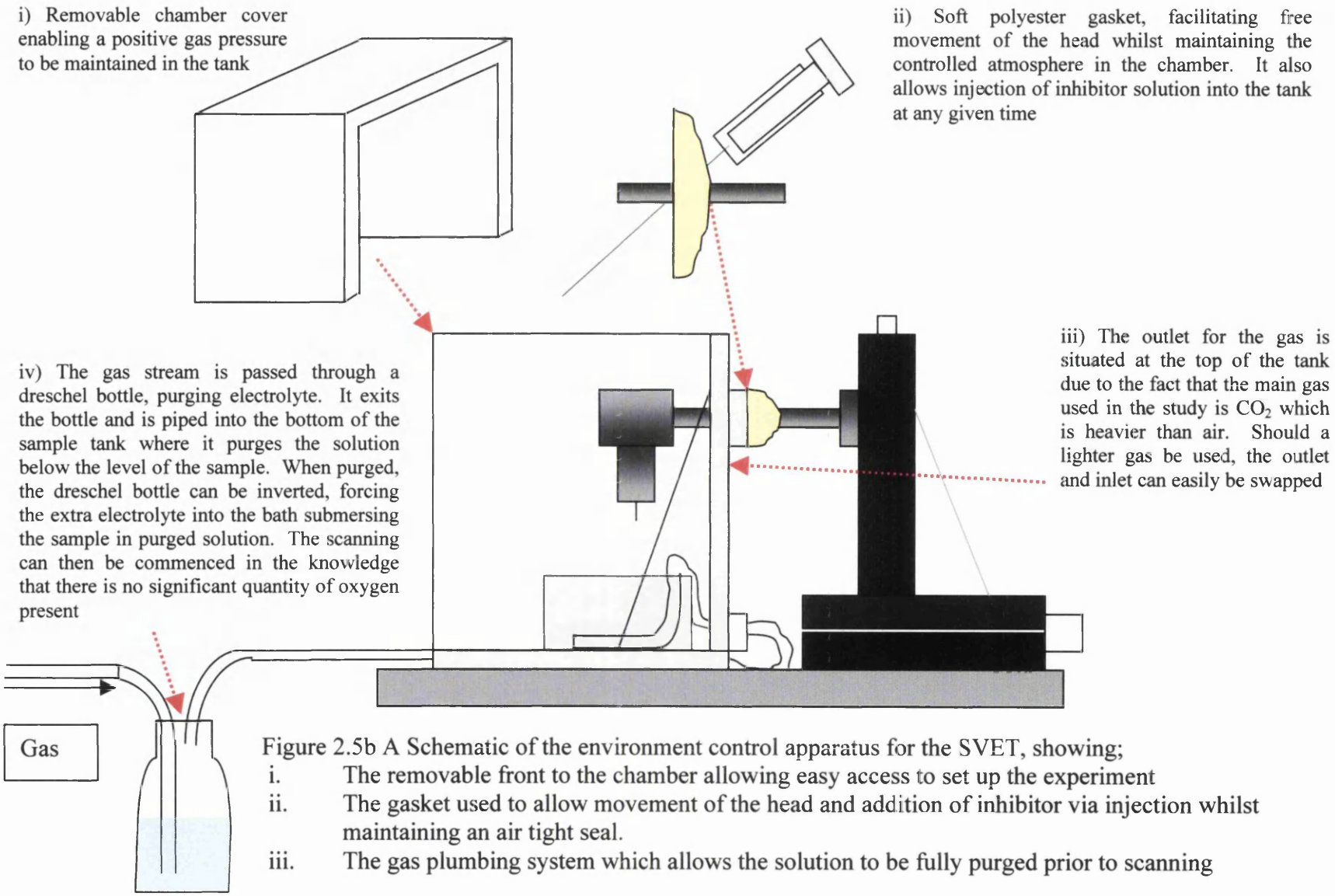

Figure 2.5b A Schematic of the environment control apparatus for the SVET, showing;

i. The removable front to the chamber allowing easy access to set up the experiment
ii. The gasket used to allow movement of the head and addition of inhibitor via injection whilst maintaining an air tight seal.
iii. The gas plumbing system which allows the solution to be fully purged prior to scanning

constructed of 10mm Perspex, it was designed with a removable front to facilitate easy access for setting up the experiment. The chamber when closed is air tight, with a gas inlet at the bottom of the chamber, and an outlet at the top of the chamber. A pipe was attached to the gas inlet, and fed into the tank so the gas bubbled through the electrolyte solution. A dreschel bottle was attached to the gas inlet line, and filled with electrolyte solution, this allowed the sample to be left unsubmerged in the chamber, whilst the electrolyte was purged with gas, then after a suitable time period, the dreschel was inverted. The gas pressure then forced the electrolyte in the dreschel into the tank, raising the electrolyte level above the sample surface to initiate corrosion, but still maintaining the oxygen free environment. The hole where the SVET head entered the tank was sealed using a flexible rubber gasket, allowing free unrestrained movement of the head around the sample area.

2.2 Sample preparation and procedure:

The samples used in these experiments, were mild carbon steel samples of pipeline steel. They were supplied mounted in chemically inert non-electrically conductive resin. Before being scanned, the samples were first metallographically prepared, by sanding the faces down on progressively finer paper (down to 1200 grade). The scratch free surface was then polished using 6μm polishing wheel followed by a 1μm polishing wheel, until a mirror finish was produced. The surface was then degreased using ethanol, and masked off using extruded Teflon self adhesive tape manufactured by 3M, leaving a $1cm^2$ area exposed. The sample was then

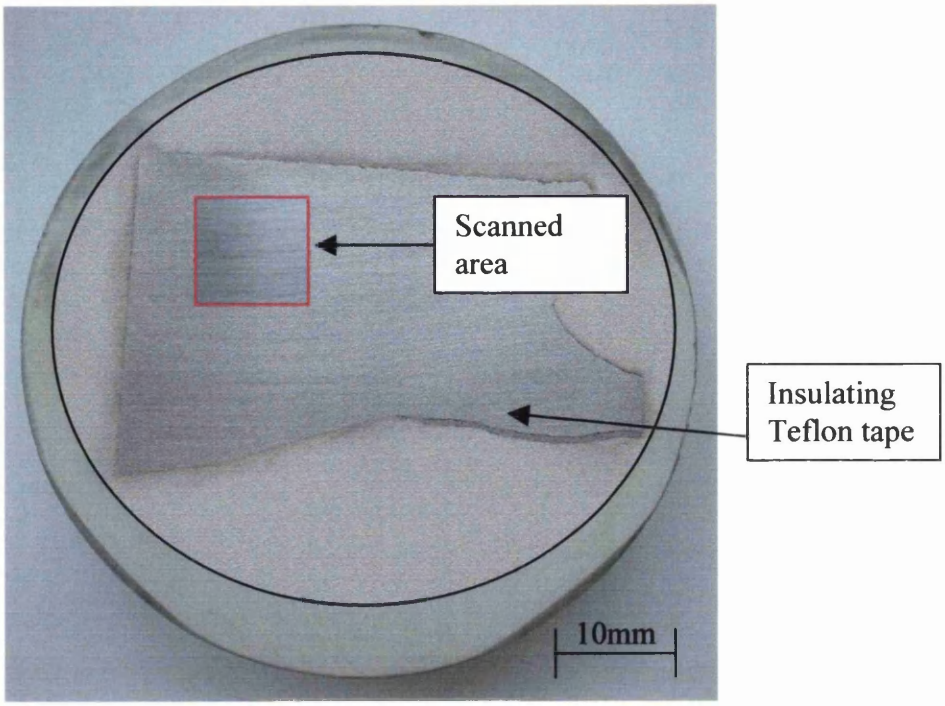

Figure 2.6a Shows the large mild steel sample, used in the inhibitor experiments. The red box shows the area that was scanned, the remaining exposed surface was sealed from the electrolyte using Teflon adhesive tape.

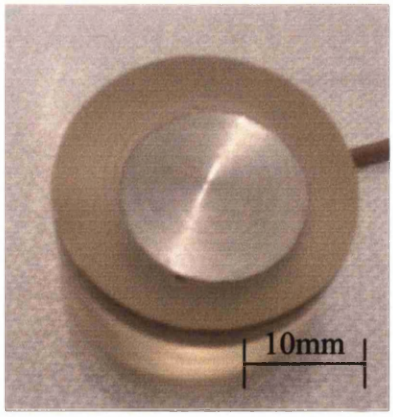

Figure 2.6b Shows the sample of similar composition steel, used in the crevice corrosion experiments.

mounted on the levelling table, and levelled using the procedure discussed in section 2.16.

2.2.1 The Electrolyte and Inhibitor Dilution:

The electrolyte used throughout this study was 0.1% NaCl (1000ppm). This involved adding 10 grams of sodium chloride to 10 litres of deionised water, thus creating 10 litres of 0.1% NaCl electrolyte.

Inhibitor dilution was more complicated, as the amounts used were very small. When adding 1ppm of inhibitor, the procedure was to first dilute to 200ppm (add 1 gram of inhibitor to 5 litres of water), then dilute the 200ppm solution into the electrolyte i.e. add 5ml of 200ppm solution to 1 litre of electrolyte.

2.2.2 Experimental Materials:

The specimens investigated during this project were supplied by Total Fina Elf. They were all composed of mild steel X65QT (see section 1.2 for a description of the material) from around welded sections of oil pipelines or steel rods representative of the composition of pipeline materials. Since each was mounted in a resin block, they could be repolished following exposure and analysed again using the SVET.

Sample A. Was a section of mild steel; away from the weld from an oil pipeline, the sample measured 25mm by 50mm. A picture of the sample is shown in figure 2.6a

Sample B. This sample is of similar composition to sample A but is circular with a diameter of 10mm. This sample was used in the analysis of crevice corrosion, as the entire sample surface could be easily scanned, including the interface between the resin and the metal where the crevice is located. (Figure 2.6b). Indeed it was this interface that was used to study crevice corrosion in section 4.

Sample C. This is a sample from the area surrounding the welded joint in an oil pipeline, it consists of the two base metals, and the weld zone as illustrated in figure 2.7a. A diagram showing the different compositions of the sample and a photograph of the sample are shown in figures 2.7a and 2.7b. It should be noted that this part failed in service for no apparent reason, although bimetallic corrosion was suspected.

Several samples of the weld were extracted and separately sectioned and polished to enable EDX analysis of the substrate.

Sample C2 (Fig 2.7c): Is a section of sample C shown in figure 2.7a, and is part of the base metal 1.

Sample C3 (Fig 2.7d): is a section taken from the heat-affected zone of sample C.

Sample C4 (Fig 2.7e): is a section of the weld material in sample C

Sample C5 (Fig 2.7f): is a section of base metal 2

Figure 2.7d Weld metal sample

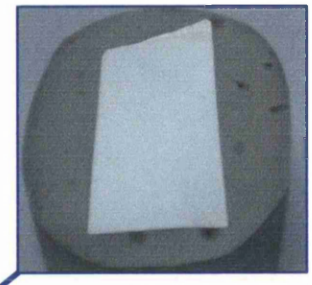

Figure 2.7e Base Metal 2

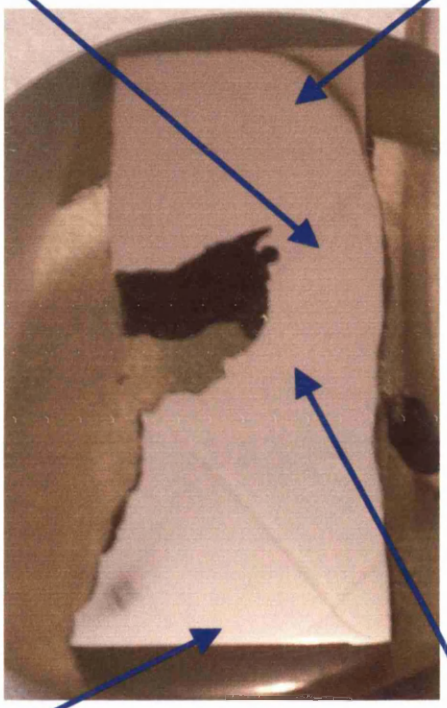

Figure 2.7a Sample of welded pipeline material.

Figure 2.7b Base Metal 1

10mm

Figure 2.7c HAZ material

Figures 2.7a-e Show the samples used in the weld corrosion experiments. Samples c-f were sections from shown locations of sample 2.9b.

2.2.3 Experimental Procedure:

For the experiments carried out in aerated conditions, the sample was prepared and levelled and placed in the tank. Electrolyte was then poured into the tank until the level was just below that of the surface to be scanned. The height of the tip above the surface was then confirmed before pouring in the remainder of the electrolyte, covering the exposed surface of the specimen. The program was then started, and the $10mm^2$ area scanned in a 40x40 matrix at a fixed height. The scans took around 10 minutes to complete and were performed at half hourly intervals for up to 24 hours.

When scanning samples in a CO_2 saturated environment, the electrolyte was first purged with CO_2 for 1 hour before carefully being poured into the tank until leaving the sample non submersed. The environment chamber was then moved into place and securely fastened. CO_2 was then passed through a dreschel containing 500ml of electrolyte and any inhibitor being used in the experiment into the chamber, and bubbled through the electrolyte in the tank. After 15 minutes, the dreschel was inverted and the pressure of the gas used to force the remaining electrolyte into the tank. Once the sample was submersed, the program was started and scanning began. By using this method, oxygen contamination was entirely avoided.

In some cases inhibitor was added after a period of scanning in CO_2 saturated solution. In these instances a syringe of CO_2 saturated NaCl containing the desired dose of inhibitor was injected 5 minutes before the next scan in the cycle and typically 2 hours after commencing immersion. This allowed an assessment of the inhibitors

effectiveness at inhibiting existing corrosion events, and the time period under which they worked.

CHAPTER 3

Calibration of the SVET apparatus.

3. Calibration:

As stated in section 1.7 the SVET records a potential which is proportional to the normal component of current flux in the plane of scan. As such the SVET can be used to spatially resolve and quantify local corrosion events. In this section we explore the use of a point current source cell to calibrate the apparatus and examine the maximum spatial resolution achievable.

3.1 Calibration Apparatus:

In order to calibrate the sample, the current density that the test cell outputs must be known precisely, thus the equipment shown in figure 3.1 is used.

- The test cell is a 25μm platinum disc micro-anode connected to the positive or negative output from the nano-galvanostat, encased in a glass sheath within a perspex block. The cell is then submersed in electrolyte (in this case 0.1% NaCl) allowing ionic flow between the exposed anode and the remote cathode.
- The remote cathode or anode used is a $2cm^2$ platinum gauze cathode is located at a relatively large distance from the anode so that current flow from the anode is omnidirectional as shown in figure 3.2
- The nano-galvanostat connects to the anode and cathode supplying a known current to the circuit in the range 10nA to 1μA.

The test cell is placed on the sample table shown in figure 2.4 and levelled; the 0.1% NaCl solution is then added to the tank, until the anode is entirely covered. The cell

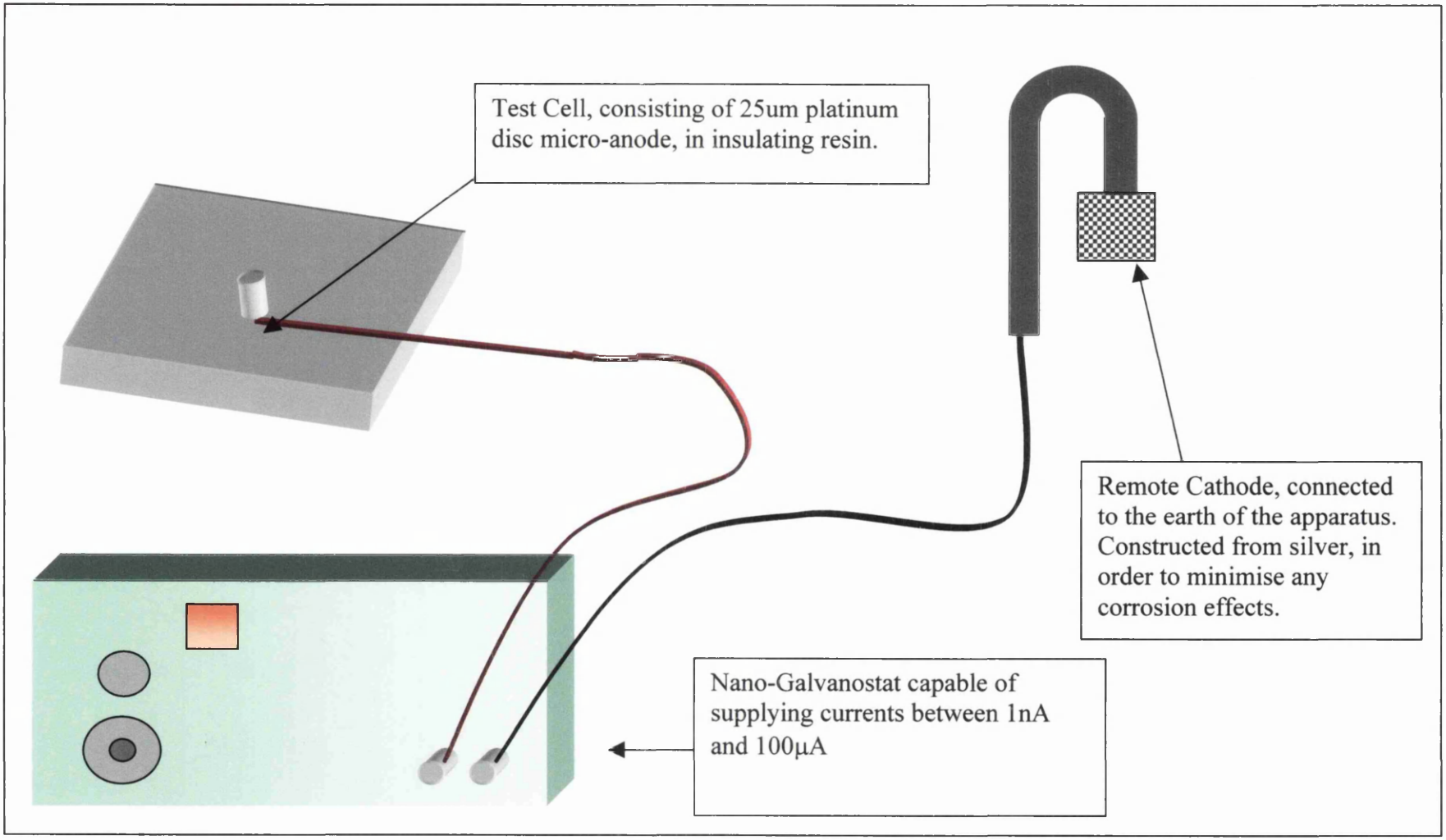

Figure 3.1 A schematic of the test cell apparatus showing the test cell, remote cathode and nanogalvanostat.

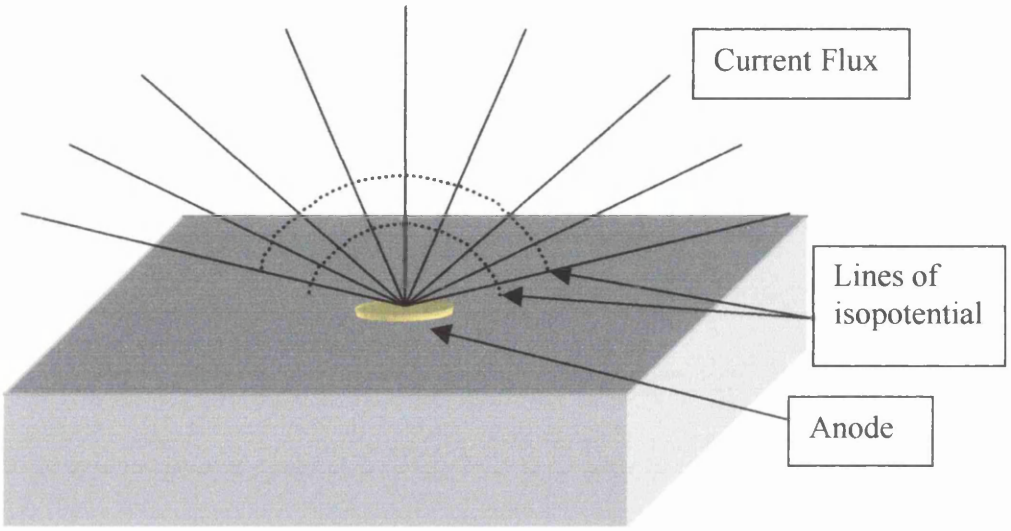

Figure 3.2 A schematic diagram of a point source, with a remote cathode. This shows the linear omnidirectional flow of the current flux, and lines of isopotential have been plotted through the current flux lines. In reality the flow is three dimensional, therefore the lines of current flux are inverted cones and the isopotentials are actually hemispherical

was then scanned at probe heights of 70μm, 100μm and 130μm at various currents between 10nA and 1μA. The resulting SVET data was used to calibrate the instrument and provide details of spatial resolution.

3.2 SVET isocurrent contour maps.

Current flow emanating from the model point source will travel in unidirectionally away from it as illustrated in figure 3.2, therefore when scanning over it a radially symmetric current density should be observed around the point source and the measured current density should be at its highest directly above the point source, and should gradually decrease as the tip move further away along the radius, equally in all directions.

A typical SVET map is shown in two reliefs in figures 3.3a and 3.3b. The SVET response to the point source shows symmetric bell shaped proportions. These maps confirm that the SVET is functioning correctly, the yellow colour represents the strongest currents, and the blue colour represents zero current. The plots are almost exactly symmetric suggesting that there is very little horizontal component to the vibrational modes of the tip. This means that we can continue to calibrate with confidence that the apparatus is functioning correctly. This calibration check can be used routinely to check the SVET response (ensuring consistent data from experiments). The absence of any other features in the scan confirms that vibration is occurring normal to the plane of scan, and the absolute magnitude of the maximum

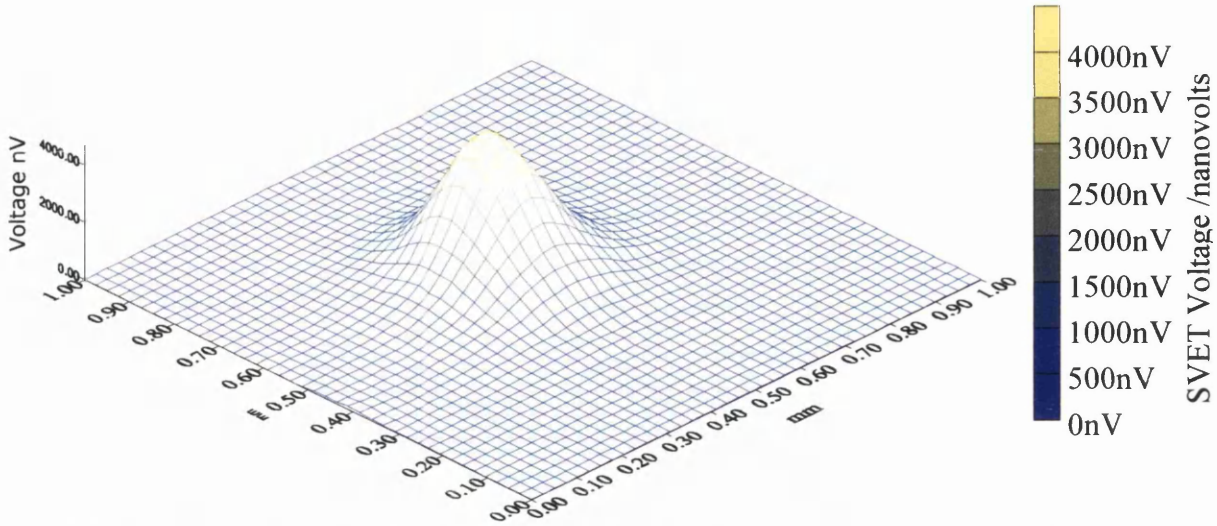

Figure 3.3a A three dimensional view of the data after scanning over the test cell in 0.1% NaCl and using a current of 0.1μA.and and a vibrational amplitude of 10μm and a scan height of 100 μm

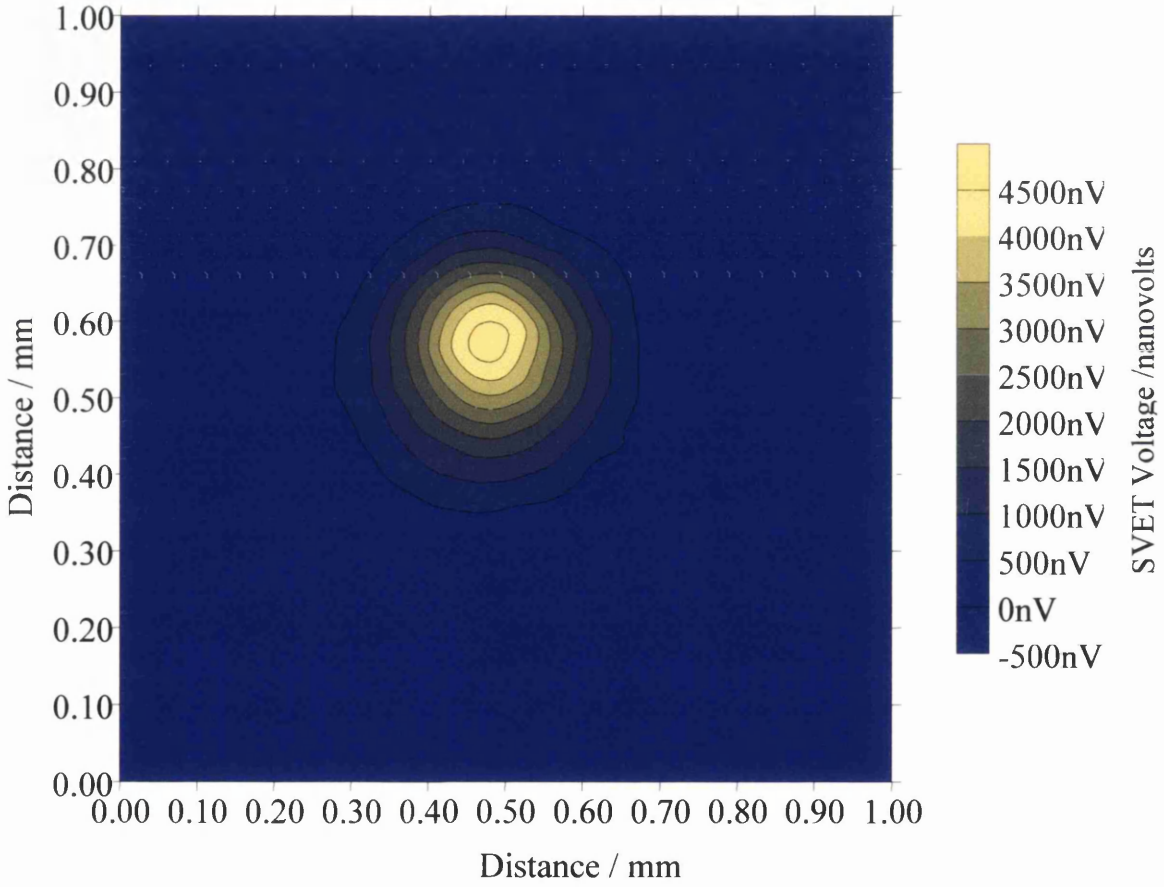

Figure 3.3b A two dimensional isocurrent contour map of the test cell scan , this is the same data as that shown in figure 3.3a but represented as a 2D contour map.

signal obtained for a set current (typically 0.5μA) can be used to calibrate and ensure consistent vibrational amplitude.

3.3 Calibration Constant:

The raw data picked up by the SVET is a potential difference measured in volts, this does not provide us with a quantitative set of data as the units do not take into account experimental variables such as amplitude of vibration or the scan height. As such a calibration factor is required to convert the potential difference into current density (Am^{-2}). These are far more useful units that are directly comparable with other SVET studies and conventional electrochemical measurement in the field and give a quantitative measure of corrosion and are height independent.

In order to obtain the calibration factor, the test cell apparatus described in above (see section 3.1) must be used. The point current source is submersed in electrolyte and the SVET tip located directly above its centre (the peak of the contour map shown in fig 3.3a) where the measured voltage is greatest. The tip is then positioned at known heights above the point current source (70μm, 100μm and 130μm) and the current varied between –1mA and 1mA in the steps shown in table 3.1, for each of the given heights. At each current, the voltage detected is recorded and the plots for each height can be seen on figure 3.4. The height effect is clearly noticeable, with the measured voltage for a given current increasing as the tip is moved closer to the surface. Next a simple calculation is used to convert the current into current density. Since the current is distributed radially the current density

Table 3.1. A table showing the current density values obtained during calibration

Current Density Values

Date:	04/04/01	Machine:	JIM	Solution:	0.1%NaCl	Cell Type:	PS

Experimental Notes:

Height (μm):	70	*Height (μm):*	100	*Height (μm):*	130
Am^{-2}	**μV**	**Am^{-2}**	**μV**	**Am^{-2}**	**μV**
-32.48062807	-5082	-15.91550775	-2968	-9.417460209	-1811
-25.98450245	-4059	-12.7324062	-2357	-7.533968167	-1450
-19.48837684	-3050	-9.549304651	-1748	-5.650476125	-1086
-12.99225123	-2036	-6.366203101	-1152	-3.766984083	-724
-6.496125613	-1001	-3.18310155	-592	-1.883492042	-363
-3.248062807	-508	-1.591550775	-293	-0.941746021	-181
-2.923256526	-459	-1.432395698	-261	-0.847571419	-162
-2.598450245	-407	-1.27324062	-233	-0.753396817	-146
-2.273643965	-352	-1.114085543	-201	-0.659222215	-127
-1.948837684	-303	-0.954930465	-169	-0.565047613	-109
-1.624031403	-254	-0.795775388	-146	-0.47087301	-92
-1.299225123	-200	-0.63662031	-110	-0.376698408	-77
-0.974418842	-153	-0.477465233	-87	-0.282523806	-53
-0.649612561	-102	-0.318310155	-57	-0.188349204	-37
-0.324806281	-51	-0.159155078	-29	-0.094174602	-18
0	0	0	0	0	0
0.324806281	49	0.159155078	28	0.094174602	17
0.649612561	108	0.318310155	55	0.188349204	35
0.974418842	150	0.477465233	84	0.282523806	54
1.299225123	199	0.63662031	111	0.376698408	76
1.624031403	252	0.795775388	144	0.47087301	88
1.948837684	304	0.954930465	168	0.565047613	105
2.273643965	350	1.114085543	196	0.659222215	123
2.598450245	410	1.27324062	230	0.753396817	140
2.923256526	455	1.432395698	243	0.847571419	155
3.248062807	515	1.591550775	291	0.941746021	177
6.496125613	1011	3.18310155	579	1.883492042	360
12.99225123	2033	6.366203101	1158	3.766984083	719
19.48837684	3050	9.549304651	1744	5.650476125	1077
25.98450245	4058	12.7324062	2320	7.533968167	1441
32.48062807	5080	15.91550775	2901	9.417460209	1801

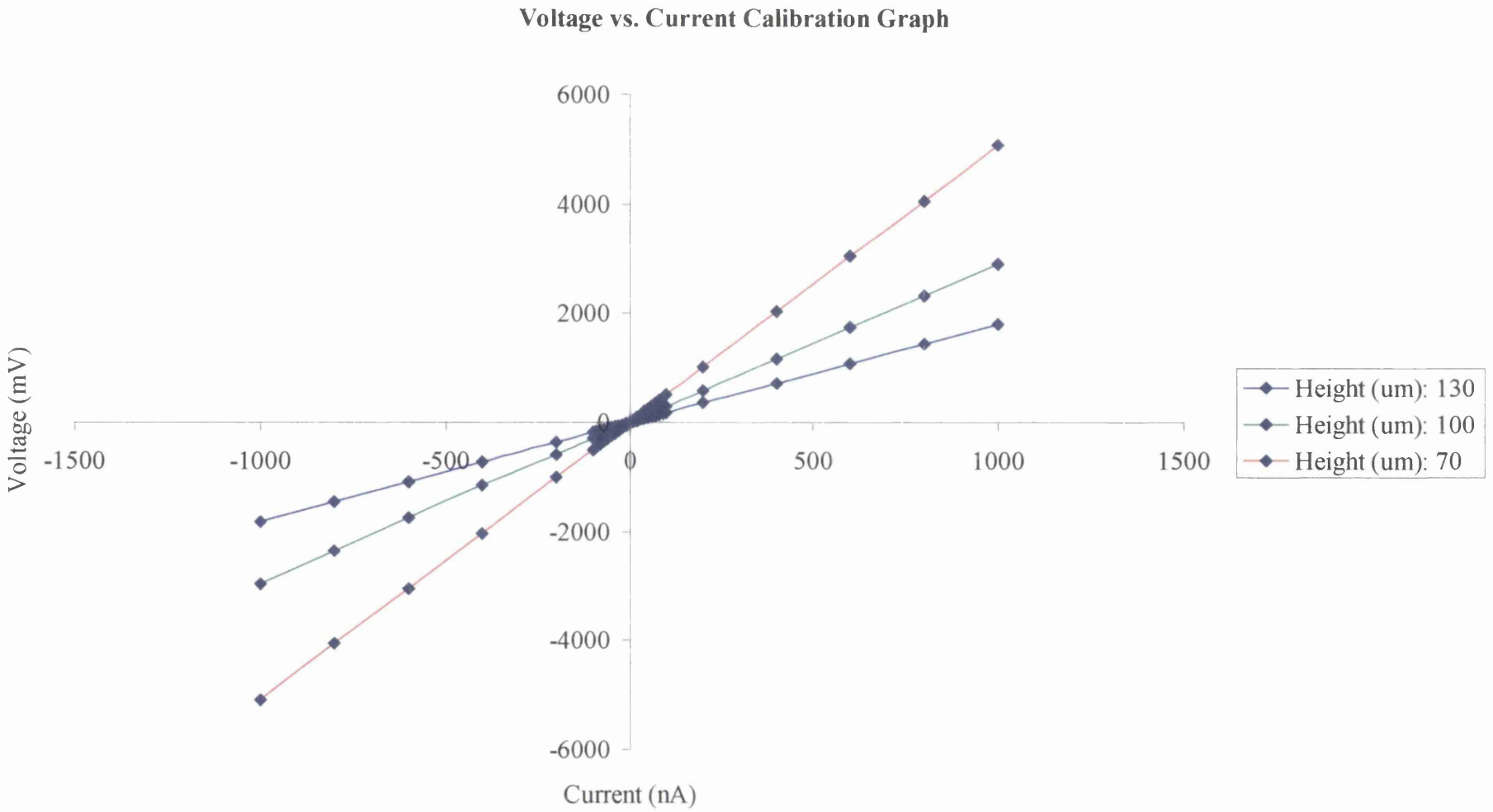

Figure 3.4 A calibration graph showing voltage against current for three different heights of 70, 100 and 130μA in 0.1%NaCl

passing through any point in a hemisphere of radius equivalent to the height will be the same. Hence for any current i, the current density is given by j.

$$j = \frac{i}{2\pi z^2} \tag{3.1}$$

When plotting current density against voltage, the height should now be accounted for. As can be seen in figure 3.5 this is the case, the three plots for 70μm, 100μm and 130μm scan heights all now lie on a single straight line. The calibration factor is the gradient of the best-fit line through the data and is 5445 $Am^{-2}V^{-1}$. Any data obtained from the SVET used in these experiments can easily be converted into current density. This point source calibration is a simple and reproducible method of instrument validation. Other current calibrations are also possible (e.g. passing known current through a set bore tube) but in this work the test cell has been used throughout.

3.4 Width at half maximum (WHM):

The WHM for a given SVET is a measure of the spatial resolution of the technique at a given scan height. When looking at a point 'r' at coordinates of (x,y) from the point source then the mathematical distance will be:-

$$r = \sqrt{(x^2 + y^2)} \tag{3.2}$$

Thus the distance at which the measured potential is halved, 0.5Fmax, will be found by substituting in equation 3.2 into equation 1.4 giving:-

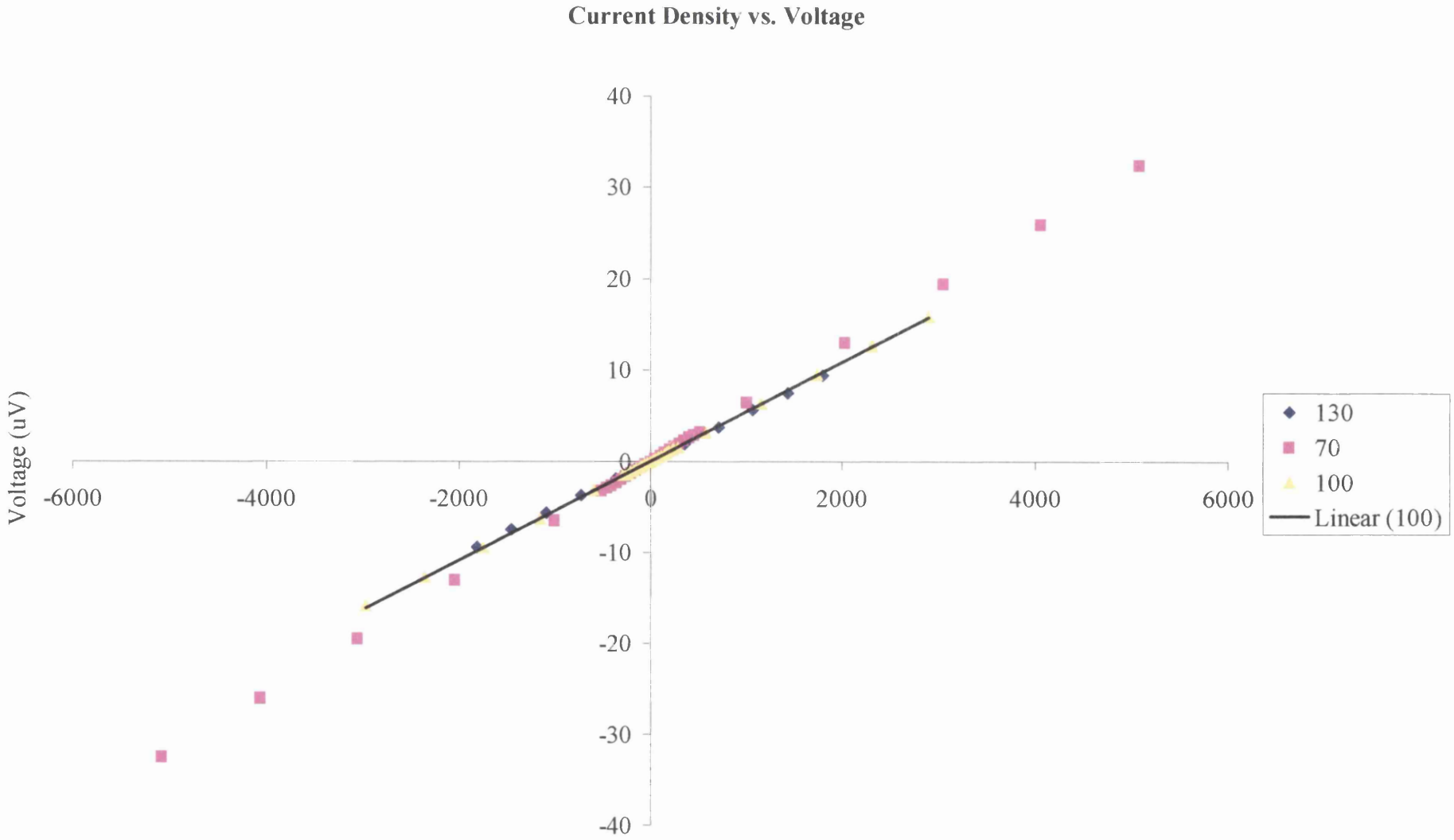

Figure 3.5 A calibration graph showing voltage against current density for three different heights of 70, 100 and 130μA in 0.1%NaCl

$$0.5F_{\max} = \frac{iz}{2\pi\kappa\sqrt{\left(r^2 + z^2\right)}} \tag{3.3}$$

Taking the ratio of equations (1.3) and (3.2) will therefore give a direct relationship between r and z and is shown thus:-

$$r = z\sqrt{\left(2^{2/3} - 1\right)} = 0.7665z \tag{3.4}$$

Solution of the point source voltage problem shows that the width of the SVET response peak will be 2r; therefore WHM will be related to the scan height by the following simple formula:

$$\text{WHM}=1.533z \tag{3.5}$$

The WHM can be reliably measured and is a reasonable estimate of the resolution. The apparatus could theoretically resolve two separate anodes at a minimum distance of 153μm apart, at a scan height of 100μm. To see how closely our apparatus fits theory, scans were performed over the test cell and the line scan over the centre of the point source recorded at several different currents and heights.

Figure 3.6 that shows the WHM of the SVET at a height of 100μm in practice for a variety of different currents. The WHM should only be dependant on height, fig 3.6 shows that at a scan height of 100μm the WHM remains independent of current, with all three currents giving the same WHM at 100μm of 220μm, around 40% more than theory predicts.

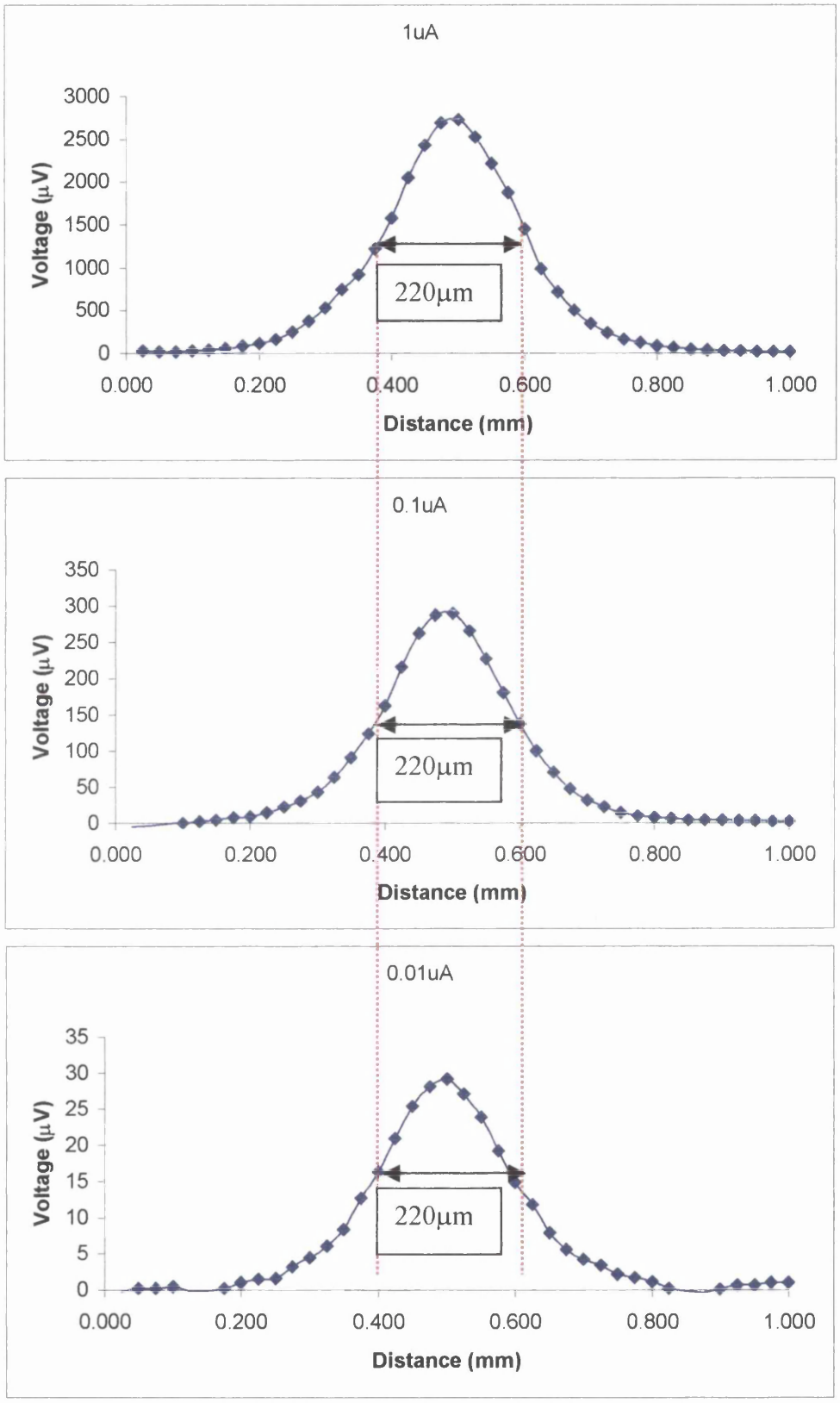

Figure 3.6 These plots show the width at half maximum at 100μm scan height and three anode currents of 1μA, 0.1μA, 0.01μA.

The experiment was repeated at a single current of 1μA with varying scan heights (70μm, 100μm and 130μm), the results of which can be seen in fig 3.7. This plot shows not only the dramatic relationship between F_{max} and scan height, but also the increasing WHM with scan height. An interesting phenomenon is that the WHM values deviate from theory as the probe gets closer to the sample surface, as shown in table 3.2.

Height (μm)	**WHM (μm)**		**Difference**
	Theoretical	Actual	**%**
70	107	190	77
100	153	220	44
130	199	260	30

Table 3.2. Difference between theoretical and actual data

The difference between actual and theoretical WHM data is shown in table 3.2. It shows that the actual WHM is 77% greater at 70 μm height, decreasing to 30% at 130μm height. The reasons for this are that in practice, the platinum tip is not a point, but has a finite size (125μm diameter) and is encased within a glass probe of approximately 200μm diameter. Thus the tip will still be detecting current flux when its centre is 100 μm from the anode, therefore decreasing the resolution. Another potential problem is the fact that the tip is vibrating, thus continuously altering its height thus the z value used in calculating the WHM will not be a true representation of the height. Finally a clear trend can be seen, in that the actual WHM becomes more similar to the theoretical value, as Z, the distance from the tip to the test cell, is

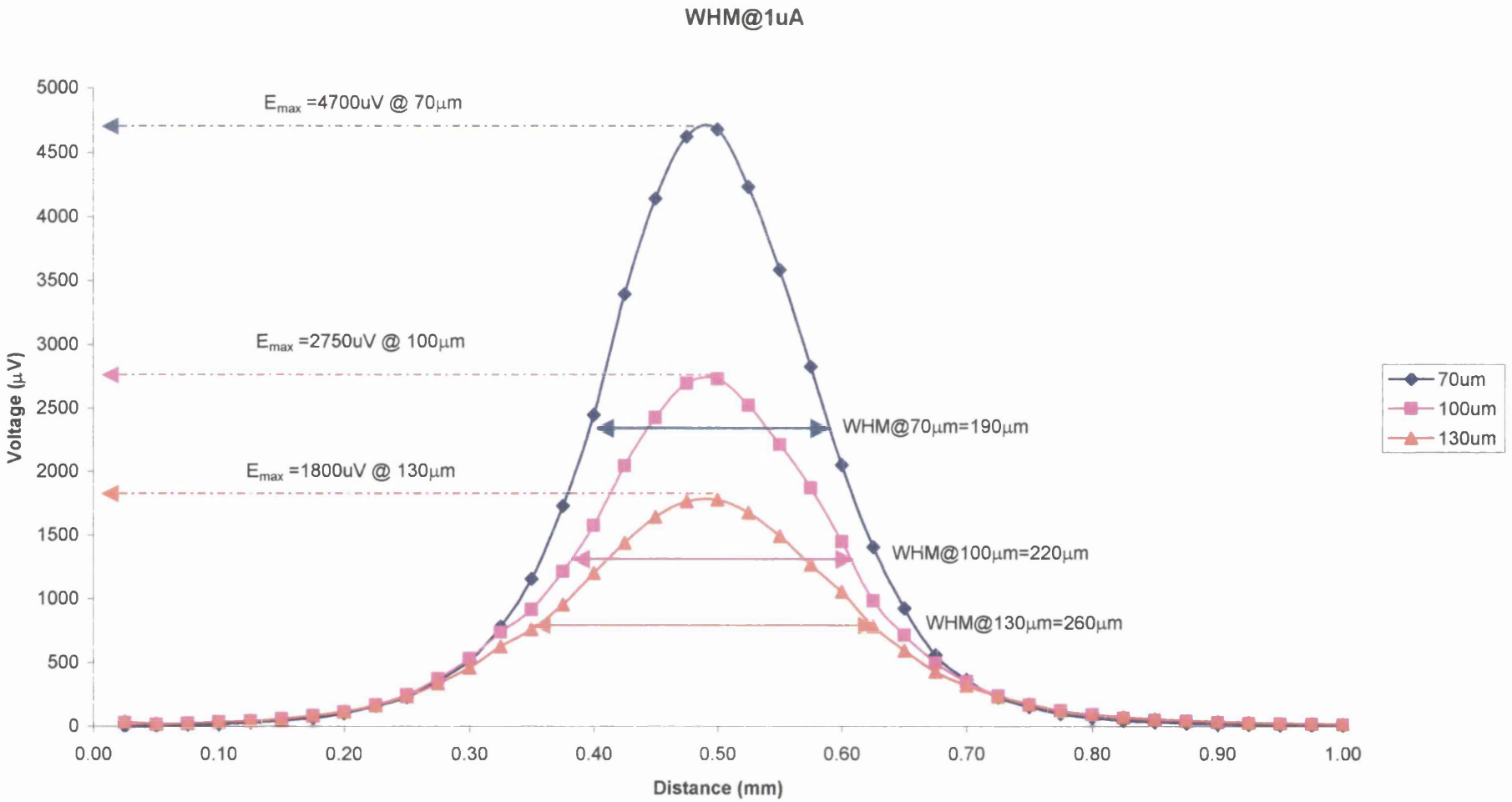

Figure 3.7 A graph showing line scans over the point source for various heights and for a set point anode current of 1μA.

increased. This is due to the physical size of the tip impinging on the current flow from the point source causing the current flux to be compressed within the narrow space between the surface and the tip. This will spread the peak as the probe impinges on the current flow, therefore lowering the resolution at lower scan heights (see figures 3.8a and 3.8b). As Z is increased, this impingement decreases, as the current has a larger area in which to flow. So at large Z values, there would be almost no impingement by the tip, leaving only the reasons mentioned previously to cause a difference between the actual and theoretical values. The WHM values for this experiment are well within expected tolerances, and suggest there will be good scan resolutions especially at heights of 100μm or more, but that resolution is limited to events separated by greater than 200μm. What is also important to realise is that this design of SVET is very sensitive with point source currents of 10nA easily quantifiable over the base line noise of the instrument.

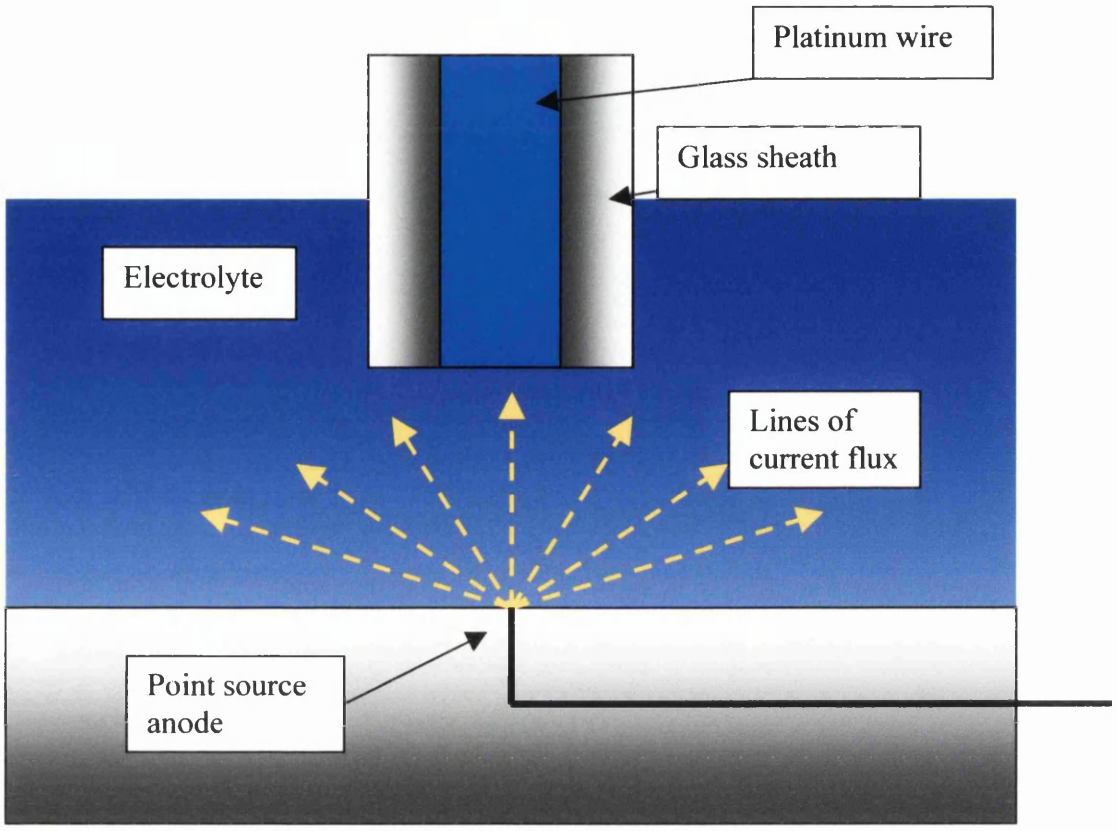

Figure 3.8a. Shows the tip at a relatively high scan height, where impingement on the lines of current flux is minimal.

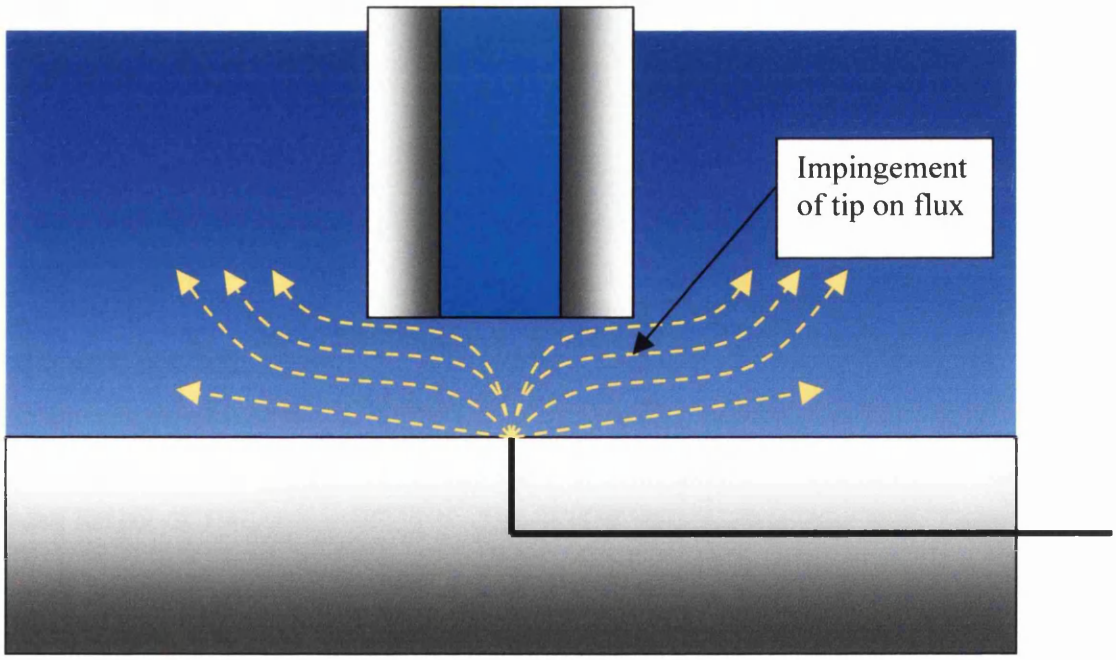

Figure 3.8b. Shows the tip impinging on the lines of current flux as the scan height is decreased, effectively spreading the peak that will be detected.

3.5 Calibration Conclusions:

Calibration is a relatively simple task, and must be carried out routinely for a number of reasons, these being:-

- To obtain an accurate calibration factor, that allows the relatively meaningless SVET potential differences to be converted into current densities. Current density accounts for the scan height and the conductivity of the electrolyte.
- Routine checking of the calibration factor is essential since variations in the value will suggest changes in the vibrational amplitude and will lead to spurious interpretation of the data.
- To ensure normal vibration of the tip. Scanning over the test cell should produce a radially symmetric bell shape with no other features, meaning that the SVET tip is vibrating normal to the plane of scan.
- To compare the spatial resolution achievable experimentally with the resolution predicted by SVET theory, and explain the reasons why there is a difference. This is particularly important when changing tips where geometry may alter the instrumental resolution.

The SVET now assembled is capable of detecting corrosion events (point source currents >10nA) in a controlled atmosphere. The spatial resolution is ~220μm at a scan height of 100μm and it is possible to convert SVET voltages recorded into current densities, using the calibration factor calibrated.

CHAPTER 4

SVET Study of the Corrosion and Corrosion Inhibition in Pipeline Materials

4.1 Results

4.1.1 Introduction

The aim of this section of work was to evaluate the changes in corrosion mechanisms on planar carbon steel samples exposed to differing corrosive atmospheres. The SVET has not, to date, been used for such studies being generally confined to studies where atmospheric control is less important such as galvanised steels[18] or aluminium[17].

In sweet corrosion[9] where CO_2 is involved, atmospheric control is critical. It was also our aim to investigate the effects of the addition of varying concentrations of inhibitor species to gauge their effectiveness against CO_2 corrosion on planar and crevice samples.

To this end results presented in this chapter are typical for each condition. The experiments were all repeated three or more times for each set of conditions to confirm the validity of the data obtained. The three experiments for each condition showed coherent results, with the corrosion intensity and mechanisms operating in a similar way for each repetition.

The same sample was scanned in air, CO_2 and 5ppm and 10ppm inhibitor containing solutions, and the corrosion behaviour monitored and recorded, with typical data for each being shown in the following sections. Furthermore the effectiveness of the inhibitor at preventing crevice corrosion was assessed.

4.1.2 Corrosion of sample 1 in Air saturated 0.1% NaCl:

After the sample was metallographically prepared (see section 2.2) leaving a mirror finish surface, the sample was encased in non-conductive chemically inert Teflon tape, leaving a $1cm^2$ square exposed. The sample was then placed on the levelling table and

levelled (see section 2.1.6). Subsequent to polishing there was a fifteen minute period prior to scanning while the sample could be set up and levelled, this period was the same for all of the experiments undertaken. The sample was then submersed in 0.1% NaCl under aerobic conditions and the scanning started. Under these conditions the oxygen concentration is $2x10^{-5}$ mol/l [28] (20ppm).

Typical SVET isocurrent contour maps for a three-hour immersion are illustrated in figures 4.1a to 4.1f. Looking at the data shown in figure 4.1a it can be seen that initially there are ten localised anodes. These anodes resemble point sources with WHM's of ~220μm. The activity of these individual point anodes appears to decreases over the scan time and after two hours very little localised activity is evident. After two hours immersion the anodic events no longer resemble point sources and have WHM values of ~0.8mm. As such although the number of localised anodic events has decreased, the level of corrosion has increased since the anodic activity is now spread over a far wider area. It should be noted that the scale for these scans goes up to 1100 mAm^{-2}. This change from localised to generalised corrosion is similar to that reported previously for iron immersed in $FeCl_3$ solution[18].

During the scanning process, corrosion products rapidly built up on the sample surface, as such the scan was terminated after three hours to prevent the deposits affecting the SVET readings, or causing damage to the probe.

Subsequent to the three-hour scanning period the sample was removed form the electrolyte and dried using ethanol and a hair dryer. The exposed surface of the sample showed extensive corrosion over approximately three quarters of the $10mm^2$ scan area. The sample was then imaged using an optical flat bed scanner; the sample was scanned at a resolution of 600x1200dpi. The final SVET scan is shown as a two dimensional contour

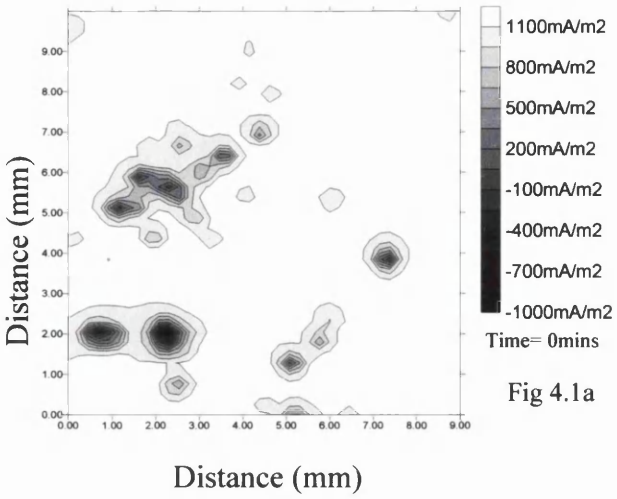

Fig 4.1a

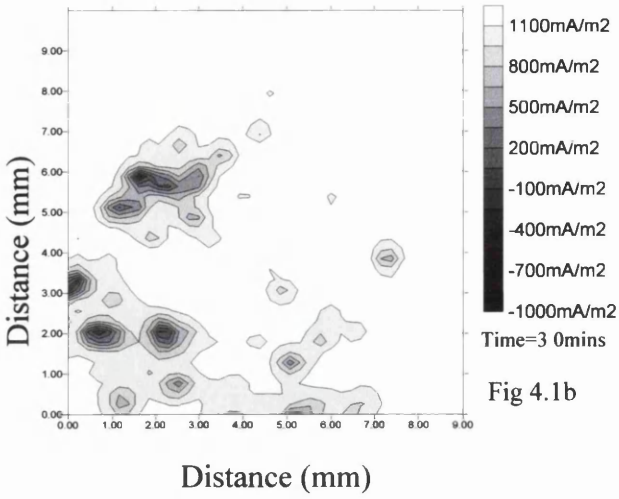

Fig 4.1b

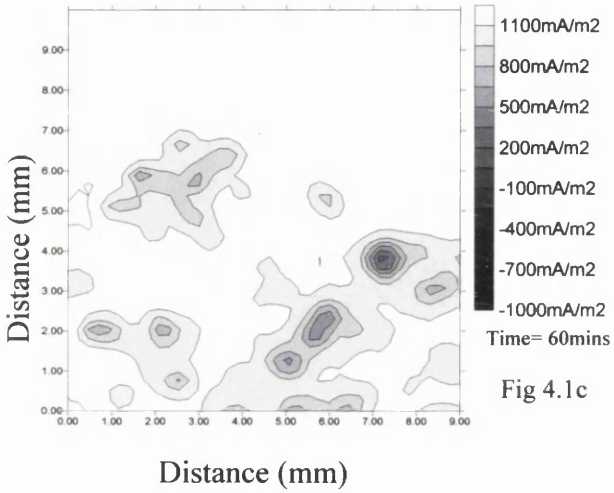

Fig 4.1c

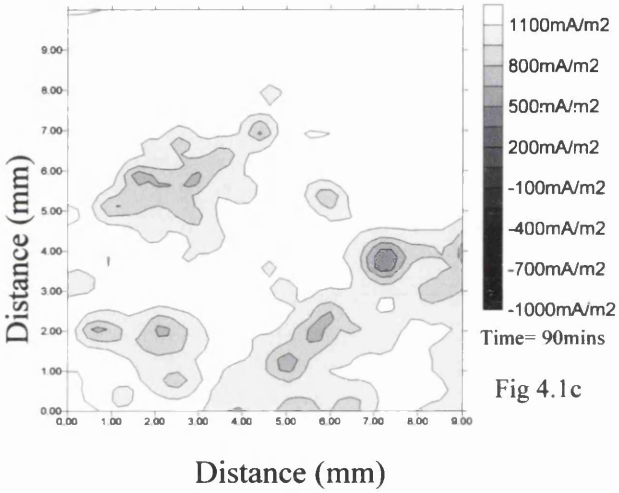

Fig 4.1c

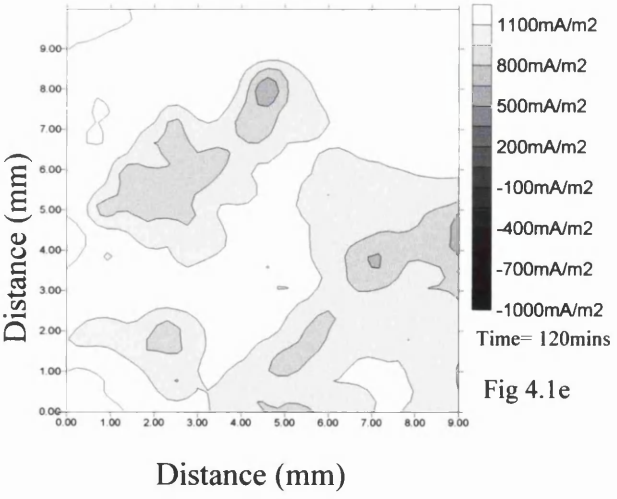

Fig 4.1e

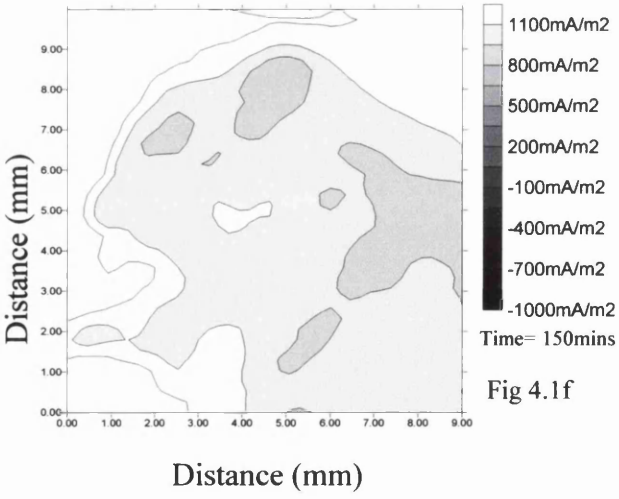

Fig 4.1f

Figures 4.1a-f Show the half hourly SVET maps obtained from scanning over the sample submersed in air saturated 0.1% NaCl electrolyte. The darker areas represent the anodic regions.

Last SVET scan before removal from electrolyte.

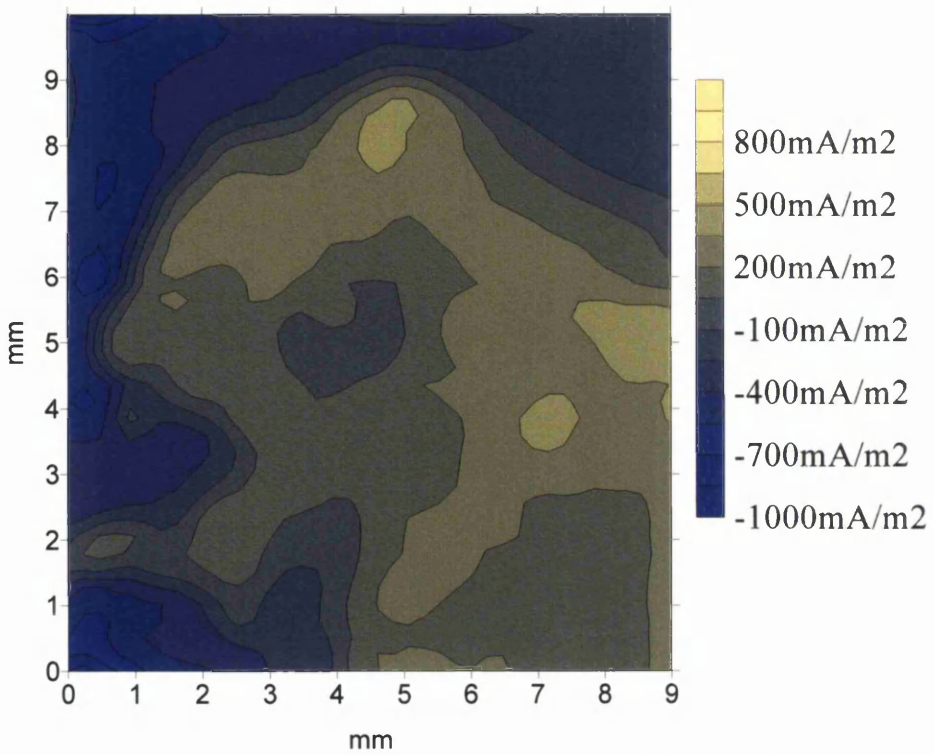

Optical scan image immediately after removal form electrolyte and drying.

Figure 4.2a and 4.2b show a SVET scan of the sample, and an optical scan of the sample after submersion in air saturated electrolyte for 3hours

map in figure 4.2a next to an optical scan (fig 4.2b) of the sample immediately after removal from the electrolyte. Comparing the SVET image fig 4.2a and the scanned image fig 4.2b, we see that the cathodic area at around the top edge of the sample remains relatively clean, and the area shown by the SVET to be generally anodic shows extensive corrosion. The SVET data can be treated semi quantitatively (see section 4.3) and as shall be demonstrated this shows an overall trend to increased corrosion activity which is less apparent from immediate analysis of the SVET maps.

4.1.3 Corrosion of sample 1 in CO_2 saturated 0.1% NaCl:

The sample was subjected to identical experimental conditions to those discussed above (i.e. repolished etc..), with the exception that this time the samples were submerged in a solution that was CO_2 purged prior to scanning. This experiment was undertaken in the environment chamber discussed in section 2.1.7. The sample was put into the electrolyte tank, with the electrolyte level just below that of the surface to scanned, the specimen was then levelled and the environment chamber sealed with CO_2 bubbling through a 500ml Dreschel bottle into the bottom of the tank. After around 30 minutes the bottle was inverted and the gas pressure forced the electrolyte in the bottle to pass into the tank, submersing the sample. Scanning commenced immediately after the sample was submersed in solution. Typical data for such a scan over 10 hours is illustrated in figure 4.3a-4.3f. Figure 4.3a shows the scan immediately after submersion in the electrolyte, there are four highly localised pits form on the surface. Looking at the scale, the intensity of these pits is not as great as that observed in the corrosion of the sample in air saturated solution. However the anodic activity remains far more focused and is persistent throughout.

The anodic activity remains relatively constant throughout the first four hours of submersion, after which the intensity begins to slowly decrease, but still remain active throughout the twelve hour scan. Furthermore the scan shows that throughout the experiment, the anodes remain in the same position, and the cathodic reactions occur all over the rest of the exposed sample surface.

After the scanning period, the sample was removed from the electrolyte and the water removed from the surface, by dousing it with ethanol and using a hot air drier to evaporate the solvent from the surface. The exposed surface was significantly 'shinier' (free from corrosion product) than the sample submerged in the air saturated solution, even though this scan was performed over an extended period of time. The four anodic pits were clearly identifiable on the surface as small black areas with rough texture; the relief of these areas was below that of the surrounding metal i.e. there was metal loss from these locations. This is shown in the optical scan of the corroded sample surface see figure 4.4b. Looking at the SVET contour map of the surface (figure 4.4a), it can be seen that the locations of the pits on the scanned sample directly correspond to the anodic areas shown by the SVET during the scanning period.

The presence of CO_2 has clearly altered the corrosion mechanism. The solution pH of 4.2 and the absence of oxygen will mean the primary cathodic process will be:

$2H^+ + 2e^- = H_2$ or $2H_2CO_3 + 2e^- = H_2 + 2HCO_3^-$ (see section 1.4.6)

In this instance it is clear that the carbonate film is incomplete allowing intense localised attack over the 24 hour submersion period. Hence this data illustrates the enormous potential that the environment controlled SVET offers as a means of studying sweet corrosion mechanisms.

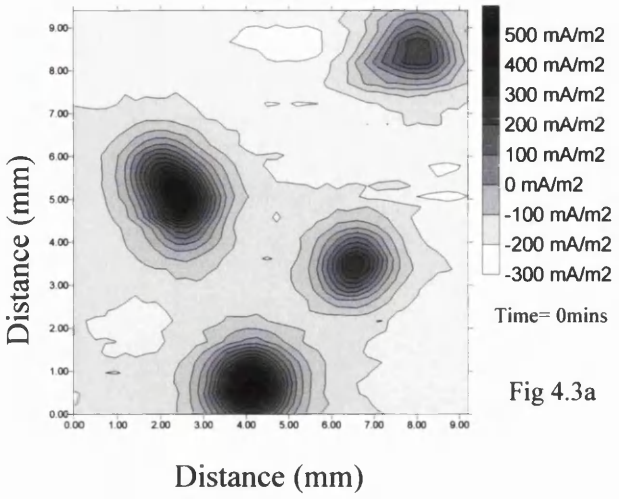

Fig 4.3a

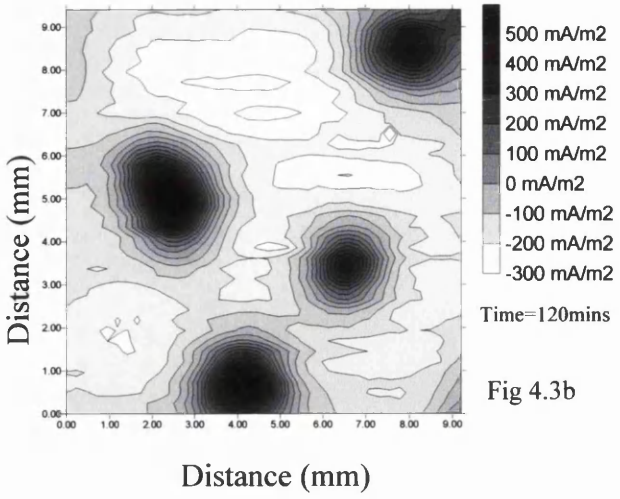

Fig 4.3b

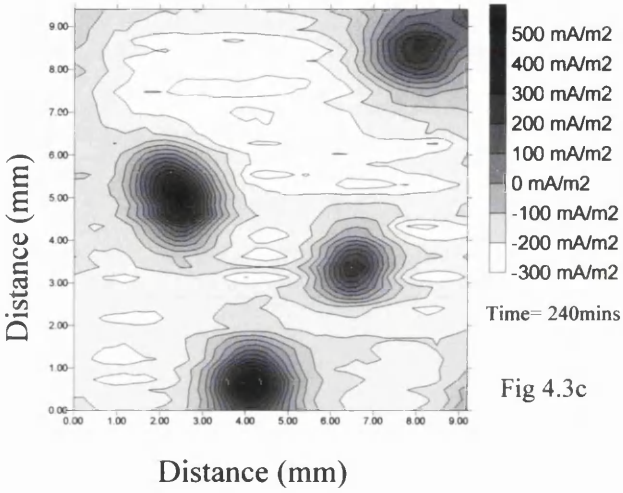

Fig 4.3c

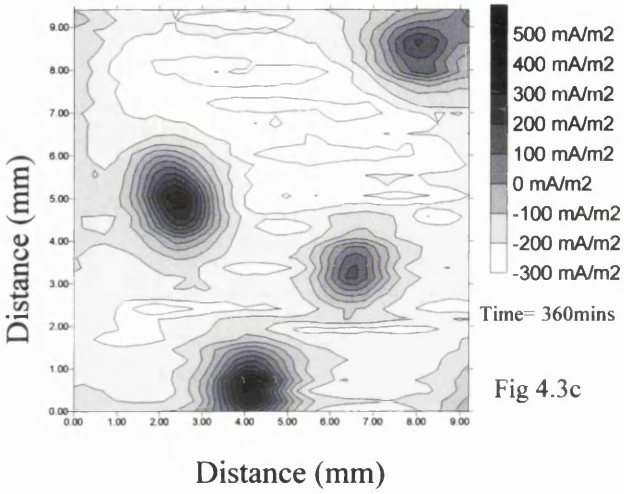

Fig 4.3c

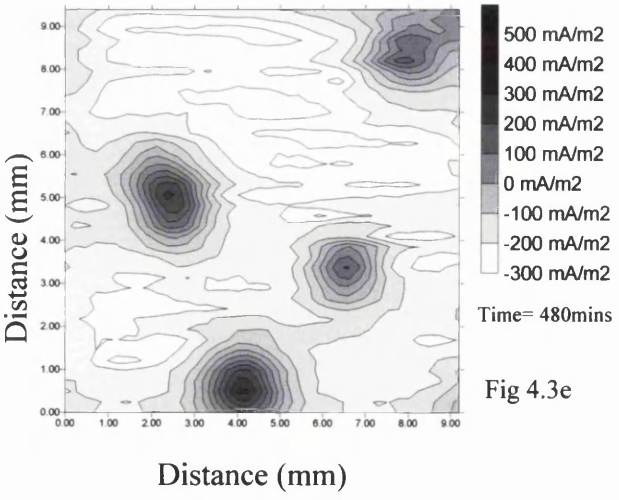

Fig 4.3e

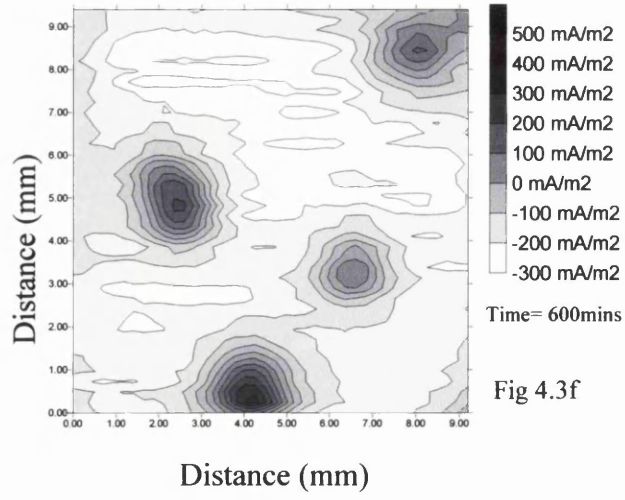

Fig 4.3f

Figures 4.3a-f Show the hourly SVET maps obtained from scanning over the sample submersed in CO_2 saturated 0.1% NaCl electrolyte. The darker areas represent the anodic regions.

Last SVET scan before removal from electrolyte.

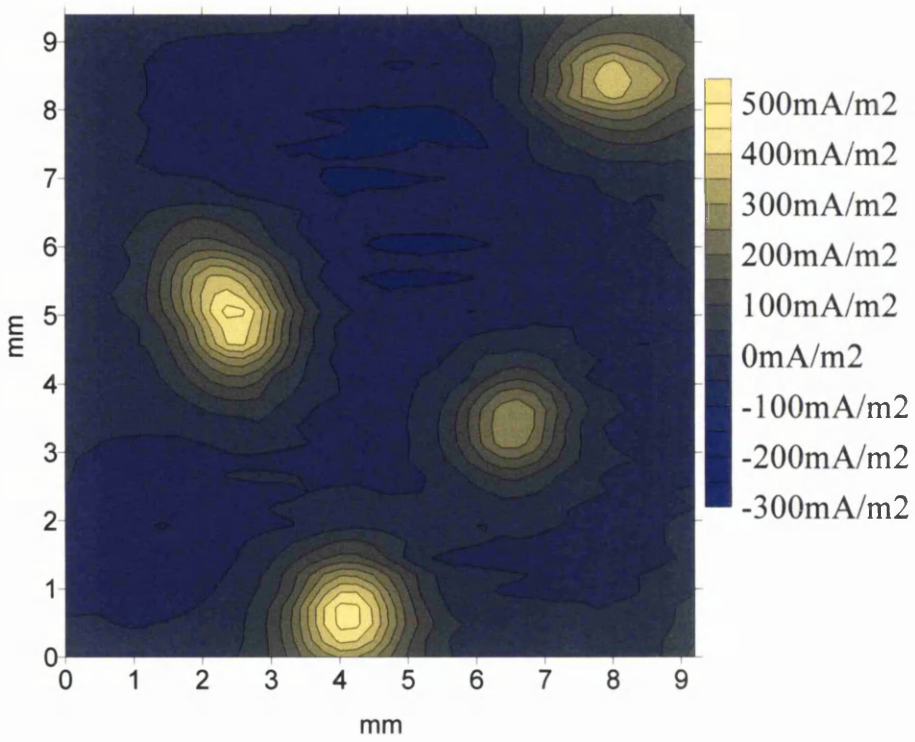

Optical scan image immediately after removal form electrolyte and drying.

Figure 4.4a and 4.4b show a SVET scan of the sample, and an optical scan of the sample after submersion in CO_2 saturated electrolyte for 12 hours.

Under conditions of CO_2 saturation iron carbonate formation can forestall corrosion but it is clear from the scans shown here that its mode of inhibition is insufficient to prevent pit development in this material. Indeed the focused pitting is indicative of partial anodic inhibition

4.1.4 Sweet Corrosion in CO_2 saturated 0.1% NaCl with 5ppm anodic inhibitor:

The inhibitor used in this work was supplied by Total Fina Elf and is a filming organic inhibitor with anodic inhibition properties. It is of the imidazoline group of inhibitors, the structure of which is shown below in figure 4.5

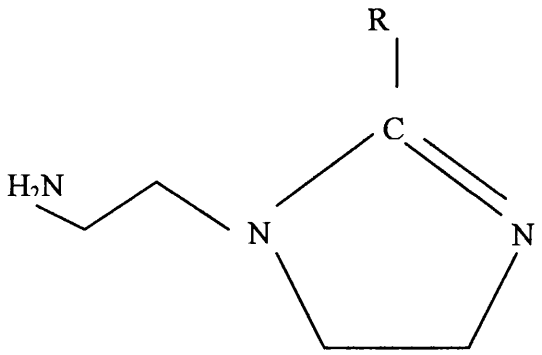

Figure 4.5 The inhibitor species 1-aminoethyl-2-nonadecyl-2-imidazone, where R is an alkyl fragment in this case $(CH_2)_{18}CH_3$

The sample was prepared in the same way as described previously; in this case the CO_2 saturated 0.1% NaCl solution was dosed with five parts per million inhibitor solution as described above, from the outset of the experiment. Typical SVET isocurrent contour maps over 10 hours are shown in figures 4.6a-f, the inhibitor addition can be seen to largely inhibit the formation of anodic sites, however, several are able to form, and looking at the scale of the data, the intensity of these anodes has initially increased in comparison to that

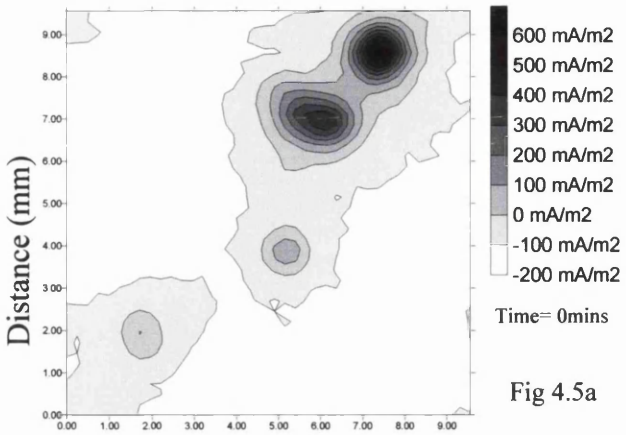

Fig 4.5a

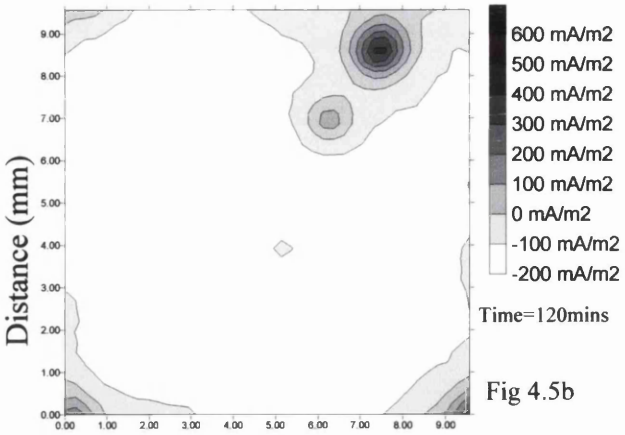

Fig 4.5b

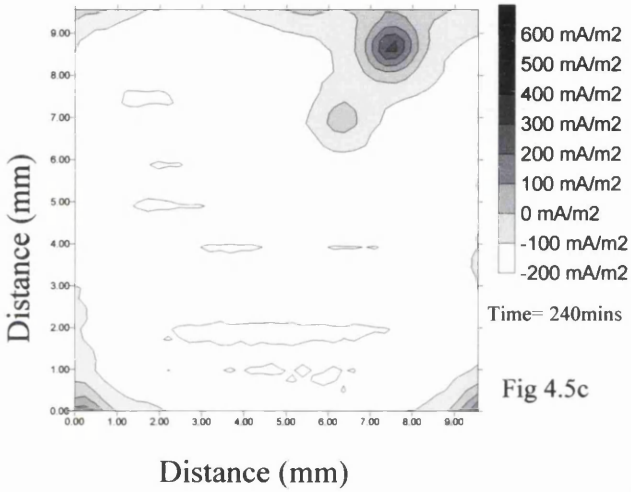

Fig 4.5c

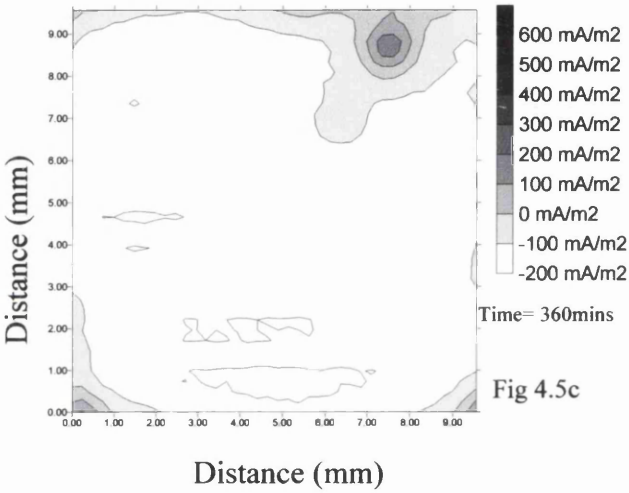

Fig 4.5c

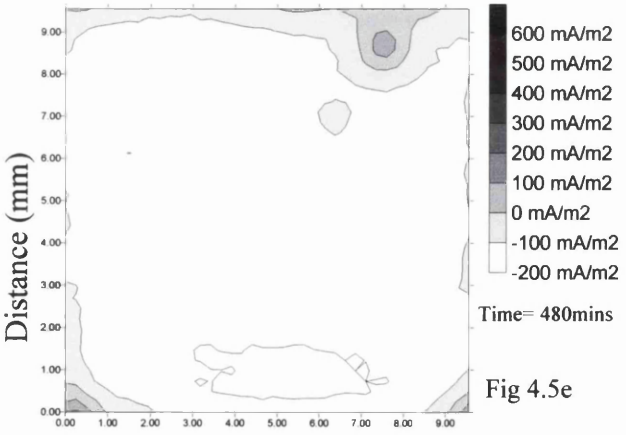

Fig 4.5e

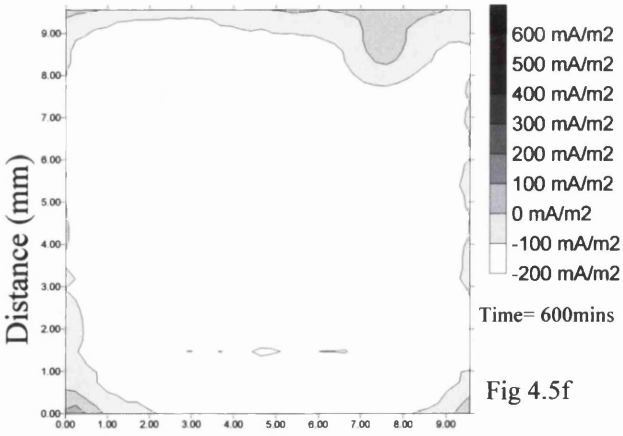

Fig 4.5f

Figures 4.5a-f Show the two hourly SVET maps obtained from scanning over the sample submersed in CO_2 saturated 0.1% NaCl electrolyte doped with 5ppm anodic filming inhibitor. The darker areas represent the anodic regions.

Last SVET scan before removal from electrolyte.

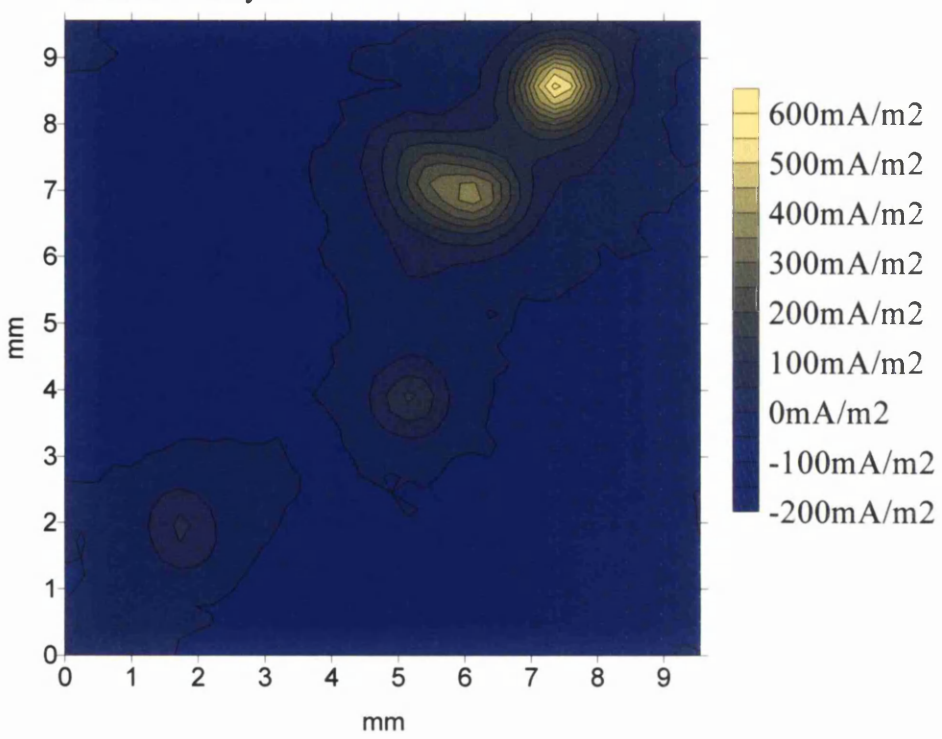

Optical scan image immediately after removal form electrolyte and drying.

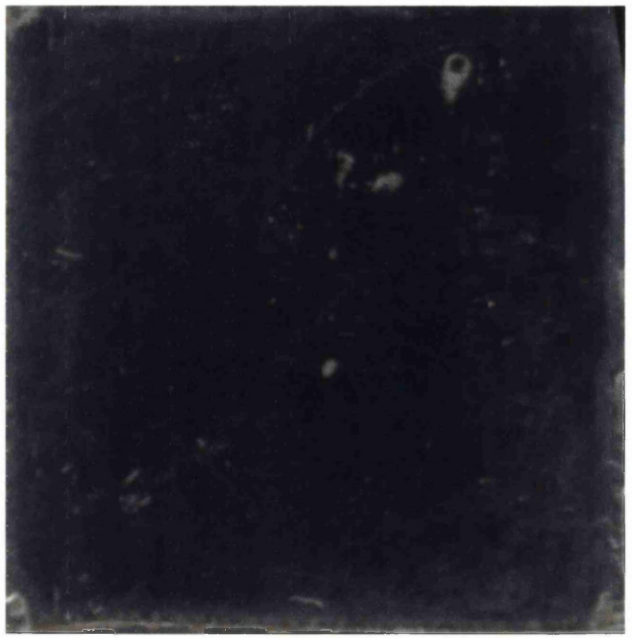

Figure 4.6a and 4.6b show a SVET scan of the sample, and an optical scan of the sample after submersion in CO_2 saturated electrolyte doped with 5ppm anodic filming inhibitor for 12 hours.

of the samples immersed in CO_2 saturated solution as shown in figures 4.3a-f. After the initial scan, all but two of the anodes are inhibited, and as time moves on the intensity of the remaining anodes slowly decreases as the inhibitor takes affect.

Upon removal and drying of the sample, the surface is relatively clean with the exception of blemishes in the same location as the anodic activity occurred. Comparing the image obtained using optical scanning of the sample (see figure 4.6b) with the SVET contour map (see figure 4.6a) shows that the location of the anodic sites during the experiment, directly tallies with the location of the blemishes on the surface of the corroded sample.

4.1.5 Corrosion of sample 1 in CO_2 saturated 0.1% NaCl with 10ppm inhibitor:

In these cases the sample was prepared, and scanned in a CO_2 saturated 0.1% NaCl solution electrolyte dosed with 10 parts per million anodic inhibitor. Typical data is shown in figures 4.7a-f for a 10 hour period of scanning. Notice in this case that the scale is significantly lower than for the other experiments, only going up to 130 mAm^{-2} as opposed to 500 mAm^{-2} for the 5ppm case. Throughout this scan, corrosion is evident around the edge of the taped off area. This is evident on all the scans, however the lower scale of the data shown in figures 4.8a-f makes it seem more prevalent in this case. During the scanning period the levels of anodic activity around the edge of the sample do increase with the maximum intensity being seen on the last scan. This suggests the initiation of underfilm type crevice corrosion

After scanning the sample maintained the mirror finish as previous to the immersion in the electrolyte. There were no blemishes on the surface, and no pits of any magnitude

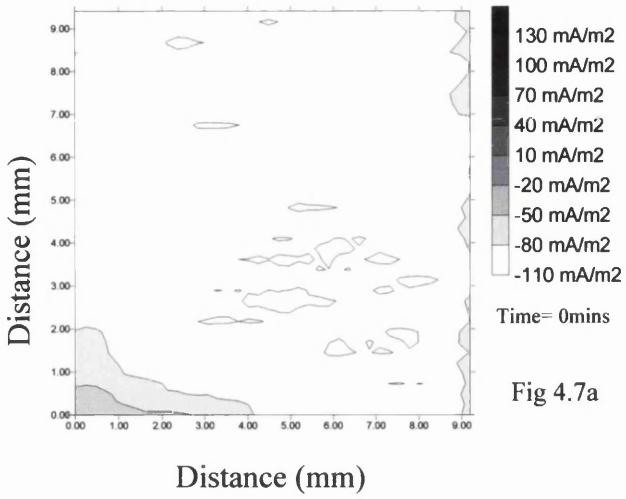

Fig 4.7a

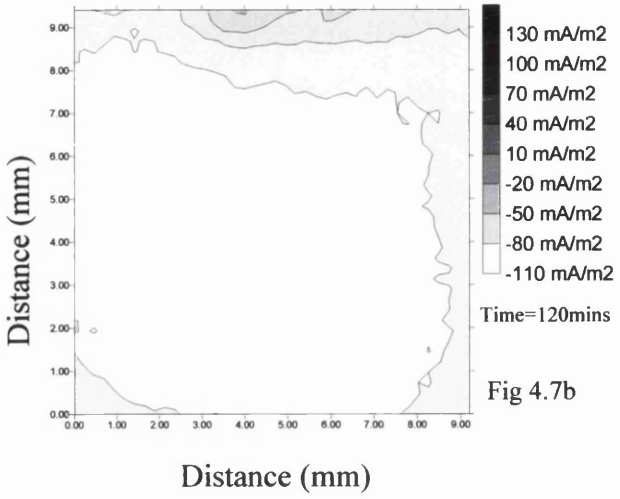

Fig 4.7b

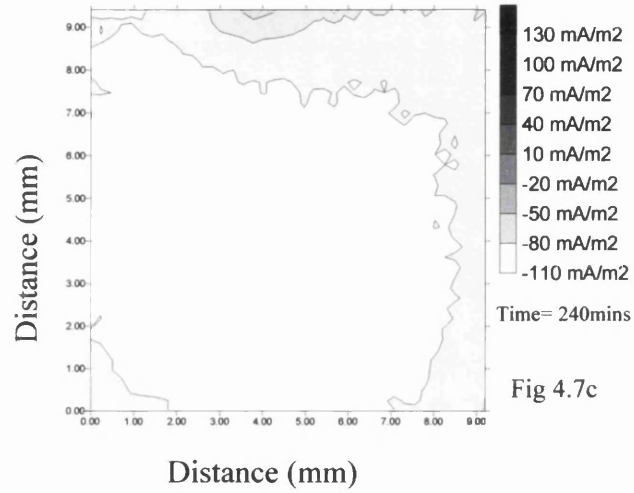

Fig 4.7c

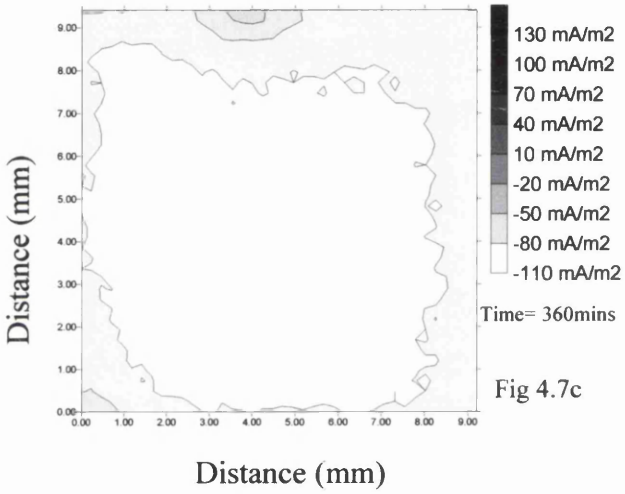

Fig 4.7c

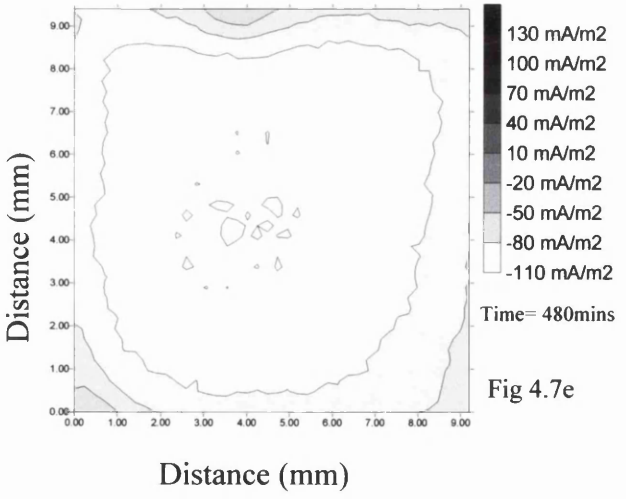

Fig 4.7e

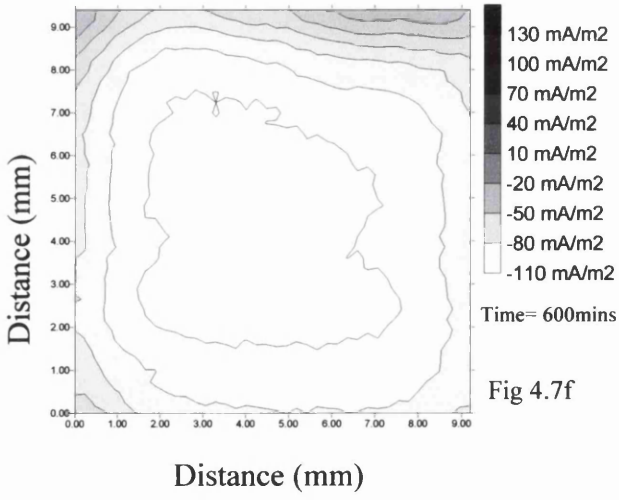

Fig 4.7f

Figures 4.7a-f Show the two hourly SVET maps obtained from scanning over the sample submersed in CO_2 saturated 0.1% NaCl electrolyte doped with 10ppm anodic filming inhibitor. The darker areas represent the anodic regions.

Last SVET scan before removal from electrolyte.

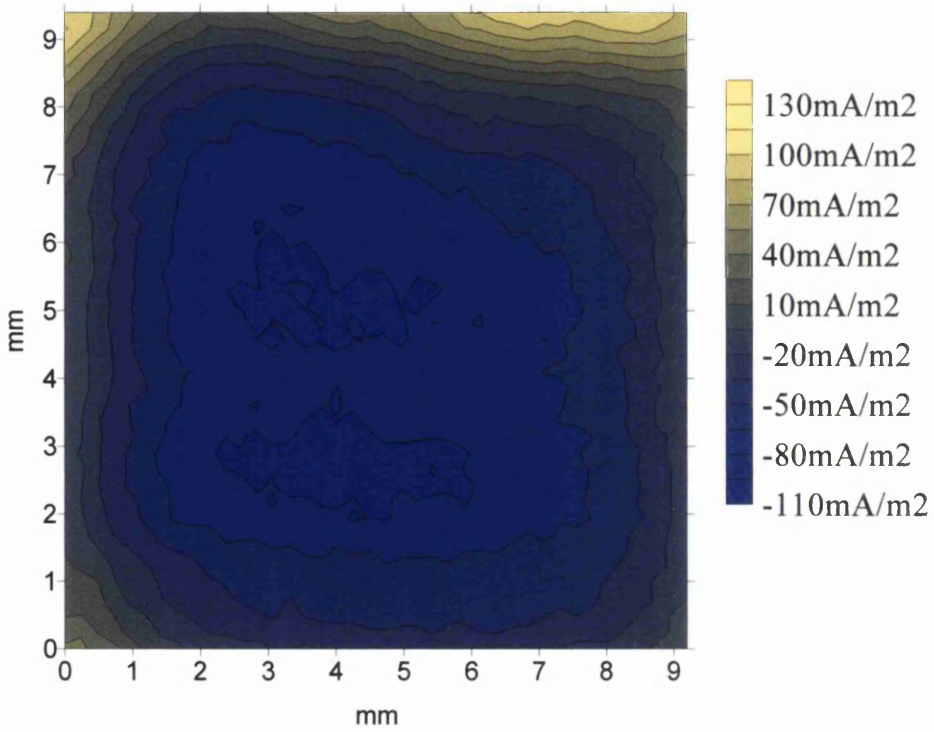

Optical scan image immediately after removal form electrolyte and drying.

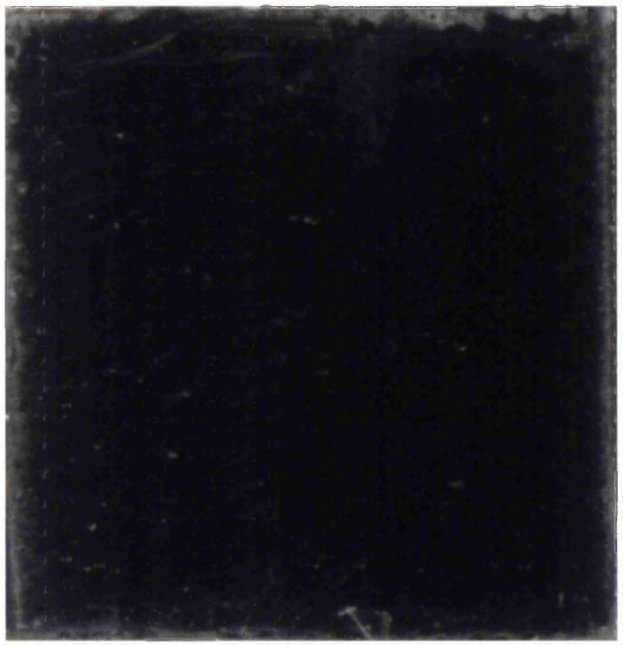

Figure 4.8a and 4.8b show a SVET scan of the sample, and an optical scan of the sample after submersion in CO_2 saturated electrolyte doped with 5ppm anodic filming inhibitor for 12 hours.

were identified by the SVET during the scanning period (see figure 4.8a and 4.8b). Small amounts of corrosion were evident in the crevice between the teflon tape and the sample surface, as seen on the scanned image (see figure 4.8b).

4.2 Total Metal Loss:

The data gathered during the scanning process has units of Am^{-2} after calibration. Therefore by integrating each SVET area map, the total current emerging in the plane of scan can be calculated. This is done by use the 'Surfer 6' program on the pc. Conversion to charge, and the use of Faraday's law allows total metal loss for the scans to be calculated, the following flow chart shows the steps taken:-

- The units of the data from the SVET are in nanovolts. (units=nV)
- This is expressed in volts by dividing by 10^9. (units=V)
- After integrating, the total volume of 'voltage' emerging in the plane of scan has units of Vmm^2

Multiplying by 10^{-6} converts this into Vm^2

- Conversion to current is performed by multiplying the Vm^2 by the calibration constant. (units=$Am^{-2}V^{-1}$) giving units of amps.
- Charge = Current x Time, thus if we multiply the current data by the scan interval we get units of charge in coulombs.
- Using Faradays law charge converted into grams

The critical assumption that has been made is that the corrosion activity between scans remains constant e.g. the total metal loss is considered for an individual scan. This is then assumed to be the level of corrosion occurring for the period immediately prior to the scan. The results of calculating the total metal loss, for each scan is shown in figure 4.10. The trends to note are:

Total metal loss (TML) for the sample in air saturated electrolyte exhibits the greatest levels of loss initially. As the time progresses, the total metal loss for the individual scan period shows a sharply increasing trend, despite decreasing localisation as illustrated in the SVET isocurrent contour maps shown in figures 4.1a-f

Looking at the sample in CO_2 saturated solution, with no inhibitor, it can be seen that the levels of TML are lower than those for the air saturated solution throughout the scanning period. The levels of TML increase up until the 2.5hr mark, before beginning to decrease. TML shows a decreasing trend towards the end of the experiment.

The TML for the sample in 5ppm inhibitor solution shows initially high levels (higher than those seen in the CO_2 solution without the inhibitor), but sharply decreases over the subsequent two scans, before levelling out just above zero. This is typical of an anodic inhibition which has been incomplete and has been backed up by an increasing E_{corr} measured at –640mV as opposed to -720mV versus SCE for the solution without inhibitor additions.

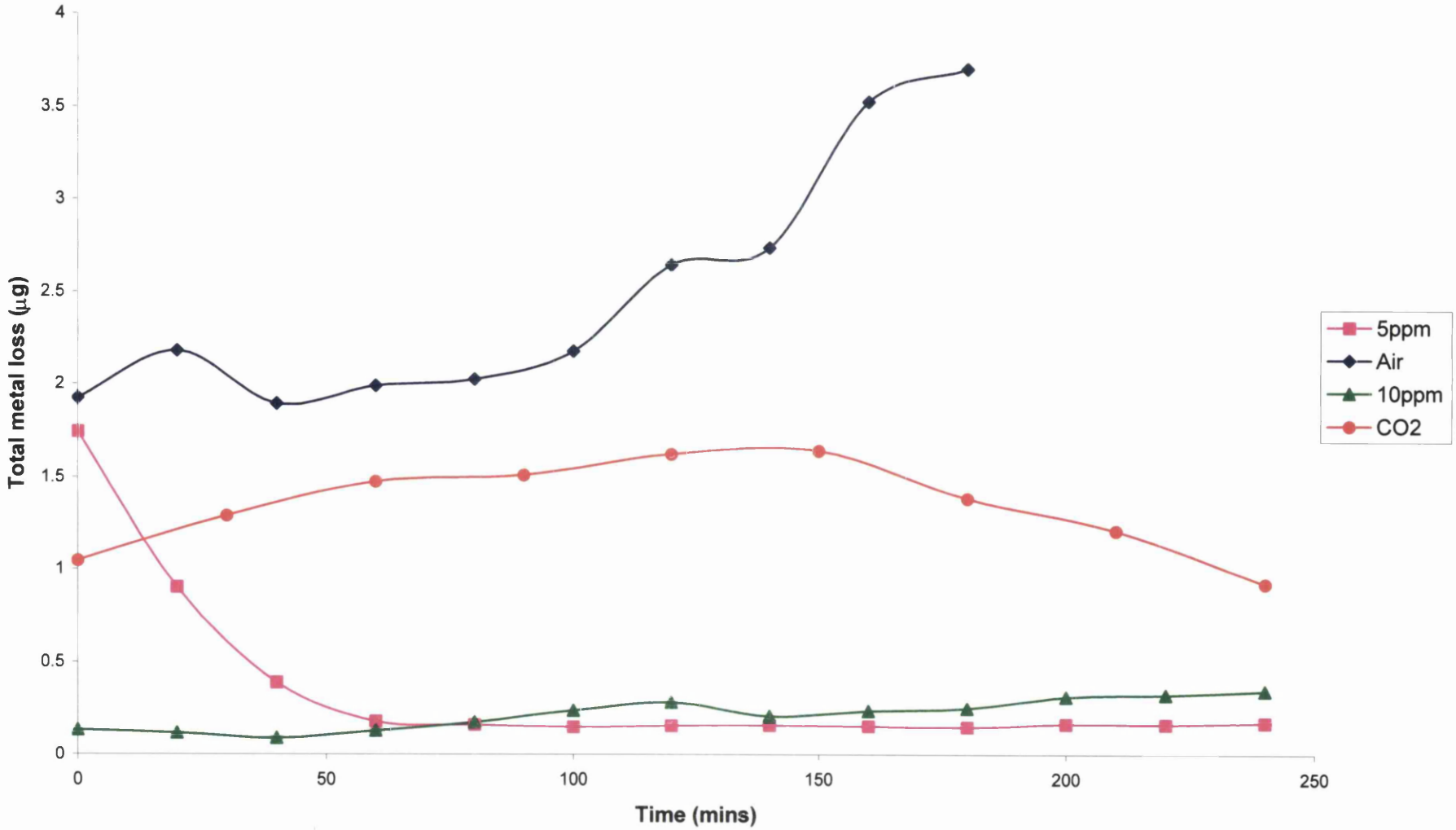

Figure 4.10. The metal loss per individual scan period for; i) the sample submerged in air saturated electrolyte ii) the sample scanned whilst submerged in CO_2 saturated electrolyte, iii) the sample submerged in CO_2 saturated electrolyte doped with 5 ppm filming inhibitor and iv) the sample submerged in CO_2 saturated electrolyte doped with 10 ppm filming inhibitor

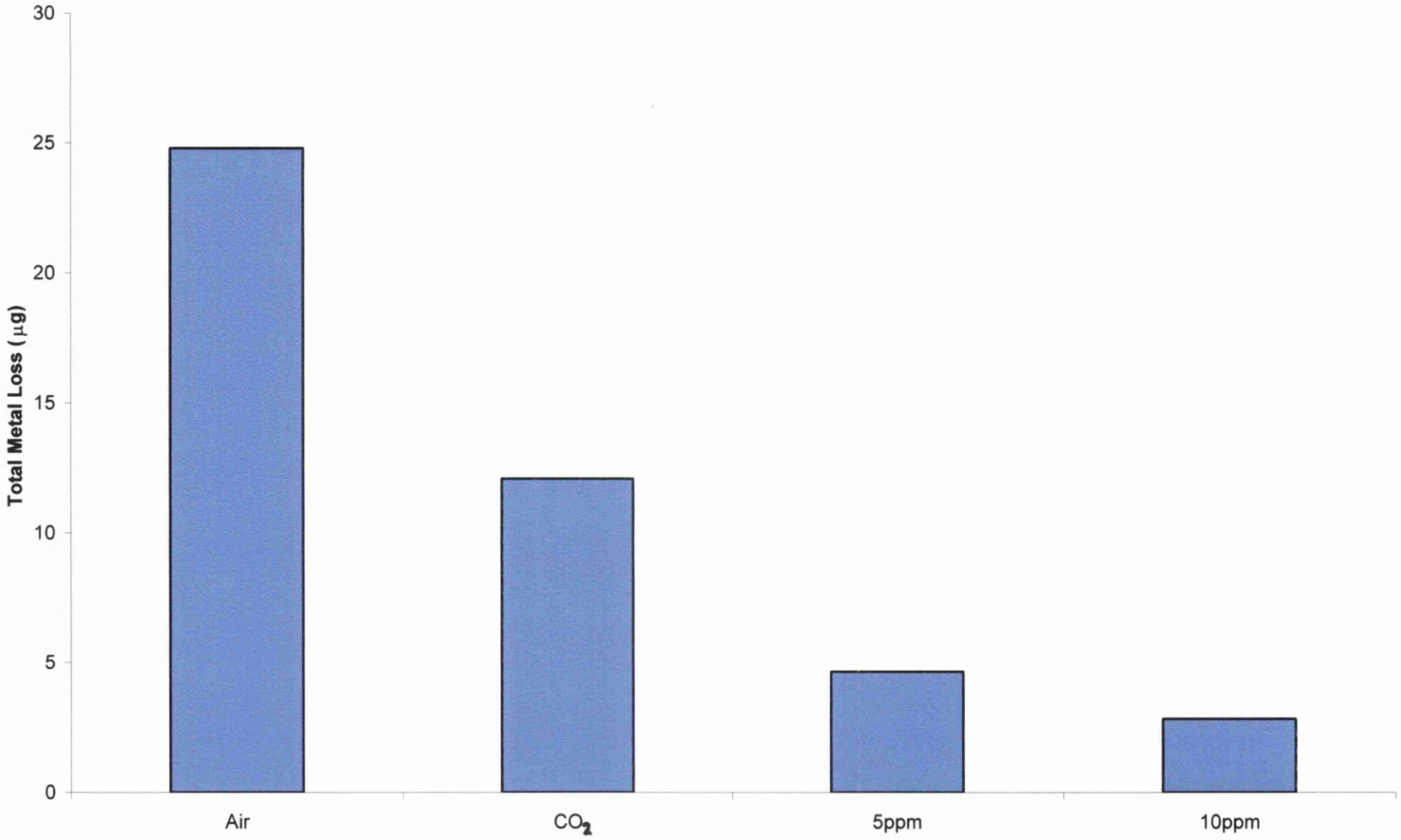

Figure 4.11 The cumulative total metal loss figures for each of the environmental conditions over 3 hours

TML for the sample in 10ppm inhibitor solution remains at very low levels throughout the scanning period. The E_{corr} measured in this case was –680mV versus SCE. This is still more positive than the uninhibited case but the slight shift in E_{corr} suggests that the filming layer is covering the surface, and actually serving to inhibit cathodic activity as well, therefore further reducing both metal dissolution and hydrogen evolution.

The sum of each of the total metal losses per scan period were added to give a plot showing the overall metal loss during the entire scanning period (see figure 4.11). As expected, the air saturated solution shows the most elevated levels of total metal loss, followed by the CO_2 saturated solution, then the 5ppm CO_2 saturated solution, and finally the 10ppm saturated solution shows the lowest levels of metal loss.

It is interesting to note the persistent crevice like corrosion in the vicinity of the tape, and separate SVET studies were performed to analyse the effectiveness of the inhibitors on preventing this corrosion as described in section 4.3.

4.3 Crevice Corrosion

The sample shown in figure 2.6b was used to assess the effectiveness of the filming inhibitor at preventing crevice corrosion. The circular sample was mounted in resin; the interface between the resin and the sample forms a primitive crevice. The sample is exposed to CO_2 purged 0.1% NaCl electrolyte doped with 5ppm inhibitor solution, as described in the inhibitor experiments (section 4.14). The effectiveness of the inhibitor at preventing crevice corrosion could then be assessed.

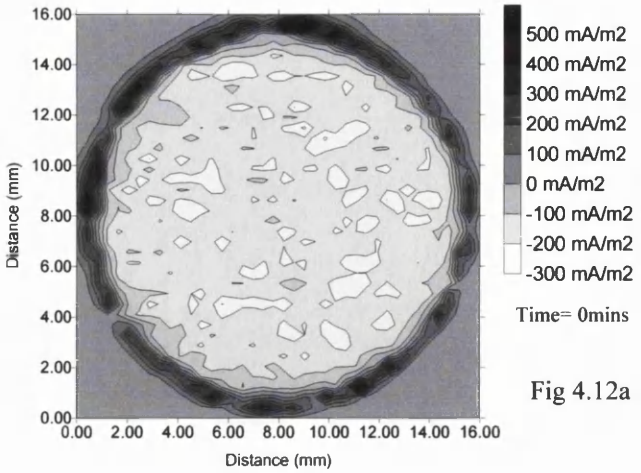

Fig 4.12a

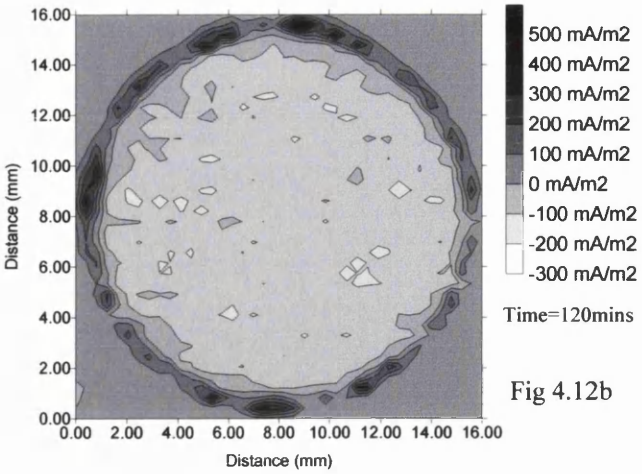

Fig 4.12b

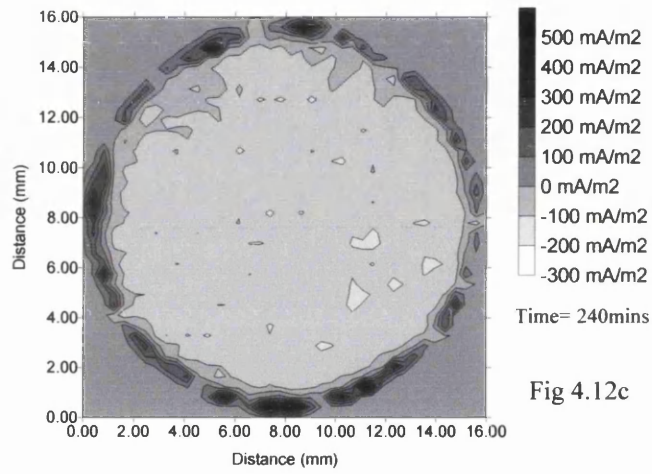

Fig 4.12c

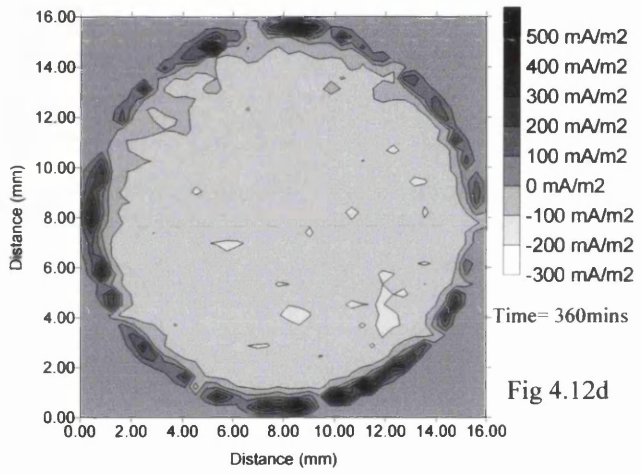

Fig 4.12d

Figures 4.12a-d Show the two hourly SVET maps obtained from scanning over the sample submersed in CO_2 saturated 0.1% NaCl electrolyte with 5ppm inhibitor, with a crevice between the metal and resin. The darker areas represent the anodic regions.

Scans 4.12a-d show the activity occurring on the specimen over a 6 hour period. There is a clearly identifiable dark ring corresponding to the metal-resin interface, the scale shows this region to be anodic. The anodic activity persists at the metal resin interface, at a constant intensity throughout the 6 hours of scanning. The remainder of the exposed metal surface shows primarily cathodic activity. Comparison between the sample submerged in 5ppm inhibitor solution without a deliberate crevice and the crevice sample under the same conditions show similar anodic intensity. However the location of the activity has been vastly altered. Instead of the focal anodes distributed around the scan area, we now see that nearly all corrosion activity occurs at the crevice site. Furthermore, the 5ppm inhibitor experiment showed the corrosion activity to decrease over time whereas the anodic intensity around the crevice remains at a high level throughout the experiment. The reasons for the location of the corrosion activity are discussed in section 4.4.3

4.4 Discussion:

4.4.1 Effects of atmosphere

Scanning of the sample in air saturated electrolyte and CO_2 saturated electrolyte showed the corrosion mechanism had been extensively altered by the change in atmospheric conditions. The anodic reaction for each is simply metal dissolution where the iron dissolves to form iron ions and electrons. It is the distribution of the anodic activity that differs, as well as the cathodic reactions. In air saturated solution there is ample oxygen dissolved in the electrolyte that can combine with the water molecules and electrons from the anodic reaction to form hydroxyl ions. The CO_2 saturated solution contains no oxygen, therefore the primary cathodic reactions for electron take up are now:

$$2H^+ + 2e^- = H_2$$

$$2H_2CO_3 + 2e^- = H_2 + 2HCO_3^-$$

Corrosion in CO_2 saturated environments is known as Sweet corrosion. With reference to section 4.1.3 after initial submersion in the purged electrolyte the sample experienced intense localised pitting corrosion. In fact with reference to the total metal loss figures (fig 4.6) initial loss figures are similar to those exhibited by the aerobically corroding sample. The probable cause of this is that as carbonates are deposited on the metal surface, they protect the underlying material, the metal then becomes polarised with CO_2 acting as an anodic inhibitor, there by increasing the E_{corr} value so those areas not protected by carbonates are corroded more vigorously. As the experiment moves on, the total metal loss for each given scan decreases. This is due to further carbonate formation on the surface leaving progressively less exposed metal. At the end of the experiment the pits identifiable

during the immersion and scanning period were clearly visible on the surface of the sample. A scanned image is shown in figure 4.2b.

The sample scanned in air saturated solution shows far less focal anodes, with corrosion activity spread across much of the scan area. Although the anodes are less intense than those seen in the scans of the CO_2 scan, their larger area means that the overall levels of corrosion are higher. The corrosion product formed by the corrosion of mild steel in oxygen saturated solution is iron oxide (rust), which does not form a coherent 'passivating' layer under normal pH conditions. The iron oxide is a gel like deposit which does not protect the metal from further attack. With ample oxygen dissolved in the electrolyte, there is a ready supply of cathodic sites, as such corrosion is largely generalised from the outset of immersion. Total metal loss shown in figure 4.6 shows corrosion to be continually increasing over time, suggesting that were this component in service under these conditions, failure would result in a relatively short period of time. In summary, the environment can vastly change the intensity, distribution, and nature of corrosion products in the corrosion of mild steel.

4.4.2 Effects of inhibitor:

Within the scope of this project is the effect that the addition of inhibitor solutions has on the corrosion behaviour of oil pipelines. The concentrations investigated were 5ppm and 10ppm of the anodic filming inhibitor 1-aminoethyl-2-nonadecyl-2-imidazoline. The tests were performed in a CO_2 environment to best mimic that found in oil pipelines in service. This particular inhibitor species is an anodic filming inhibitor, and reduces corrosion activity by forming a passivating film preventing the anodic reaction of metal

dissolution. The environment is CO_2 saturated so that the primary method of attack would be sweet corrosion.

Initially the solution was doped with 5ppm inhibitor solution, a concentration well below that used in the field. E_{corr} measurements of –640mV vs SCE versus –720mV in the CO_2 purged uninhibited solution confirm that the inhibitor is indeed operating to impede the anodic reactions. Referring to the scans shown in figure 4.5, it can be seen that there are only a few localised 'pits', however the intensity of these pits actually exceeds that of the sample submerged in inhibitor free solution by approximately 20%. This is due to the fact that the concentration of filming inhibitor is insufficient to protect all the anodic sites. As much of the surface is protected, the surface is polarised and the E_{corr} increases therefore increasing the intensity of the corrosion activity at the unprotected sites. As the experiment progressed, the intensity of the pits decreased due to the exposed anodic sites being protected by carbonate/inhibitor film build up. This was confirmed by analysis of the total metal loss data. The experiment was repeated using a 10ppm inhibitor solution which is a concentration far more common in the field although even higher quantities are often used to ensure total filming protection. The primary mechanism of corrosion will be sweet, however in this case sufficient inhibitor is added to protect the entirety of the exposed metal surface. Due to the formation of a complete filming layer, there is no corrosion activity on the bulk of the sample throughout the experiment. There is however limited anodic activity around the edge of the scan area at the interface between the Teflon tape and the metal surface. This is highlighted due to the small scale of the plots (maximum value is 130 mAm^{-2} compared to 600 mAm^{-2} for the 5ppm experiment). The increased corrosion activity is due to the function of crevice actions which are discussed in section 4.4.3. After removal from the electrolyte the metal had an unblemished shiny finish. Dosing of oil

pipelines is achieved using "pigs". The pipeline is initially dosed with a high concentration of inhibitor to build up a sufficiently thick inhibitor layer to withstand erosion from the flowing liquid for a reasonable period of time. However, the inhibitors are costly with the cost of under inhibiting even greater. As such to play it safe, the pipelines are re dosed with inhibitor well before the previous inhibitor has ceased to protect the pipeline surface. Better understanding of how much inhibitor is required to stop corrosion, and how long it stops corrosion for is an important factor. This investigation concluded that 10ppm inhibitor solution served to effectively eliminate corrosion. However this would not be a suitable dose for a pipeline in service as the inhibitor must last several months and not be washed away by the flow of fluid through the pipe.

4.4.3 Analysis of crevice corrosion

The samples supplied were mounted in a non-conductive resin. The steel and the resin have a different coefficient of thermal expansion (although efforts are made to make them as similar as possible). Therefore after mounting and cooling the interface between the metal and resin will not be coherent even after polishing. It is this interface that was used to assess the crevice corrosion protection characteristics of the inhibitor under investigation. The sample was submersed in 0.1% NaCl electrolyte for a period of six hours and scanned every two hours. The effectiveness of the inhibitor was then assessed.

Immediately after submersion the corrosion activity is concentrated around the crevice region with the bulk surface of the sample being the cathode. The intensity of the anodic activity is similar to that experienced when scanning the sample under the same conditions without the presence of a significant crevice, although the location of the corrosion activity differs immensely. Further more the levels of anodic activity now persist

throughout the experiment at the crevice. It should be noted that the inhibitor has eliminated corrosion activity on the bulk of the sample surface.

The reason that the inhibitor is not effective at preventing crevice corrosion is possibly due to the positively charged nature of the imidazoline. As the metal corrodes in the crevice, metal ions are released in to the electrolyte in the crevice. The combination of these ions with negative anions is more difficult due to the inaccessibility of the crevice. As such there is a net positive charge in the crevice, so that the positively charged inhibitor species is repelled from the crevice. The crevice will also attract negatively charged ions e.g. Cl^- which further serve to accelerate corrosion in the crevice. As previously discussed the 'insulating' of the metal surface will increase the E_{corr} so that those unprotected areas i.e. the crevices will experience increased corrosion levels.

CHAPTER 5

Results: Analysis of Galvanic corrosion

In Welded Pipeline Materials

5. Welded Sample C

5.1 Introduction

As highlighted in chapter 1, it is necessary to join carbon steel sections using welded joints and these are often focal points for corrosion failure.

The aim of this section of work was to evaluate the environmental SVET as a means of imaging localised corrosion activity on a failed welded joint supplied by Total Fina Elf

Sample C is a section of a weld that failed in service prematurely. The purpose of this analysis is to scan the mounted sample, and take quantitative measurement of the corrosion characteristics and mechanisms. A digital image of the sample is shown in figure 2.7, it is a section of the failed pipeline wall at a welded joint.

5.2 Results of scanning welded sample C:

A photograph of the samples is shown in the experimental procedure section in figure 2.7. In this case the specimen was metallographically prepared, ensuring a totally planar surface for scanning (again, as for all experiments the time period between polishing and scanning was fifteen minutes). It was mounted and levelled in the SVET tank. This experiment was conducted in a CO_2 purged 0.1% NaCl environment, with no inhibitor present. It was then scanned over a 12 hour period, typical results of this are shown in figure 5.2 a-l.

The first scan at time = 0mins shows the corrosion occurring in bands. The centre section of the sample, corresponding to the welded section of the sample as shown in figure 5.3a, shows predominantly anodic activity, this anodic activity remains prevalent in this area throughout the scanning period. The lower zone of the regions identified on the SVET

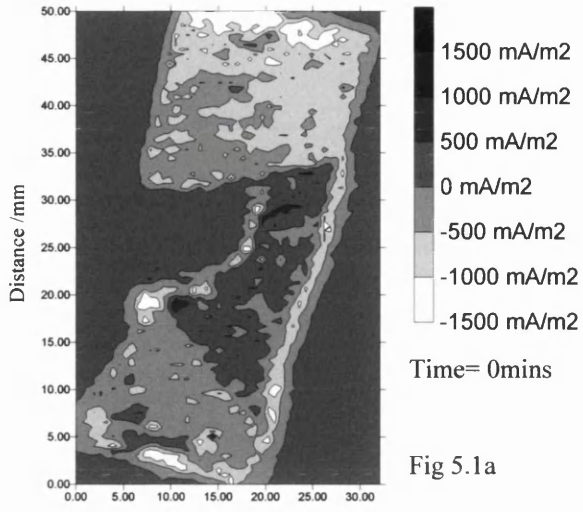

Fig 5.1a

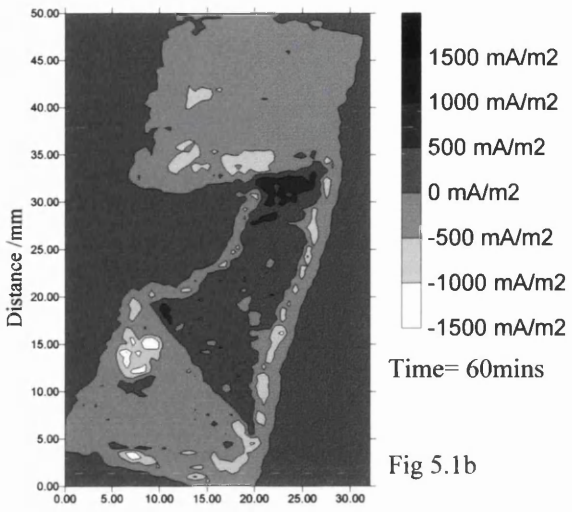

Fig 5.1b

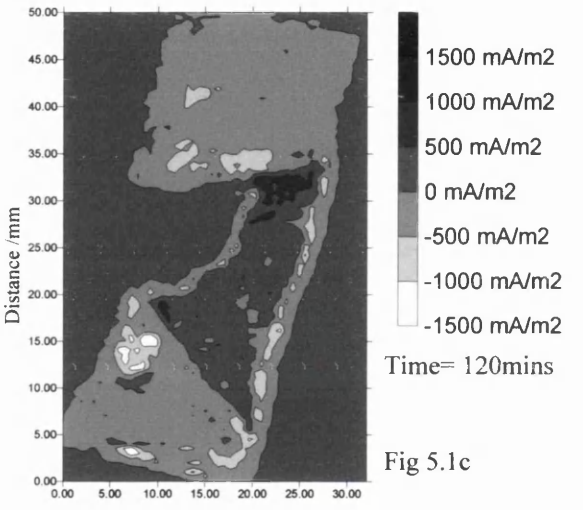

Fig 5.1c

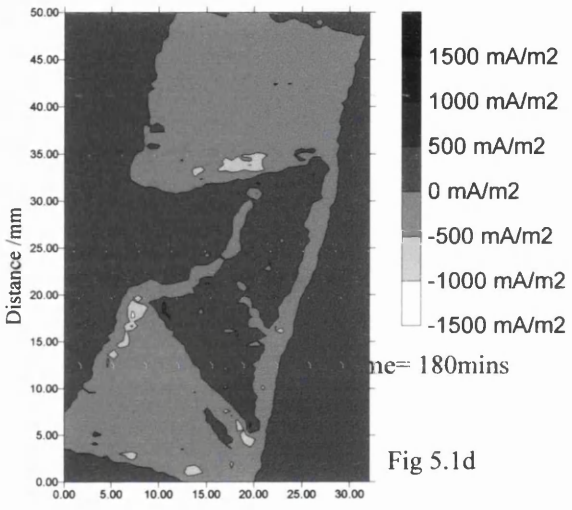

Fig 5.1d

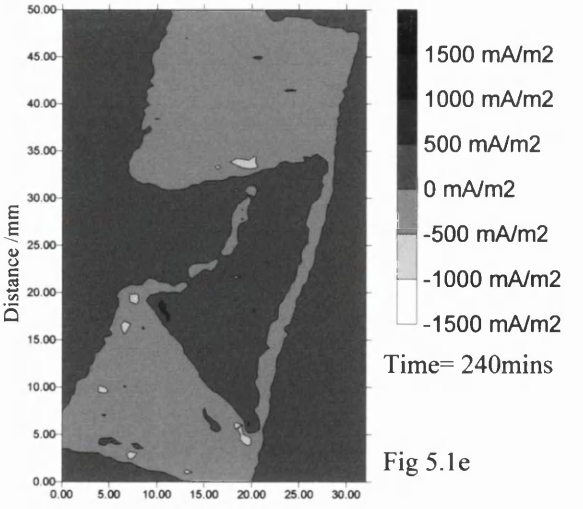

Fig 5.1e

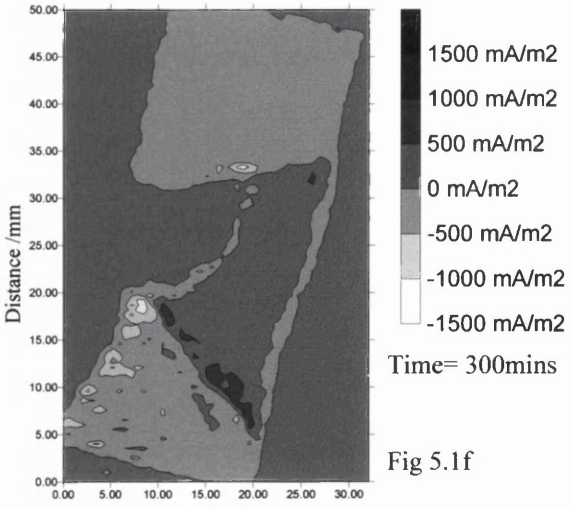

Fig 5.1f

Figures 5.1a-l Show the hourly SVET maps obtained from scanning over the weld sample submersed in 0.1% NaCl electrolyte. The darker areas represent the anodic regions.

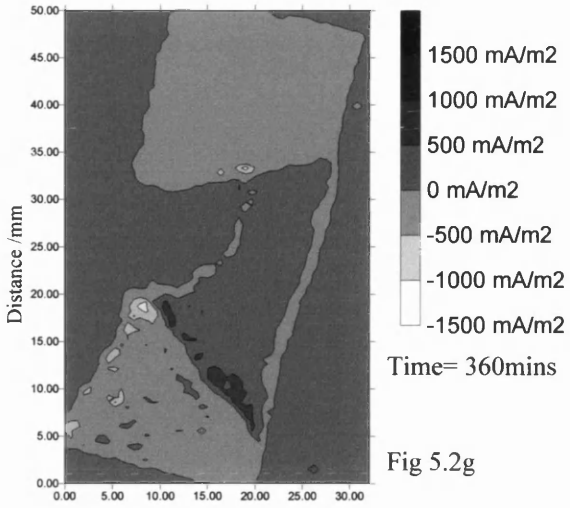

Fig 5.2g

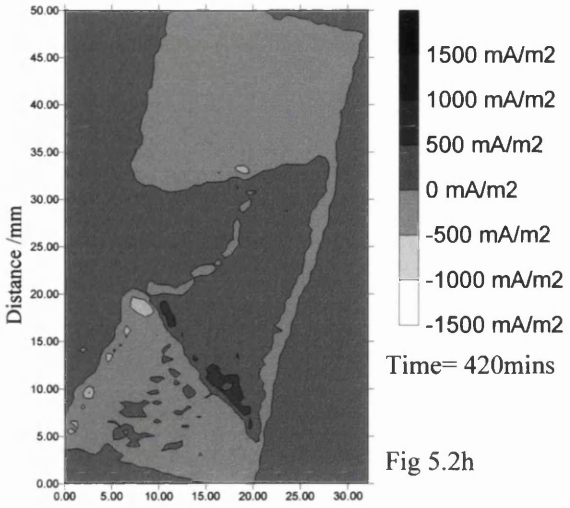

Fig 5.2h

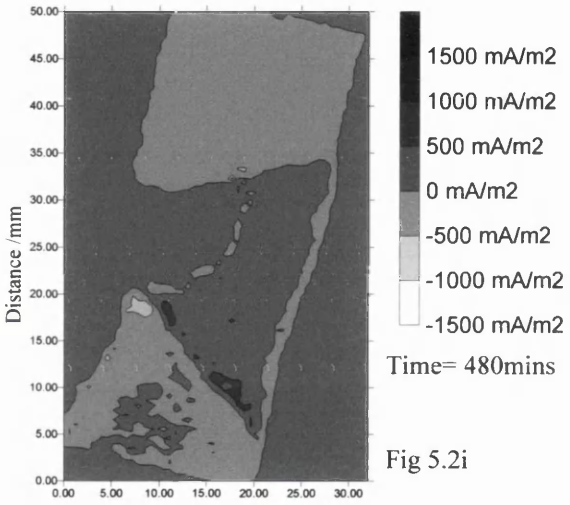

Fig 5.2i

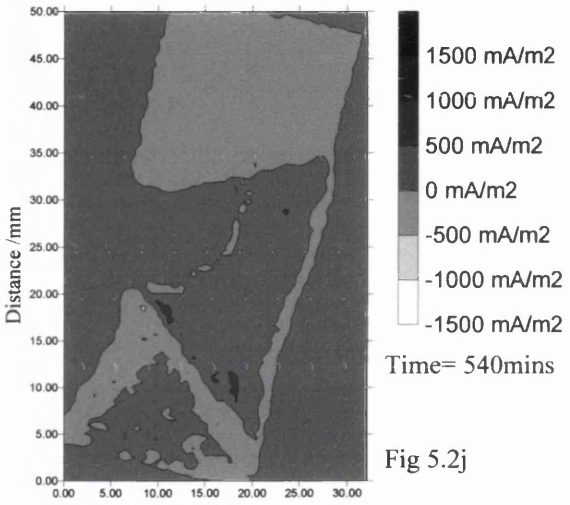

Fig 5.2j

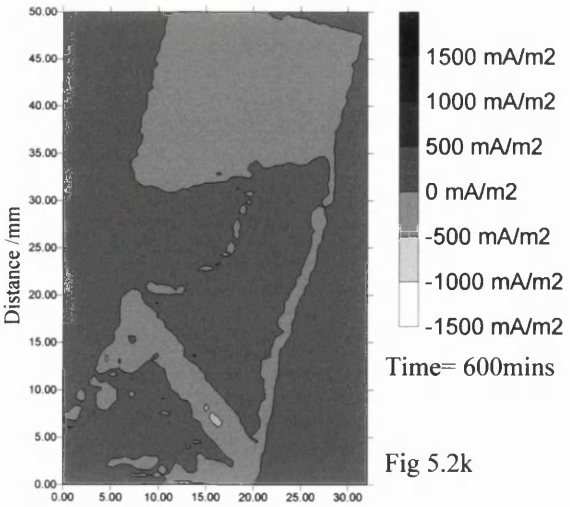

Fig 5.2k

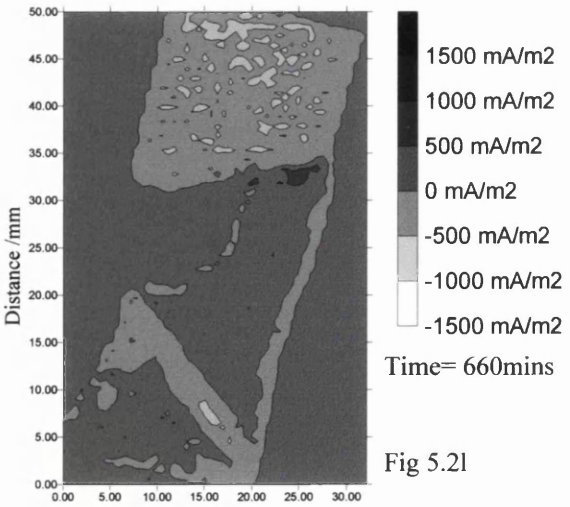

Fig 5.2l

scans corresponds to base metal 2 on figure 5.3a. This shows predominantly cathodic activity with anodic activity occurring over the latter scans. The upper zone of the scans correspond to base metal 1 on figure 5.3a. The reactions in this area are primarily cathodic throughout the experiment, with very little anodic activity occurring.

Figures 5.2a and 5.2b show the image formed by the final scan of the SVET and a digital camera image of the sample immediately after the experiment. The middle third of the sample exhibited extensive corrosion, with the lower third (base metal 2) showing lesser signs of activity. Base metal 1 was significantly less corroded than the other sections of the sample.

Figures 5.3b and a show the corroded sample, and an acetate of the differing metallic regions on the sample. Notice the correlation between the differing compositions and corrosion behaviour: each of the three regions experiences quite different levels of corrosion.

Compositional analysis of the different zones of the sample was achieved using the EDX technique. Specimens of the welded area as described in section 2.2.2 are analysed.

Sample 2.7b. Is a section of sample C shown, and is part of the base metal 1

Sample 2.7c is a section taken form the heat affected zone of sample C.

Sample 2.7d is a section of base metal 2

Sample 2.7e is a section of the weld material in sample 2.7a

Last SVET scan before removal from electrolyte.

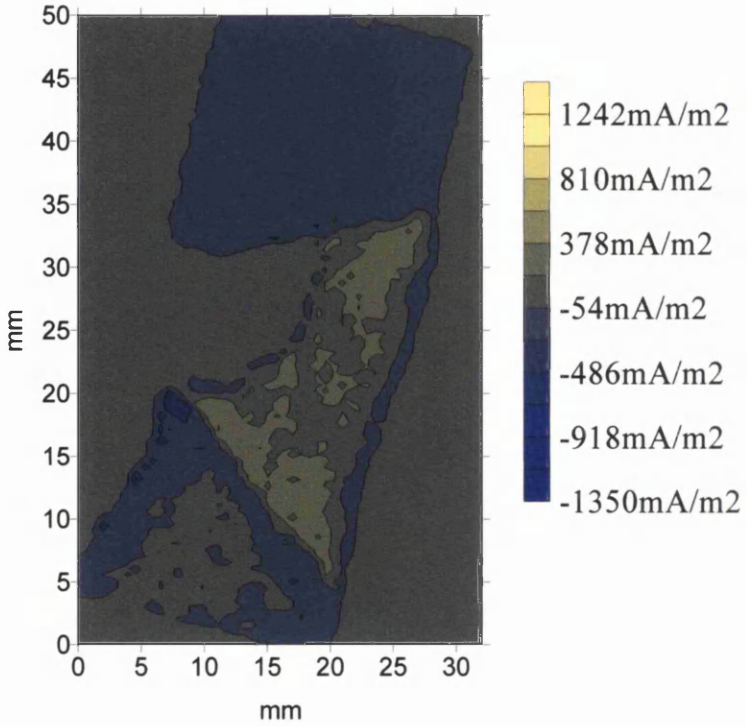

Digital Camera image immediately after removal form electrolyte and drying.

Figure 5.2a and 5.2b show a SVET scan of sample C, and a digital photo of the sample after submersion in CO_2 saturated electrolyte for 12 hours.

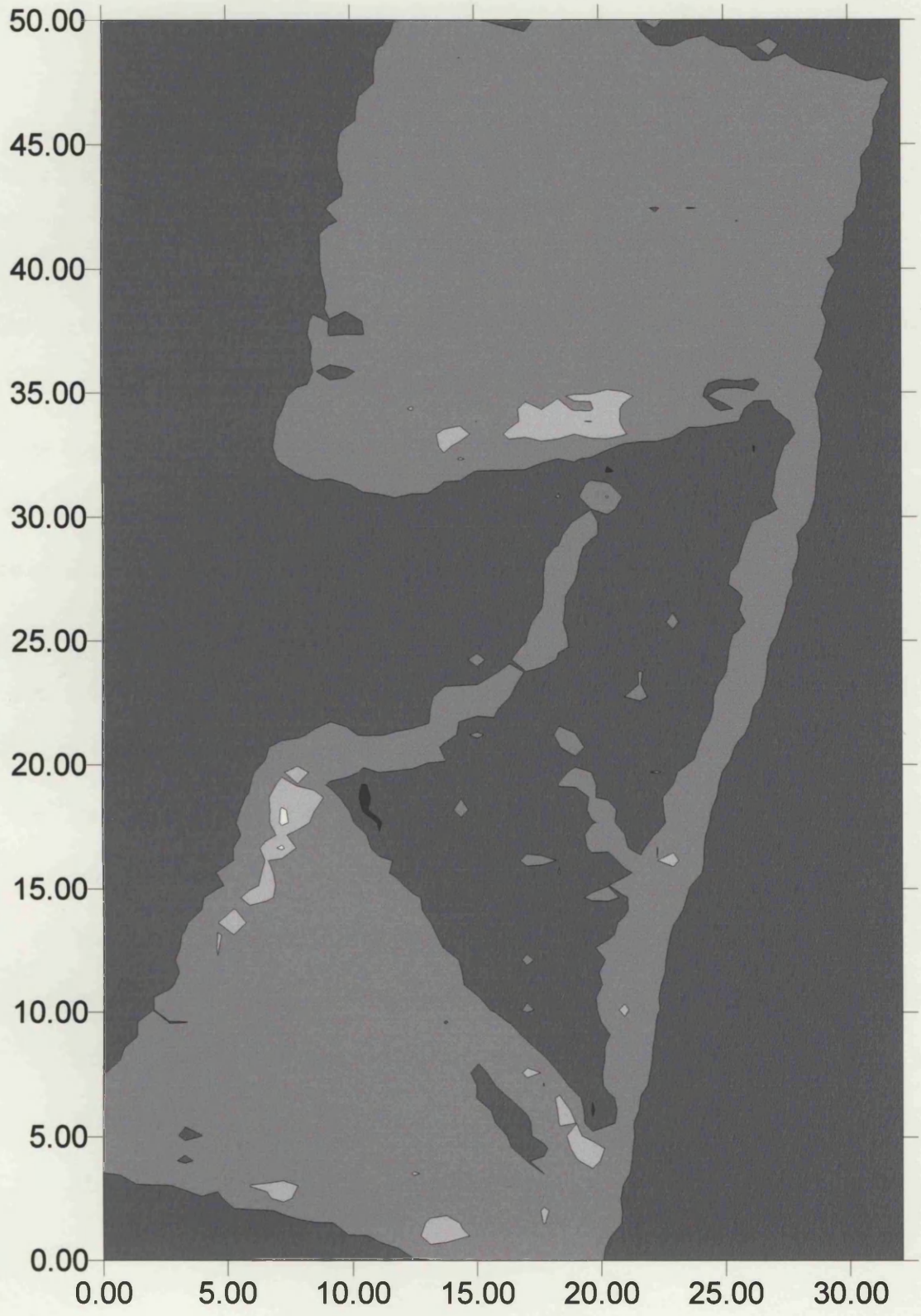

Fig 5.3b Shows the SVET scan of the sample after 3 hours, showing the areas of anodic and cathodic activity, which correspond to the differing compositional regions

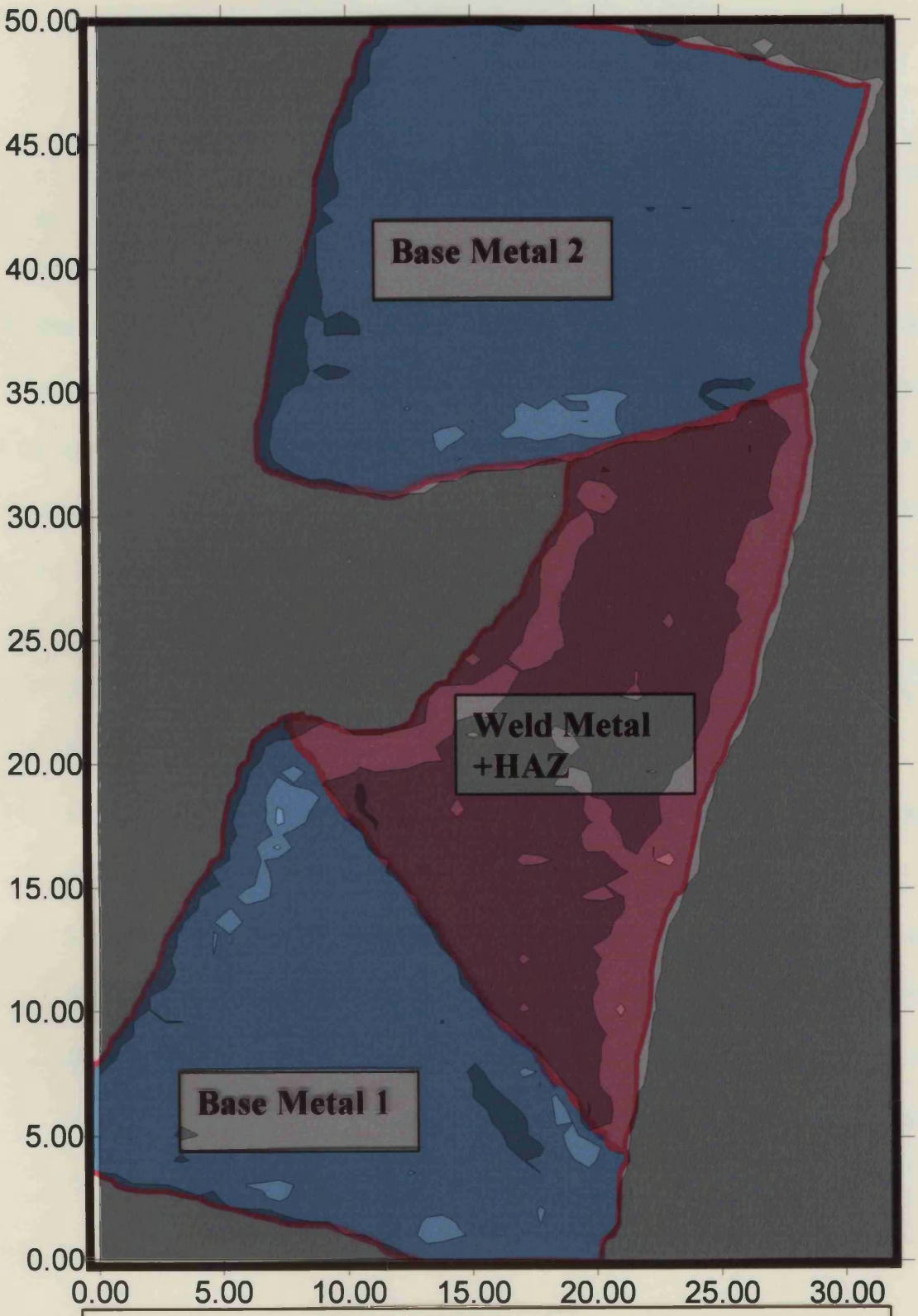

Fig 5.3a Shows the differing compositional zones of the sample being scanned; base metal 1, base meta 2, weld metal and HAZ

Fig 5.3b Shows the SVET scan of the sample after 3 hours, showing the areas of anodic and cathodic activity, which correspond to the differing compositional regions

	Mn	Cr	Al	Si	Ni
	Elemental % of iron content				
Base Metal 2	1.01	0.89	0	0	0
Base Metal 1	0.913	0	0	0	0
Weld	0.901	0	0.42	0.25	1.15
HAZ	1.02	0	0	0	0

Table 5.1 A table showing the elemental compositions of the four different sections of the sample.

The levels of manganese, chromium, aluminium, silicon and nickel have been expressed as a percentage of the iron content detected by the EDX technique. This is due to limitations of the apparatus's ability to detect carbon. Spurious carbon level measurements can give false representations of the overall elemental levels. Taking the elements as a percentage of the iron level serves to minimise this effect.

- EDX analysis of base metal 1 (fig 2.7b) shows that the sample is carbon steel, with 0.91% manganese present.
- Base metal 2 (fig 2.7e) has similar levels of manganese, but in this case there is additionally 0.89% chromium.
- The heat affected (fig 2.7c) zone of the weld again showed similar properties to the base metals, as expected, however the levels of manganese were elevated to 1.02%.
- EDX of the weld metal (fig 2.7d) showed the composition to have a lower Manganese content, with 0.901%. Aluminium (0.42%), Silicon (0.25%), and Nickel (1.15 %) are also present in the weld material.

5.2.1 Total Metal Loss

As for the other experiments, total metal loss was calculated for the welded sample in order to give a quantitative measure of the corrosion activity. The data was handled in exactly the same manner to produce the graph shown in figure 5.4. Initially the corrosion is quite fierce, and over the four hour period tails off. The data cannot be directly compared to that obtained from previous scans due to the differences in scan area. Therefore if one looks at total metal loss per unit area then the results can be compared. The sum of all the metal loss data for the large sample is 205μg compared to 24.8, 12.1 4.65 and 2.84μg for the air saturated, CO_2 saturated, 5ppm and 10ppm scans. The area of the weld sample is 872mm^2 compared to 100mm^2 for the other samples. In order to compare, we must look at the TML per mm^2.

	TML (μg)	Area (mm^2)	TML/mm^2
Weld	205	872	0.24
Air	24.8	100	0.25
CO_2	12.1	100	0.12
5ppm	4.65	100	0.05
10ppm	2.84	100	0.03

Table 5.2 Showing the Total Metal Loss per mm^2 for each of the samples

Thus the TML per mm^2 is double that of the sample under the same environmental conditions, but without the weld joint. The corrosion levels are near those seen in the sample corroding in aerated solution.

Thus the total loss per mm^2 is larger for the weld due to galvanic coupling. Since anodic activity is localised in the weld then this is particularly damaging. In the case of the welded pipe the cathode area will be very large indeed leading to rapid component failure.

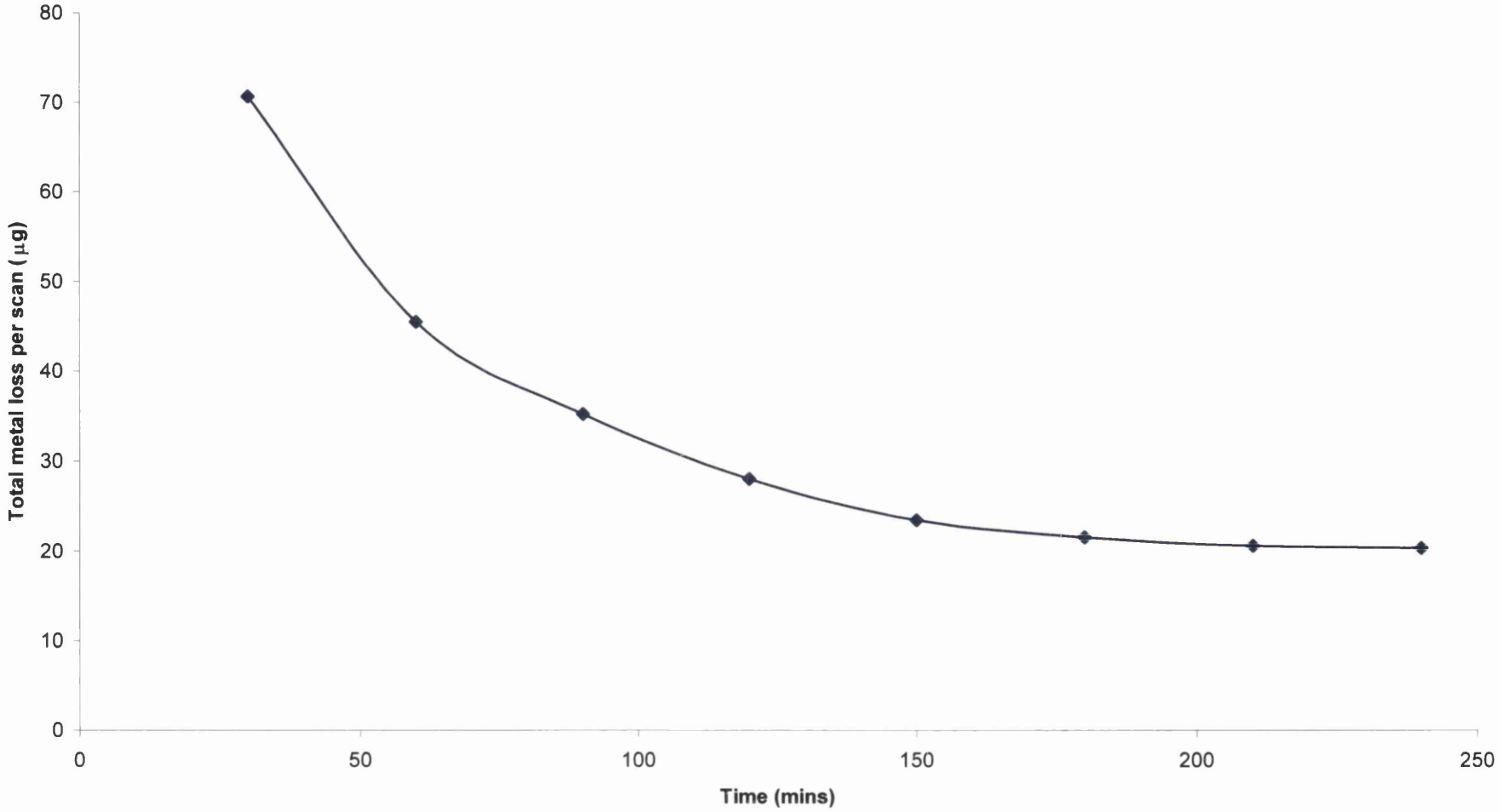

Figure 5.4. The cumulative total metal loss for the weld sample over 4 hours

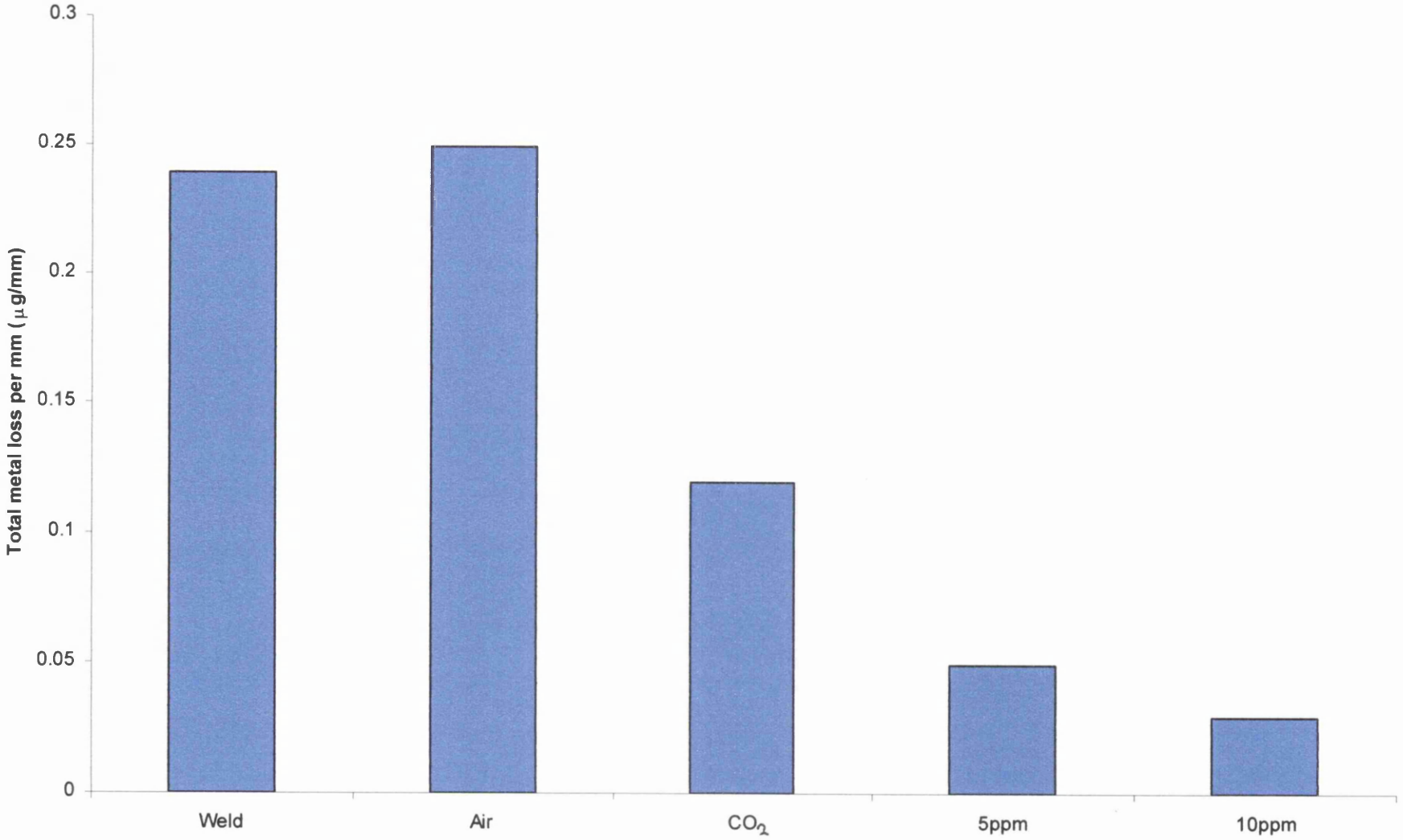

Figure 5.4. The total metal loss per mm figures for each of the samples

5.2 Discussion of the welded sample C.

This sample is a section of a failed weld in a pipeline. It has three separate metallic regions, base metal 1, base metal 2 and the weld material (see section 2.2.2). This sample was scanned in CO_2 purged electrolyte with no inhibitor present. It is immediately apparent that the corrosion is occurring in bands correlating with the different regions of materials as shown in figure 5.2b. Base metal 2 remains as a cathodic zone throughout the scan, base metal 1 is primarily cathodic, but does exhibit more anodic activity through the latter stages of the scan. The weld region shows extensive anodic activity throughout the scans see fig 5.2c-n.

Extensive galvanic coupling suggests that each of the three materials holds different positions in the galvanic series. The weld area has effectively become the sacrificial anode, which would account for the premature failure of this component. Furthermore base metal 1 shows no anodic activity and would therefore hold a lower position in the galvanic series; finally base metal 2 sits in between the two. An EDX was conducted on metal from each of the three zones on an attempt to discover why these materials had coupled so extensively. The results of which can be seen in table 5.1.

The EDX has picked up 0.89% chromium in base metal 2 with none in the other samples. The chromium will offer increased corrosion resistance explaining why the material is the most noble of the three and therefore remains cathodic. Base metal 1 is of similar composition to 1 but does not contain any chromium, therefore it does corrode slightly during the period of scanning. The weld area is again chromium free, but does contain aluminium, silicon and nitrogen. The aluminium and silicon were most likely

deliberate additions to the filler metal, in order to reduce the melting point and increase the wettability of the weld. The nitrogen could well have been included due to poor welding practice (incomplete shielding of the weld etc.). The weld metal is likely to have a different microstructure when compared to the base metals. This could have also affected its corrosion performance.

Total metal loss calculations using the scan data show that the corrosion intensity is double that of the non welded sample subject to the same CO_2 saturated conditions, and nears the corrosion intensity experienced by the sample scanned in air saturated solution. This is due to the galvanic coupling of the weld metal and base metals. Base metal 2 with its elevated chromium content is the cathode, base metal 1 experiences limited corrosion activity and the weld metal with its elevated levels of aluminium and silicon acts as the anode. As such the vast majority of metal dissolution occurs on the weld metal, and due to the relatively small area of this region, failure could precipitate very rapidly. The effects seen in experimentation could be further accelerated due to the fact that the sample used in experimentation has a limited cathode area, whereas in the field the cathode are could be a very large area compared to the welded joint.

5.4 Conclusions

The SVET could be a good technique to investigate weld corrosion and ability of materials to inhibit corrosion, as well as the potential for galvanic coupling of the weld material and the base materials. A further problem is that the sample must be planar to within ten microns, both ensuring that the sample is flat and level becomes particularly awkward when scanning large samples such as the one studied. As such development of a 3D height scanning SVET with environmental control. This could then be used to develop new understanding of welding processes and the link between localised corrosion and the microstructure.

CHAPTER 6

Summary

& Future Work

6. Summary:

The primary objectives of this project were as follows:

- Construct an SVET with environmental control.
- Assess the effects of atmosphere on corrosion mechanisms on pipeline carbon steel samples.
- To investigate the effect of imidazoline filming inhibitor and concentrations on the corrosion mechanisms on the bulk sample and at crevice locations.
- Assess the corrosion mechanisms occurring on welded joints which had been a field failure to ascertain if there was galvanic coupling.

6.1 Building of the SVET apparatus:

A large portion of this project was dedicated to constructing an environment controlled SVET. The improvement in the performance of the technique under environmentally controlled conditions was marked, the addition of the CO_2 flooded chamber prevented any significant oxygen contamination during scanning. As was shown in sections 3.1 and 3.2, there is a marked effect on the corrosion mechanisms in the presence of air as opposed to CO_2. Due to the extreme height sensitivity of the apparatus, many efforts were taken to eliminate any sources of movement of the apparatus. The SVET and environment chamber were mounted on a 60Kg concrete slab, to which the chamber was bolted to prevent movement when the lid was put on or removed. The final iteration of the equipment design yielded excellent data reproducibility and environmental control.

Levelling table redesign aided in a more user friendly and adaptable design with sample levelling being able to be performed in significantly reduced periods. The design also facilitated the addition of sample specific adapter plates that allowed secure mounting of the samples to the table, critical due to the height sensitivity of the apparatus. Calibration of the SVET had to be performed regularly to ensure correct operation of the equipment. Calibration was performed in non CO_2 purged solution. It would however have been more accurate to calibrate in CO_2 saturated solution, as the lower pH of the solution would have increased conductivity by approximately 10%.

6.2 The effect of atmosphere on corrosion mechanisms:

Samples immersed in air saturated solution rather unsurprisingly showed the highest overall levels of corrosion activity spread across the surface of the sample. The corrosion product formed was iron oxide (rust). Intense anodic activity remained throughout submersion in the electrolyte. The purging of the solution with CO_2 changed the mechanism of corrosion to sweet corrosion. In this case the anodic activity was far more focused giving more intense local anodes initially, but lower overall levels of corrosion. As the experiment continued, the level of corrosion activity decreased due to the formation of a carbonate layer on the metal surface, effectively shielding it from further corrosion activity.

6.3 The effects of inhibitor addition, the concentrations and crevice corrosion

One area of testing involved the addition of anodic filming inhibitor to the electrolyte at two different concentrations of 5 and 10ppm. The addition of 5ppm largely eliminated corrosion activity, but was not sufficient to protect the entire surface. As such the remaining exposed areas experienced increased corrosion activity due to the fact that the inhibitor had increased the $E_{corr.}$ Over all activity was less than for the inhibitor free solutions, the initial intensity of the focal anodes were actually greater. 10ppm inhibitor addition was sufficient to form a complete protective layer, and as such corrosion activity remained very low throughout experimentation with the sample maintaining an unblemished surface even after extended periods of submersion. Interestingly from the scans it was clear however that limited activity was occurring at the interface between the insulating tape and the metal. This prompted further investigation into the effectiveness of the inhibitor at preventing crevice corrosion. Investigation showed that when scanning a planar sample, with a crevice between the metal and mounting resin, the inhibitor solution was not able to prevent corrosion activity in the crevice region. The main reason suggested for this is that the inhibitor is a positively charged species, and due to the fact that metal ions released in the crevice struggle to combine with negative anions from the cathodic sites away from the crevice region, there is a net positive charge to the crevice which will therefore repel the like charged inhibitor molecules. The problem is accentuated by the fact that the use of an anodic inhibitor increases the $E_{corr.}$ Therefore corrosion at unprotected areas is increased.

6.4 Study of the welded sample

The SVET has demonstrated itself a useful technique to investigate weld corrosion and the ability of materials to inhibit corrosion, as well as the potential for galvanic coupling of the weld material and the base materials. This was a prime case of galvanic coupling, the weld was a relatively small area of metal that was more anodic than either of the base metal materials it was joining and therefore acted as a sacrificial anode. Due to the massive disparity in cathode to anode size in the field, it is unsurprising that this welded joint failed prematurely. The presence of chromium in base metal 2, whilst no where near the levels required to make the material 'stainless', was sufficient to make the material significantly more noble than the weld and base metal 1. Base metal 2 therefore acted as the cathode and experienced virtually no anodic activity. The failure could have been avoided with a more careful materials selection, using metals and weld material with similar corrosion properties.

6.5 Future Work

There are numerous permutations of experiments that could be conducted using the apparatus constructed. Other conditions could be analysed, the inclusion of acetic acid, other types of inhibitors, changing the temperature of the solution etc. Of particular interest would be to quantify how long the inhibitor provides protection for at a given concentration, and the effects of flow on its longevity (does it wash away).

In the field, 'pigs' are used to dose the pipes. An investigation into how delivery of the inhibitor effects performance could be undertaken. Finally, use of a

3D height scanning SVET would enable non-planar samples to be scanned. Currently the samples must be ground to a mirror finish, which is unlikely to be the conditions found in an actual pipeline. The 3D SVET could scan specimens in their 'in service' condition.

Initial work has shown environmental SVET has wide ranging appeal. There are significant opportunities for study including:

1. The effects of atmosphere: This subject was only touched on in this project; the apparatus has now been constructed that allows the atmosphere in and around the SVET to be carefully controlled. Experimentation could be performed with a wide range of gases. Furthermore temperature control could enable a closer simulation of the conditions found in the field.
2. 3D Height Scanning: As has been briefly discussed, the current SVET can only scan planar samples, a 3D profiling environmental SVET would enable scans to be made of contoured samples.
3. The effects of acetic acid on the corrosion mechanisms- precise pH control
4. A wider range of metals could be investigated, different grades of steel etc...
5. Investigations could be made into corrosion under moisture films by means of the Kelvin probe, since immersion corrosion is only part of the failure model observed.
6. Microstructural analysis of the specimens to allow investigations to be made into why certain sites become local anodes would enable a precise link between certain defect sites and the initiation of corrosion to be made.